

Sheffield Hallam University

Development of optical bio-sensing methods for detection of toxins produced by algae.

AL-AMMAR, Rukaiah.

Available from the Sheffield Hallam University Research Archive (SHURA) at:

<http://shura.shu.ac.uk/19231/>

A Sheffield Hallam University thesis

This thesis is protected by copyright which belongs to the author.

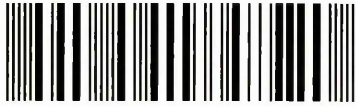
The content must not be changed in any way or sold commercially in any format or medium without the formal permission of the author.

When referring to this work, full bibliographic details including the author, title, awarding institution and date of the thesis must be given.

Please visit <http://shura.shu.ac.uk/19231/> and <http://shura.shu.ac.uk/information.html> for further details about copyright and re-use permissions.

Learning and Information Services
Adsetts Centre, City Campus
Sheffield S1 1WD

102 048 297 4



Sheffield Hallam University
Learning and Information Services
Adsetts Centre, City Campus
Sheffield S1 1WD

REFERENCE

ProQuest Number: 10694111

All rights reserved

INFORMATION TO ALL USERS

The quality of this reproduction is dependent upon the quality of the copy submitted.

In the unlikely event that the author did not send a complete manuscript and there are missing pages, these will be noted. Also, if material had to be removed, a note will indicate the deletion.



ProQuest 10694111

Published by ProQuest LLC (2017). Copyright of the Dissertation is held by the Author.

All rights reserved.

This work is protected against unauthorized copying under Title 17, United States Code
Microform Edition © ProQuest LLC.

ProQuest LLC.
789 East Eisenhower Parkway
P.O. Box 1346
Ann Arbor, MI 48106 – 1346

Development of Optical Bio-sensing Methods for Detection of Toxins Produced by Algae

Rukaiah Al-Ammar

**A thesis submitted in partial fulfilment of the requirements of
Sheffield Hallam University
For the degree of Doctor of Philosophy**

March 2015

DECLARATION

I hereby declare that this thesis submitted for the degree of PhD is the result of my own research and that this has not been submitted for a higher degree to any University or institution.

Signed

Rukaiah Al-Ammar

ABSTRACT

The main aim of this work is to develop an optical method for the detection of microcystin-LR, one of the most dangerous toxins released by cyanobacteria. Photosynthetic cyanobacteria (also known as blue-green algae) exist in any type of water (including drinking water) and possess a serious threat to humans and animals, and generally to the environment. Microcystin-LR (MC-LR) is perhaps the most toxic from a large family of cyanotoxins; it is known to cause liver damage and also acts as a carcinogen. The World Health Organization has set the limit of $1\mu\text{g/l}$ for MC-LR in drinking water. However existing detection methods, such as ELISA, cannot provide such high sensitivity. The relatively low molecular weight of MC-LR (995.2 m/mol) makes it difficult to detect using conventional QCM and SPR based analytical methods. Therefore, the development of highly sensitive, reliable, and (at the same time) inexpensive and easy-to-use methods of detection of microcystin is of very high importance today. The method of Total Internal Reflection Ellipsometry (TIRE) is particularly attractive for the above task considering its high sensitivity and particular suitability for detection of low molecular weight analytes. In this work MC-LR was detected in direct immunoassay with MC10E7 monoclonal antibodies raised against MC-LR in mouse, using TIRE as a detection method. Also the TIRE method was used to study the protein- protein interaction (the protein chaperon with its receptors in the chloroplast) and to detect other types of toxins such as Aflatoxin B1.

At first, the TIRE immunoassay was calibrated using aqueous solutions with known concentration of MC-LR. The study of binding kinetics of MC-LR to MC10E7 yielded the association constant close to 10^8 l/mol which is typical for highly specific immune reactions. The detection limit for MC-LR between 0.1ng/ml and 1ng/ml was achieved using the TIRE detection. Then, the concentration of the MC-LR toxin produced naturally by algae *microcystis aeruginosa* was evaluated using calibration data obtained for solutions spiked with known concentrations of MC-LR. The role of environmental factors (temperature, pH, nutrition contents, and salinity) on the efficiency of production of MC-LR by *microcystis aeruginosa* was studied. Purification of solutions contaminated with MC-LR (both commercial and naturally produced) was achieved using MnCO_3 microparticles coated with polyelectrolytes and functionalised with MC10E7 antibodies as an absorbent for MC-LR. Also, the concentration of MC-LR in solutions was reduced as a result of direct electrolysis.

ACKNOWLEDGMENTS

I would like to express my deepest appreciation to my Director of study, Dr. Alexei Nabok, for all of his encouragement, being patient and offering truly valuable support during this work, and for his useful advice. I greatly enjoyed the learning process and worthwhile research studies under him. His wide knowledge was a great value to me.

I would like to thank the additional members of my PhD committee, Dr. Abbass Hashim, and Dr. Tom Smith, for their fantastic guidance and important discussions regarding this work.

Thanks are also due to all MERI support staff, especially Veny for his technical help and support throughout this work. I would also like to thank Zaki for his help and Hakin. It has been a pleasure working with my colleges in the Laboratory.

Most importantly, I would like to give special thanks to my husband, Maytham, for his unconditional love and support. His prayers and belief in my ability always encouraged me to move forward. Thank you.

Finally, I want to say thank you to all my children, Aya, Noralhuda, Sara, and Fatima for their loving support, patience and understanding throughout my study.

LIST OF ABBREVIATION

MC-LR	microcystin-LR
AFT	Aflatoxin
Ab	Antibody
SEM	Scanning electron microscopy
AFM	Atomic force microscopy
BSA	Bovin Serum Albumin
DNA	Deoxyribonucleic acid
ELISA	Enzyme-linked immunosorbent assay
IgG	Immunoglobulin G
K_A	Association constant
K_D	Dissociation / affinity constant
LC	Liquid chromatography
$MnCO_3$	Magnesium carbonate
MS	Mass spectroscopy
PAH	Poly(allylamine) hydrochloride
PSS	Poly-styrene sulfonate
SPR	Surface Plasmon Resonance
TIRE	Total internal reflection ellipsometry
WHO	World health organization
RACE	Rapid Amplification of cDNA Ends
IP injections	Interapretoneal injection

LIST OF PUBLICATIONS

Journals publications:

1. **R. Al-Ammar**, A. Nabok, A. Hashim, (2014) optical detection and purification of contaminated substances microcystin-LR produced by algae. *Sensors & Actuators: B. Chemical*, (in press).
2. **R Al-Ammar**, A Nabok, A Hashim and T Smith. (2013) Optical detection of microcystin produced by cyanobacteria. *J. Phys.: Conf. Ser.* **450**, (1), 012006.
3. A. Nabok, V. Erokhin, S. Erokhina, A. Szekacs, M. K. Mustafa & **R. Al-Ammar**. (2013) Extraction of mycotoxins from aqueous solutions using functionalized polyelectrolyte-coated microparticles. *BioNanoSci*, **3** (1), 79-84.
4. V. Kriechbaumer, A. Nabok, M.K. Mustafa, **R. Al-Ammar**, A Tsargorodskaya, D.P. Smith, B.M. Abell. (2012) Analysis of protein interactions at native chloroplast membranes by ellipsometry, *PLoS One.*; **7**(3):e34455.

Conference papers:

1. A. Nabok, V. Kriechbaumer, M.K. Mustafa, A.Tsargorodskaya, R.Al-Ammar, B. Abell, D. Smith. The study of interaction of chaperones with respective receptors assembled on the surface. 12th European Conference on Organized Films, ECOF 12 conference, 17-20 July, 2011, Sheffield, UK.
2. R. Al- Ammar, A. Nabok, A. Hashim & Prof. T. Smith, 21 May 2011. Detection of water Pollution using Bio-Sensing Technologies (poster). student day Sheffield Hallam University.
3. R. Al- Ammar, A. Nabok, A. Hashim & T. Smith, 23 Dec 2011. Optical detection of Microcystin-LR produced by cyanobacteria, BMRC ,Sheffield Hallam University, Sheffield UK.
4. R. Al-Ammar, A. Nabok, A. Hashim, T. Smith, Detection of Microcystin in Direct Immunoassay Format Combined with Total Internal Reflection Ellipsometry, 11th European Conference on Optical Chemical Sensors and Biosensors, EUROPTRODE XI, 1-4 April, 2012, Barcelona, Spain.
5. R.Al-Ammar, A. Nabok, A. Hashim, T. Smith, Optical detection of toxins released by cyanobacteria, 14th International conference on organized molecular films, ICOMF 14 (LB 14), 10-13 July, 2012, Paris, France.
6. R.Al-Ammar, A. Nabok, A. Hashim, T. Smith, Detection of microcystin in direct immunoassay format combined with Total Internal Reflection Ellipsometry. Institute of Physics, Sensors & their Applications XVII, 16-18 September, 2013, Dubrovnik, Croatia

7. R. Al-Ammar, A. Nabok, T. Smith, Optical detection of microcystin produced by cyanobacteria and purification of contaminated substances using functionalised polyelectrolyte micro-particles, 12th European Conference on Optical Chemical Sensors and Biosensors (EUROPTRODE XII), 13-16 April, 2014, Athens, Greece
8. R. Al-Ammar, A. Nabok, A. Hashim, T. Smith. Detection of water pollution using bio-sensing technologies, MERI, student day. (Presentation). 20 June 2012. Sheffield Hallam University.
9. R. Al- Ammar, A. Nabok, A. Hashim, T. Smith. Optical detection of Microcystin-LR produced by cyanobacteria, BMRC, 17 Dec 2012, Sheffield Hallam University, Sheffield UK.
10. R. Al- Ammar, A. Nabok, A. Hashim & T. Smith . Production of microcystin by cyanobacteria.Purification of substances Containing microcystin with functionalized microparticules.BMRC/ MERI Winter Poster Even 22 Dec 2013.

Prizes:

- 1- **Third prize** – poster in student day (2011). Sheffield Hallam University
R. Al- Ammar, A. Nabok, A. Hashim & T. Smith
Detection of water Pollution using Bio-Sensing Technologies (poster).
- 2- **Third prize** (poster), BMRC/ MERI Winter Poster Event (2013). Sheffield Hallam University. R. Al- Ammar, A. Nabok, A. Hashim & T. Smith. Production of microcystin by cyanobacteria.Purification of substances containing microcystin with functionalized microparticules.BMRC/ MERI Winter Poster Even 2013.

I was the reviewer With IEEE Sensors Journal for the paper:
Part-Per-Trillion Level Detection of Microcystin-LR using a Periodic Nanostructure.(2014).

Contents

- I. Declaration**
- II. Acknowledgement**
- III. Dedication**
- IV. Abstract**
- V. List of Publications**
- VI. List of Abbreviations**

Chapter	Topics	P.
1.	INTRODUCTION	
1.1	Problem outline	1
1.2	Detection of microcystin.	2
1.3	Mycotoxins: detection and purification of contaminated substances.	3
1.4	Protein-protein interaction.	4
1.5	Aims and objectives.	5
2.	BACKGROUND OF ALGAE AND TOXINS PRODUCED BY ALGAE	
2.1	Algae	7
2.2	Cyanobacteria	10
2.3	Microcystin-LR.	12
2.4	Presence of Microcystins in Aquatic Systems	16
2.5	Liver toxicity of microcystin-LR	17
2.6	Health-Based Criteria for Safe Exposure to Microcystin	17
2.7	Domestic Animal Poisonings	18
2.8.	Effects of Microcystins on Fish and Wildlife	19
2.9	Detection of Microcystin-LR	21
2.10	Current Treatment Technologies for Microcystin-LR	22
3.	THE CONCEPT OF BIOSENSORS	
3.1	Biosensors: definitions and classification	24
3.1.1.	Importance of biological sensing system	26
3.1.2	Biosensors world market	27
3.1.3	The need for label-free detection	27
3.2	Immunosensors	28
3.2.1	Avidity and Affinity	29
3.2.2	Antibody - Antigen interaction	30

3.2.3	Antibody immobilization	34
3.3	Antibodies production and purification	35
3.4	Optical biosensors and detection of Immune reaction	36
3.4.1	ELISA method	37
3.4.2	SPR (BIACORE)	37
3.5	Summary	39
4.	OPTICAL IMMUNOSENSING METHODS: TOTAL INTERNAL REFLECTION ELLIPSOMETRY (TIRE)	
4.1	Theoretical background of evanescent wave technique	40
4.1.1	Ellipsometry	42
4.1.2	Surface Plasmon Resonance (SPR)	44
4.2	Total Internal Reflection Ellipsometry (TIRE)	47
4.2.1	TIRE experimental set up	51
4.2.2	Methodology of TIRE experiments	54
4.2.3	TIRE kinetics analysis	56
5.	COMPLEMENTARY EXPERIMENTAL TECHNOLOGUES	
5.1	UV-vis. Absorption Spectrophotometry	58
5.2	Scanning electron microscopy (SEM)	60
5.3	Infinite Focus Microscopy (IFM)	62
5.4	Fourier Transform Infrared Spectrometry FT-IR	62
5.5	Hemocytometry	65
5.6	Fluorescence Microscopy	67
5.7	Langmuir–Blodgett trough	68
5.8	Edwards E360A evaporation unit	70
6.	FURTHER DEVELOPMENT OF TIRE METHOD FOR OTHER APPLICATIONS	
6.1	Protein-protein interaction	72
6.1.1	Study of chaperone interaction with receptors	73
6.1.2	Sample preparation	73
6.1.3	TIRE measurements and data fitting	75
6.1.4	Analysis of chaperone binding kinetics	79
6.2	The study of Aflatoxin B1 binding to polyelectrolyte capsules	81
6.2.1	Functionalization of microcapsules	81
6.2.2	UV-vis absorption spectra study	83
6.2.3	Conclusions	87

7.	OPTICAL DETECTION OF MICROCYSTIN-LR	
7.1	Detection of Microcystin LR using TIRE	89
7.1.1	Samples preparation and TIRE measurements	89
7.1.2	TIRE study of the immune reaction between MC LR and MC10E7	90
7.1.3	The study of MC-LR and MC10E7 binding kinetics	93
7.2	Fourier Transform Infrared spectrometry (FT-IR) measurements	97
7.3	UV-vis spectral study of microcystin-LR	98
7.4	Detection of MC-LR produced by cyanobacteria; effect of environmental factors on algae and toxin production.	100
7.4.1	Selection of microorganism and growth of algae	100
7.4.2	The growth in optimal condition	101
7.4.3	Growth microcystis aeruginosa under increased and decreased nutrient levels in broth and changing the environmental condition	105
7.4.4	Extraction of MC-LR	108
7.4.5	Effect of salinity on the algae growth	112
7.5	TIRE detection of naturally produced microcystin-LR	114
7.6	Microcystin-LR cleansing with functionalized polyelectrolyte micro-particles	117
7.7	Conclusion	117
8.	THE USE OF FUNCTIONALIZED MICROPARTICLES AS ABSORBENT FOR MICROCYSTIN-LR	
8.1	Micro encapsulation	118
8.2	Polyelectrolyte microcapsules	119
8.3	Preparation of microparticles	121
8.3.1	UV-vis measurement	123
8.3.2	TIRE measurements	124
8.4	Comparison between purification of natural and commercial toxin by microcapsules	126
8.5	Removing the core of the microcapsules	127
8.6	Microcystin-LR removal by electrolysis	133

Conclusions	135
9. CONCLUSIONS AND FUTURE WORK	
9.1 Conclusions	136
9.2 Future work	137
References	138

LIST OF FIGURES

Figure		Page
Figure 2.1	Chemical structure of microcystin-LR.	14
Figure 3.1	Configuration of a biosensor.	25
Figure 3.2	Affinity and Avidity.	30
Figure 3.3	Diagram of the basic unit of immunoglobulin (antibody).	32
Figure 3.4	the antibody structure.	32
Figure 3.5	Chemical structures of (a) PAH and (b) PSS; (c) Multilayered film of alternated layers of PAH And PSS deposited on negatively charged surface.	34
Figure 3.6	(a) various orientations of antibodies on surface, (b) Improvement of antibody orientation using proteins Protein A (or G)	35
Figure 3.7	Production of antibodies.	36
Figure 3.8	ELISA methods.	38
Figure. 4.1	(a) Reflection and transmission of light at the n_1 - n_2 interface; (b) Total internal reflection; (c) The formation of evanescent wave.	41
Figure 4.2	Schematic diagrams of evanescent waves propagating along a metal- Dielectric interface.	41
Figure 4.3	The formation of evanescent wave at total internal reflection at the Boundary between two media with different wave motion properties.	42
Figure 4.4	Changes in polarization of light reflected from the surface.	42
Figure 4.5	The schematic of rotating analyzer spectroscopic ellipsometry.	44
Figure 4.6	Kretschmann (a) and Otto (b) configurations of an Attenuated Total	

	Reflection setup for coupling surface plasmons.	45
Figure 4.7	(a) Typical set-up of an SPR biosensor.	46
Figure 4.8	Experimental setup for surface Plasmon resonance enhanced ellipsometry.	49
Figure 4.9	Typical TIRE spectra bare gold film on glass.	50
Figure 4.10	(a) J.A. Woollam M2000 Ellipsometry	51
Figure 4.11	The flow-chart of data analysis in TIRE.	52
Figure 4.12	Typical time dependencies of ψ and Δ extracted from dynamic TIRE scan at selected wavelength.	55
Figure 5.1	Electronic transitions in organic materials.	59
Figure 5.2	Operation principle of UV-vis Absorption Spectrophotometry.	59
Figure 5.3	Operation principle of SEM.	61
Figure 5.4	The view of IFM (Alicona) instrument.	62
Figure 5.5	(a) the principles of a classical spectrometer.	64
Figure 5.6	Haemocytometer slide and its cover.	65
Figure 5.7	Standard Haemocytometer chamber.	66
Figure 5.8	Example of using Haemocytometer for counting cells.	66
Figure 5.9	Schematic diagram of Fluorescence Microscope	68
Figure 5.10	Schematic diagram of Langmuir trough for isotherm measurements	69
Figure 5.11	Schematic diagram of surface pressure – area per molecule isotherm.	70
Figure 6.1	(a) typical Π -A diagram of chloroplast membranes on a water surface;	74

	(b) Recording Π during Langmuir-Schaefer deposition of chloroplast.	
Figure 6.2	Spectral shift caused by binding of Hsp70 chaperones.	75
Figure 6.3	Hsp70 (a) and Hsp90 (b) chaperones binding to receptors.	78
Figure 6.4	Dynamic TIRE measurements and evaluation of the association constants.	80
Figure 6.5	IFM image of microcapsules functionalized with antibodies to Aflatoxin B1	82
Figure 6.6	SEM image microcapsule with antibodies to Aflatoxin B1.	82
Figure 6.7	Uv-vis absorption spectra of 100 μ g/ml aqueous solution of AFT B1.	83
Figure 6.8	Spectra of AFT B1 solutions of 20mg/ml (a) and 50 mg/ml (b) Concentrations mixed with capsules and incubated for a different time.	84
Figure 6.9	The dependence of 362nm band intensity of AFT B1 on the incubation time.	85
Figure 7.1	(a) Series of TIRE spectra recorded after each deposition step. (b) Calibration curve for MC-LR.	91
Figure 7.2	Spectral shift without deposited protein A or G.	93
Figure 7.3	Typical dependencies of $\Psi(t)$ and $\Delta(t)$ Evaluation of the during MC-LR & MC10E7 binding.	94

Figures 7.4	the evaluation of the association constant K_A .	94
Figures 7.5	Binding kinetics yields the association constant K_A .	96
Figure 7.6	the negative test for blocking spaces between the antibody and protein A.	96
Figure 7.7	Spectral shift for negative control without antibody.	97
Figure 7.8	(a) FT-IR spectra of 1 MC-LR, antibody MC10E7, and MC10E7/ MC-LR .	98
Figure 7.9	UV-vis spectra of MC-LR solution.	99
Figure 7.10	Optimal condition 25C & sun light.	102
Figure 7.11	Calibration curve for microcystis aeruginosa cells.	103
Figure 7.12	Peak of commercial toxin in UV-vis at 238 nm.	104
Figure 7.13	Calibration curves for toxin (microcystin-LR) in OD.	104
Figure 7.14	Calibration curves for microcystin-LR by the UV-vis.	105
Figure 7.15	MC-LR release after <i>microcystis aeruginosa</i> grown in cultures with increase and decrease nutrient.	106
Figure 7.16	Cell growths with change in environmental conditions.	107
Figure 7.17	Effect of environmental conditions on MC-LR released by <i>M.aeruginosa</i> .	108
Figure 7.18	MC -LR extracted from culture which increased 5ml nutrient in it.	109
Figure 7.19	(a) <i>Microcystis aeruginosa</i> growth in optimal condition.	111
Figure 7.20	Effect of salinity on rate growth of <i>Microcystis aeruginosa</i> .	112
Figure 7.21	a series of dilutions was made from natural MC-LR.	114

Figure 7.22	kinetic reactions between natural MC-LR and antibody MC10E7.	115
Figure 7.23	Calibration curve obtained from TIRE measurements.	116
Figure 7.24	Correlation between the optical density (absorbance) and the concentration of MC-LR.	116
Figure 8.1	Formation of polyelectrolyte capsules.	119
Figure 8.2	Typical SEM image of hollow microcapsule.	120
Figure 8.3	SEM images of 4 μm microcapsules at different resolutions: scale (a) 200 μm , (b) 5 μm , and (c) 1 μm .	121-122
Figure 8.4	6 μm microcapsules coted with after (PAH/ PSS) shell and functionalized with antibodies.	123
Figure 8.5	UV-vis absorption spectra of MC-LR (25.9 $\mu\text{g}/\text{ml}$) during treatment with functionalized microparticles.	124
Figure 8.6	TIRE measurements taken on commercial MC-LR samples before and after treatment with functionalized capsules.	125
Figure 8.7	TIRE data, thickness increment of natural MC-LR and After treatment with microcapsules..	125
Figure 8.8	Effect of microparticle treatment on concentration of MC-LR: Abs. at 238nm.	126
Figure 8.9	standerd curves for MC-LR after treatment with capsules.	127

Figure 8.10	(a) Microcapsules with core MnCO_3 6 μm and eight layers (PAH/ PSS).	128
Figure 8.11	(a) Microcapsules with core MgCO_3 tested in FT-IR.	129
Fig. 8.12	(a) microcapsules stained with SYTO-9 Green Fluorescence stain, and (b) Propidium iodide red Fluorescence stain.	130
Figure 8.13	Processes of fill microcapsules with organic dye.	132
Figure 8.14	Absorption spectra of Microcystin-LR samples during electrolysis.	134
Figure 8.15	FT-IR spectrum of MC-LR solution after 24h electrolysis.	134

LIST OF TABLES

Table	Page
Table 4.1. Four-layer TIRE model.	53
Table 6.1 Four-layer TIRE model.	77
Table 6.2 Calculation of the absorbance reduction caused by adsorption of AFT on functionalized microparticles.	87
Table 7.1 TIRE data fitting for the immune reaction between microcystin-LR and MC10E7antibody.	92
Table 7.2 Concentration of microcystin-LR released by <i>microcystis aeruginosa</i> under different invironmental conditions.	110
Table 7.3 the increase in thickness for natural MC-LR.	115

CHAPTER 1

INTRODUCTION

1.1 Problem outline

The presence of Cyanobacteria (blue-green algae) in surface water is of increasing concern in Iraq as well as in other parts of the world. Cyanobacteria under the microscope come into view as small, unicellular organisms, some of which form colonies and thus reach sizes visible to the naked eye as tiny green particles. These organisms are usually finely dispersed throughout the water and may cause considerable turbidity if they reach high densities. Human activities (e.g., extensive agriculture, inadequate sewage treatment, runoff from roads) have led to excessive fertilization (eutrophication) of many water bodies. This has led to the excessive propagation of algae and Cyanobacteria into fresh water and thus has had a considerable impact upon recreational water quality. In hot climates, Cyanobacterial dominance is most pronounced during the summer months, which coincides with the period when the demand for recreational water is highest. Even though many species of freshwater algae reproduce quite intensively in eutrophic waters, they do not accumulate to form dense surface blooms of extremely high cell density, as do some cyanobacteria which naturally produce harmful compounds, called cyanotoxins, due to cell lysis during Cyanobacterial blooms. These toxins may cause mass mortality of wild and domestic animals, farmed fish and shellfish, as well as human illnesses such as nervous system injury or liver damage, and in extreme cases, death [1].

Microcystins are the most frequently occurring class of cyanotoxins, of which microcystin-LR is known to be one of the most toxic cyanotoxins in water resources [2]. When in contact with skin or consumed, microcystin-LR can lead to skin irritation or liver injury and may initiate liver tumour-promoting activity [3]. Due to these adverse health effects, the World Health Organization (WHO) has established a provisional guideline of 1 part per billion ppb (1 $\mu\text{g/L}$) for microcystin-LR in drinking water [4].

1.2 Detection of microcystin

The contamination of water resources with microcystin-LR produced by some algae species has prompted the development of detection methods for recognition and quantification of toxins. The most widespread analytical method for the determination of microcystin-LR in drinking or raw water is high-performance liquid chromatography (HPLC); it is precise but requires expensive equipment, complex procedures, and a long period of analysis.

The other methods are liquid chromatography combined with mass spectrometry (LC/MC), thin-layer chromatography (TLC), and capillary electrophoresis (CE) [5]. Although the sensitivity of chromatographic techniques is very high (typically in the range from 1pg/L to 1µg/L), these methods require time-consuming sample preparation procedures that usually need pre-concentration of samples prior to LC analysis. A major problem in quantitative analysis of MCs is the lack of standards [6]. Enzyme-linked immunosorbant assay (ELISA) method has been widely employed to monitor microcystin-LR at levels below 1µg/L [7]. Protein phosphatase inhibition assays (PPIA) [8] may yield false positives if the enzyme is inhibited by other compounds present in the sample. Recently, a commercial flow dipstick method (Microcystin ImmunoStrip) was introduced which is based on colloidal gold particles functionalized with specific antibodies [9]. Surface plasmon resonance (SPR) has become a widely used analytical technique which has led to the development of an SPR based immunosensor for the determination of MC-LR [10]. Furthermore, the Quartz crystal microbalance (QCM) method was developed in combination with Au nanoparticle amplified sandwiched immunoassay lowering the detection limit for (MC-LR) to 0.11pg/L [11]. Another detection method using color-changeable polydiacetylene vesicle achieved the 1pg/L detection level [12]. Some studies have focused on developing and improving antibodies against (MC-LR), e.g. monoclonal and polyclonal antibodies [13]. Recently developed method of total internal reflection ellipsometry (TIRE), which records simultaneously two parameters Δ and Ψ related to the amplitudes and phases of p- and s-components of polarised light, has been particularly suitable for detection of low molecular weight molecules [14], and it could be utilized for detection of MC-LR. Another interesting technology of polyelectrolyte microcapsules [15], functionalized with specific antibodies, could be used for detection of microcystin-LR as well as for purification of substances contaminated with microcystin-LR, also these technique was used for purification of substances contaminated with micotoxin.

1.3 Mycotoxins detection and purification of contaminated substances

Mycotoxins contaminate the diet of a large proportion of the world's population, especially in low income and developing countries. In 1985 the World Health Organization (WHO) estimated that approximately 25% of the world's grain was contaminated with mycotoxins.

Mycotoxins are toxic chemical compounds found in certain fungi that can grow on crops in the field, after harvest, or during storage. Since they are produced by fungi, mycotoxins are associated with mouldy crops. Nowadays there are hundreds of mycotoxins of different chemical structures and different modes of action, but only five of them are regularly found in staple foods and animal foodstuffs such as grains and seeds. These mycotoxins are aflatoxins, zearalenone, ochratoxins, fumonisins and deoxynivalenol/nivalenol.

Most mycotoxins are hydrophobic molecules of low molecular weight and thus are not soluble in water but in organic solvents such as methanol, chloroform, acetone, or acetonitril. All mycotoxins are dangerous to human and animal health in connection with high hepato- and nephro-toxicity, and have carcinogenic, genotoxic, cytotoxic, and mutagenic actions [16, 17].

Aflatoxin, a common and naturally widespread mycotoxin that is produced by *Aspergillus* fungi species, most notably *A. flavus* and *A. paraciticus*, contaminates a variety of staple food. The favorable host plants for aflatoxin are grain cultures and cereals (maize, rice, wheat, etc.), spices (chili and black pepper, coriander, ginger), high oil content nuts (almond, pistachio, walnut, coconut, Brazil nut) as well as coffee and cocoa beans, and fruit products [18-20]. It can colonize and contaminate grains before harvest or during storage. The toxin can also be found in milk and milk products of animals that are fed with contaminated food [21-23]. Within the aflatoxin group, the most dangerous toxin is aflatoxin B1 (LD50 = 6.5-16.5 mg/kg). The toxicity of AF-B1 is ten times that of potassium cyanide, 68 times that of arsenic and 416 times that of melanin [24].

In addition to a wide range of analytical methods for detection of mycotoxins [25-27], the method of TIRE was successfully adapted for detection of these low molecular weight analytes [28, 29]. In this work, however, the main focus was not on the detection

mycotoxins but on purification of substances contaminated with mycotoxins. The technology of microparticles functionalized with antibodies to aflatoxin B1 was further exploited in this work. The TIRE method along with UV-vis absorption spectroscopy was used here as an analytical tool for evaluation of aflatoxin B1 concentration in liquid samples before and after such treatment.

1.4 Protein-protein interaction

An additional task in this project was the further development of the TIRE method through its application to studying protein-protein interaction. Some of the types of biological interactions are well studied, namely immune reactions (i.e. binding of antigen to specific antibodies), enzyme reactions (decomposition of small molecules catalyzed by enzymes), hybridization of single DNA strands due to hydrogen bonding, etc. However, the interaction of proteins in general is not well-studied and not fully understood. Very often, we associate molecular binding which does not have a feasible explanation with so-called non-specific binding.

In this project, we attempted to study in more detail the interaction between chaperones and their specific receptors. Chaperone proteins play an important role in cells protecting proteins from high temperatures and other cellular stresses, stabilizing protein structure and preventing them from aggregation and degradation. It was recently suggested that molecular chaperones, such as heat shock proteins Hsp70 and Hsp81, can form complexes with freshly translated proteins and thus prevent their aggregation [30]. Furthermore, the recent finding of chaperone receptors in plants [31, 32] indicates more specific involvement of molecular chaperones in protein targeting. The study of the mechanisms of protein targeting may have a substantial impact in a number of applications, including the origin of neurological diseases. It was shown recently in our research group that the novel receptor OEP61, extracted from leaves is capable of specific binding of Hsp70 while not binding to Hsp81 [33]. In this work, the interaction of chaperones with different receptors (including OEP61) electrostatically immobilized on the surface was accessed with the TIRE measurements. Apart from confirming the binding properties of OEP61, this work showed clear separation of specific and non-specific binding, in terms of both the sensor response (i.e. thickness increment) and the affinity of binding.

1.5 Aims and objectives

The main aim of this research was to develop an effective technology for the detection of toxins released by algae, particularly microcystin, using optical biosensing techniques. Another important problem to be addressed is the purification of waters contaminated with algae was achieved.

The research project focuses on the development of optical bio-sensing methods for detection of microcystin in both purified form and naturally produced by algae. The optical methods of spectroscopic ellipsometry in total internal reflection configuration (TIRE) [34-35], UV-visible absorption, and luminescent spectroscopy were utilized for the detection of microcystin-LR. The immune sensing principles were exploited in this study in conjunction with the TIRE transducing technique. The antibodies specific to microcystin-LR were immobilized on solid surfaces (Au, Si, glass) using the technique of electrostatic deposition via intermediate layers of polyelectrolytes (PAH or PSS) and Protein A (or G) [36]. Polyelectrolyte microparticles [37] made of PAH/PSS consecutive layers and modified with antibodies specific to MC-LR were used for detection of MC-LR, as well as for the purification of water contaminated with MC-LR. To achieve the project aims, the following objectives were identified:

- To develop further the methods of polyelectrolyte microparticles and TIRE through a series of experiments on detection of aflatoxin B1 and purification of substances contaminated with aflatoxin, as well as in the study of interaction of chaperon proteins with their specific receptors.
- To adapt the TIRE method for detection of microcystin (MC-LR) involving the immobilization of MC10E7 antibodies specific to MC-LR on the surface of gold alongside a series of TIRE spectral measurements. The TIRE immune sensing part of the project will begin with the use of commercially available MC-LR and will be followed by the detection of MC-LR produced by algae (see the next task).
- To grow different algae species and to extract microcystin from the algae culture. To study the role of external factors, i.e. pH, temperature, light, nutrients, stimulating the production of microcystin.

- To prepare polyelectrolyte microcapsules from CaCO_3 or MgCO_3 core particles by consecutive coating with layers of PAH and PSS and functionalise them with antibodies specific to MC-LR.
- To study the structure and morphology of polyelectrolyte thin films and capsules modified with active bio-molecules (antibodies) using complementary physical methods of optical microscopy, IFM, SEM, AFM, TEM, FT-IR and Raman spectroscopy.
- To develop a methodology of purification of substances containing MC-LR (in both purified and natural forms) using functionalized microparticles (see the task above) in conjunction with optical methods of TIRE and UV-visible absorption and fluorescence spectroscopy.

CHAPTER 2

BACKGROUND OF ALGAE AND TOXINS PRODUCED BY ALGAE

2.1 Algae

Algae are an enormous group of various organisms from different phylogenetic groups, representing many taxonomic divisions generally, and algae can be referred to as plants; they are usually photosynthetic and aquatic organisms, though without true roots, stems, leaves, and vascular tissue and have simple reproductive structures. They are distributed worldwide in the sea, freshwater, and wastewater. Most are microscopic, but some are extremely large, e.g. some marine seaweeds can exceed 50 m in length. Micro-algae include a huge group of photosynthetic, heterotrophic organisms which have a potential for excellent cultivation as energy crops. They can be cultivated under difficult agro-climatic conditions and are able to produce a wide range of commercially interesting by products, such as fats, oils, sugars and functional bioactive compounds. In addition, some aquatic species release toxins in water. The algae have chlorophyll and can produce their own food through the process of photosynthesis [38]. Recently they have been classified in the kingdom of protista, which include a variety of unicellular and some simple multinuclear and multicellular eukaryotic organisms that have cells with a membrane-bound nucleus. Almost all the algae are eukaryotes and conduct photosynthesis within membrane-bound structures called chloroplasts, which contain DNA. The exact nature of the chloroplasts is different among the different lines of algae.

There are known many groups of algae:

(a) *Charophyta*, (green algae), or *Chlorophyta* and the *Streptophyta*. There are about 4,300 species of mostly marine organisms, both unicellular and multicellular. The latter include the sea lettuce, while the other group within the Viridiplantae are the mainly freshwater or terrestrial *Streptophyta* (or *Charophyta*), which contain several groups of green algae plus the stonewort's and land plants. (The names have been used differently, e.g. *Streptophyta* to mean the group which excludes the land plants, *Charophyta* for the

stonewort alone or the stonewort's plus the land plants.) *Streptophyte* algae are either unicellular or form multicellular filaments, branched or unbranched. The genus *Spirogyra* is a filamentous streptophyte alga familiar to many, as it is often used in teaching and is one of the organisms responsible for the algal "scum" which pond-owners so dislike. Generally Chlorophyta is a division of the kingdom of protista consisting of the photosynthetic organism normally known as green algae. This diverse species can be unicellular, multi-cellular, coenocytes (having more than one nucleus in a cell), or colonial. *Chlorophyta* are mainly aquatic or marine, a few types are terrestrial, occurring on moist soil, on the trunks of trees, on moist rocks and in snow banks. Various species are highly specialized [39].

(b) Diatoms (brown algae) are unicellular organisms of the kingdom Protista, characterized by a silica shell of often intricate and beautiful sculpturing. Most diatoms exist singly, although some join to form colonies. They are usually yellowish or brownish, and are found in fresh- and saltwater, in moist soil, and on the moist surface of plants. Fresh-water and marine diatoms appear in greatest abundance early in the year as part of the phenomenon known as the spring bloom, which occurs as a result of the availability of both light and (winter-regenerated) nutrients. They reproduce asexually by cell division. When aquatic diatoms die they drop to the bottom, and the shells, not being subject to decay, collect in the swamp and eventually form the material known as diatomaceous earth. Diatoms can occur in a more compact form as a soft, chalky, lightweight rock, called diatomite. Diatomite is used as an insulating material against both heat and sound, in making dynamite and other explosives, and for filters, abrasives, and similar products. Diatoms have deposited most of the earth's limestone, and much petroleum is of diatom origin. The surface ooze of a pond, channel, or loch will almost always yield some diatoms.

(c) Euglenophyta is a small phylum of the kingdom protista, consisting of mainly unicellular aquatic algae. Some euglenoids have chloroplasts with photosynthetic pigments; others are heterotrophic and can swallow or ingest their food. Propagation occurs by longitudinal cell division. They mainly live in freshwater environments. *Euglena* is the most featured genus, ordinary in ponds and pools, particularly when the water has been polluted by overflows from fields or lawns on which fertilizers have been used. There are about 1000 species of euglenoids.

(d) Rhodophyta (red algae), a phylum of the kingdom Protista consisting of the photosynthetic organisms usually known as red algae. Members of the division have a characteristic clear red or purplish colour imparted by accessory pigments called phycobilins. The red algae are multicellular and are characterized by a great deal of branching, but without differentiation into complex tissues. Most of the world's seaweeds belong to this group. Although red algae are found in all oceans, they are most common in warm-temperate and tropical climates, where they may occur at greater depths than any other photosynthetic organisms. Most of the coralline algae, which secrete calcium carbonate and play a major role in building reefs, belong here. Red algae are a traditional part of oriental cuisine. There are 4000 known marine species of red algae; a few species occur in freshwater [40].

(e) Cyanobacteria, or blue-green algae, are a phylum of prokaryotic aquatic bacteria that obtain their energy through photosynthesis. They are often referred to as blue-green algae, even though it is now known that they are not related to any of the other algal groups, which are all eukaryotes. Cyanobacteria may be single-celled or colonial. Depending upon the species and environmental conditions, colonies may form filaments, sheets or even hollow balls. Some filamentous colonies show the ability to differentiate into three different cell types. Despite their name, different species can be red, brown, or yellow; blooms (dense masses on the surface of a body of water) of a red species are said to have given the Red Sea its name. There are two main sorts of pigmentation. Most cyanobacteria contain chlorophyll *a*, together with various proteins called phycobilins, which give the cells a typical blue-green to grayish-brown colour. A few genera, however, lack phycobilins and have chlorophyll *b* as well as *a*, giving them a bright green colour.

(f) Dinoflagellata is a large group of flagellate protists. Some species are heterotrophic, but many are photosynthetic organisms containing chlorophyll. Various other pigments may mask the green of these chlorophylls. Other species are endosymbionts of marine animals and protozoa, and play an important part in the biology of coral reefs. Other dinoflagellates are colourless predators on other protozoa, and a few forms are parasitic. Reproduction for most dinoflagellates is asexual, through simple division of cells following mitosis. The dinoflagellates are important constituents of plankton, and as such are primary food sources in warmer oceans. Many forms are phosphorescent, being

largely responsible for the phosphorescence visible at night in tropical seas. There are approximately 2000 species of Dinoflagellates.

(g) *Chrysophyta* is a large group of eukaryote algae, commonly called golden algae, found mostly in freshwater. Originally they were taken to include all such forms, except the diatoms and multicellular brown algae, but they have since been divided into several different groups based on pigmentation and cell structure. In many chrysophytes the cell walls are composed of cellulose with large quantities of silica. Formerly classified as plants, they contain the photosynthetic pigments chlorophyll *a* and *c*. Under some circumstances they will reproduce sexually, but the usual form of reproduction is cell division.

(h) *Phaeophyta* is a phylum of the kingdom Protista consisting of those organisms commonly called brown algae. Many of the world's familiar seaweeds are members of phaeophyta. Like the chrysophytes brown algae derive their colour from the presence, in the cell chloroplasts, of several brownish carotenoid pigments, such as fucoxanthin. With only a few exceptions, brown algae are marine, growing in the colder oceans of the world, many in the tidal zone, where they are subjected to great stress from wave action. Others grow in deep water. There are approximately 1500 species of *Phaeophyta*.

The scientists believe that the evolution of plants has resulted in increasing levels of complexity, from the earliest algal mats, through bryophytes, lycopods and ferns, to the complex gymnosperms and angiosperms of today. The groups which appeared earlier continue to thrive, especially in the environments in which they evolved. Evidence suggests that an algal scum formed on the land 3,500 million years ago.

2.2 Cyanobacteria

Cyanobacteria are organisms traditionally included among the algae, but they have a prokaryotic cell structure. Cyanobacteria, also known as blue-green algae, blue-green bacteria or *Cyanophyta*, are very prehistoric organisms that are not really algae. They photosynthesize like algae, but they are actually bacteria. Scientists refer to them as “cyanobacteria” to acknowledge that they are bacteria. “Cyan” means “blue”, which refers to the fact that these organisms often appear blue-green in colour. Cyanobacteria are a phylum of bacteria that obtain their energy through photosynthesis. The name cyanobacteria come from the colour of the bacteria. Planktonic cyanobacteria are a natural component in most surface waters of the world. Cyanobacteria are mostly known for the critical

insights they have provided into the origins of life. The fossil record shows that cyanobacteria already existed 3.5 billion years ago. Cyanobacteria played a major role in the oxygenation of the air by converting carbon dioxide and water with using solar energy into glucose and releasing oxygen in photosynthesis process. Another important aspect is the existence of cyanobacterial strains dangerous to human and animal health. Some species of cyanobacteria produce toxins [41]. The blue-green algae split into two major groups, the planktonics and the mat-formers. The planktonic blue-greens are microscopic and cause the typical pea-soup green colour to water. The most common of the planktonic blue-green are *Anabaena*, *Aphanizomenon*, and *Microcystis* (commonly referred to as Annie, Fannie, and Mike!). In addition to causing water to turn green, they can rise to the surface of calm or static waters and form surface scum. This yellowish-green scum formation is typical of most planktonic blue-greens. The formation of surface scum tends to block the light to the other types of algae and aquatic plants that live deeper in the water column. By shading out their competitors, blue-greens can completely dominate a body of water Blue-green algae (one of eleven groups of algae) are microscopic plants that grow mainly in brackish ponds and lakes throughout the world [42]. Of the more than 1500 known species, some are useful as food, while others have been reported to cause gastroenteritis and hepatitis. Normally they appear green and sometimes may turn bluish when dying. Taste and odor problems commonly occur with large concentrations of blue-green algae and some species are capable of producing toxins.

Blue-green Algae Blooms. When conditions are optimal, including light, temperature, levels of nutrients (i.e., phosphorous and nitrogen, and the ratio of the two), and lack of water turbulence, blue-green algae can quickly multiply into a bloom. Blue-green algae blooms are likely to occur more often in warmer months, some blooms occur in water bodies, exposure to the blue-green algae and their toxins can pose risks to humans, pets, livestock and wildlife. Exposure to blue-green algae can cause rashes, skin and eye irritation, allergic reactions, gastrointestinal upset, and other effects. At high levels, exposure can result in serious illness or death. Risks to people may occur when recreating in water in which a blue-green when algae bloom is present, or from the use of drinking water that uses a surface water source in which a blue-green algae bloom is present. Exposure depending on the particular Cyanobacterium, and the amount to which one is exposed, blue-green algae have the potential to cause a variety of adverse health effects, including liver toxicity (e.g., *Microcystis aeruginosa*) and neurotoxicity

(e.g., *Anabaena circinalis*). Microcystin toxins may also promote tumour growth. Destruction of Cyanobacteria cells may release the toxins into surrounding waters, so care must be taken in dealing with blue-green algae blooms, and these threats are not just theoretical. Several dog deaths have been reported following exposure to blue-green algae in water bodies, while worldwide animal poisonings and adverse human health effects have been reported. The concentration of cyanobacterial cells in blooms was reported to be up to 250,000 cells/mL, which is approximately 300 mg/L cyanobacterial biomass [43].

Cyanobacterial cells have been shown to contain an average of 0.2 pg of toxin per cell [44], ranging from 4 to 605 µg toxin/g dry weight of biomass [45, 46] reported that total concentrations of cyanotoxins in highly contaminated waters is 130–300 µg/L. Cyanotoxins lead to serious health problems for humans such as irritation of the skin (dermatotoxins), cell damage (cytotoxins), liver damage (hepatotoxins), and damage to the nervous system (neurotoxins) [47]. The consequences of cyanobacterial blooms have been reported in the United States as well as other parts of the world. For example, exposure to cyanotoxins has been linked to increased liver cancer in China, the deaths of 76 dialysis patients in Brazil, and elevated kidney failure and liver injury in Australia [48, 49]. Recently, harmful cyanobacterial blooms have resulted in health alerts in New York, Florida, and Nebraska [50, 51]. In the Great Lakes, cyanobacterial blooms have emerged as a serious problem in the last decade [52].

2.3 Microcystin-LR

Microcystin-LR (MC-LR) is the most studied and the most toxic representative of the cyanotoxin family. It is a cyclic peptide, stable and resistant to chemical hydrolysis or oxidation near neutral pH. It remains potent even after boiling. In natural water and in the darkness it survives for months or even years, but at 40⁰C and pH 1 it may break down in ten weeks [53, 54-59]. Its formal name is cyclo[2,3-didehydro-N-methylalanyl-D-alanyl-L-leucyl-(3S)-3-methyl-D-β-aspartyl-L-arginyl-(2S,3S,4E,6E,8S,9S)-3-amino-9-methoxy-2,6,8-trimethyl-10-phenyl-4,6-decadienoyl-D-γ-glutamyl]. The molecular formula of MC-LR is C₄₉H₇₄N₁₀O₁₂.

The chemical structure of MC-LR shown in Figure 2.1 consists of two variable L-amino acids, three D-amino acids (alanine methyl-aspartic acid and glutamic acid) and two

unusual amino acids (Mdha) and (Adda), the latter being one important for the biological activity of the toxin [60, 61]. Concern regarding the effects cyanobacteria on human health has grown in recent years since human poisoning incidents attributed to toxic cyanobacteria have been reported worldwide. The use of water from reservoirs containing cyanobacterial blooms and insufficient water treatment are the main reasons of having microcystin in drinking water. Microcystins, released from *Microcystis*, *Anabaena*, *Oscillatoria*, and *Nostoc* are the most ubiquitous class of cyanotoxins [62]. A recent study found that 82% of 181 samples of Canadian and U.S. utility waters tested were positive for the presence of microcystins [63]. More than 60 structural variants of microcystins have been identified [64], of which microcystin-LR has shown to be the most commonly occurring and one of the most toxic congeners [62,16]. The chemical structure of microcystin-LR is shown in Figure 2.1. Microcystin- LR is a monocyclic heptapeptide containing five amino acids invariant in all microcystins, and two specific amino acids, Leucine and Arginine, designated “L” and “R”, respectively [17]. The size of microcystin-LR is approximately 3 nm in diameter, with a molecular weight of 995.2 [18]. Microcystin-LR is an amphiphatic molecule [18,19]. Hydrophilic functional groups include carboxyl groups on glutamic acid and methylaspartic acid and the amino group on arginine, while the ADDA residue is hydrophobic (see Figure 2.1). The net charge of microcystin-LR is negative (-1) at most pH values ($3 < \text{pH} < 12$), as the net result of the dissociation of two carboxyl groups and the single positive charge of the amino group [17]. Microcystin-LR is an extremely acute toxin. The lethal dose (LD50) by the intraperitoneal route ranges from 25 to 150 $\mu\text{g}/\text{kg}$ while the oral LD50 is 5000 $\mu\text{g}/\text{kg}$ in mice [24].

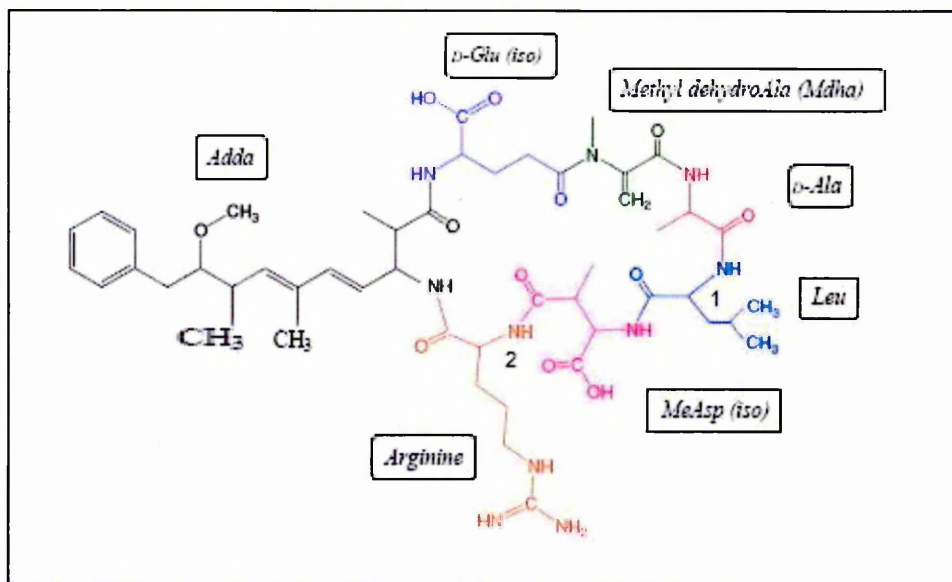


Figure 2.1 Chemical structure of microcystin-LR [15]

There are 80 known toxic variants of microcystins. The toxic effect of MCs on humans is mostly related to the liver damage (MCs promote the formation of hepatic tumors by chronic ingestion through food or drinking water). Microcystin-LR can also affect the kidney and the gastrointestinal tract. Less acute microcystin-LR toxicosis symptoms generally include headaches, blurred vision, abdominal pain, nausea, and vomiting. Their toxicity is related to the inhibition of the protein phosphatases, thus disrupting the cellular processes [65]. The World Health Organization (WHO) has adopted a provisional guideline value of 1 µg /L for microcystin-LR in drinking water (as it is the most toxic and frequent microcystin), and many countries have followed this guideline for drinking water and food as well. After a drought in February, 1996, all 126 patients in a haemodialysis unit in Caruaru, north-east Brazil, developed signs and symptoms of acute neurotoxicity and sub-acute hepatotoxicity following the use of water from a lake with a massive growth of cyanobacteria (blue-green algae). 60 patients died [66].

requirement of such sensors with increased accuracy, smaller size, high versatility and predominantly less financial outlay are therefore always in demand, from both commercial and scientific bodies. Microcystin-LR is cyclic peptides which has a comparatively large natural products, its molecular weight (MW) being 800-1,100, although it is still small compared to many other cell oligopeptides and polypeptides (proteins) (MW > 10,000) and diameter (3 nm). It contains seven amino acids, with the two terminal amino acids of the linear peptide being condensed (joined) to form a cyclic compound.

The site of action of microcystins is the hepatocyte, the commonest cell type in the liver. They act by disrupting the cytoskeleton, the adaptable protein framework that constantly shapes and reshapes the cell as it responds to the environment. The cells die, and this destroys the finer blood vessels of the liver, leading to massive hepatic bleeding. The molecular targets are a group of enzymes called protein phosphatases that play a role in regulating protein interactions and activities. Very well-defined types of protein phosphatase (Type 1 and Type 2A) are inhibited very specifically by very low concentrations of microcystins. Microcystins also activate the enzyme phosphorylase, which plays a very important role in the affairs of the hepatocyte [67, 68]. The combination of inhibition and activation is rapidly lethal to the cell. The specificity of some of these toxins makes them valuable research tools. In aquatic environments, these toxins usually remain contained within the cyanobacterial cells and are only released in substantial amounts on cell lysis. Along with their high chemical stability and their water solubility, this containment has important implications for their environmental persistence and exposure to humans in surface water bodies. Microcystin-LR cause damage to the liver which is rapid and irreversible. Dialysis or liver transplants may be the only effective treatments. The antibiotic rifampin shows protective effects in animal studies and could be used prophylactically if a genuine threat of an attack exists [69].

No plastics were used in the preparation of the aqueous microcystin-LR solutions as adsorption of the toxin on polypropylene surfaces is known to occur. The mechanisms of microcystin binding could be based on either simple hydrophobic, electrostatic or hydrogen bonding interactions or a combination of those. Microcystins are amphipathic molecules which are characterized by a cyclic heptapeptide structure containing a hydrophobic β -amino acid (Adda) with a terminal phenyl group and conjugated double bonds in its side chain. MC-LR contains a number of charged functional groups: i.e. the guanidine group of the arginine residue is positively charged, and the two carboxylic acid groups are negatively charged at neutral pH giving a negative net charge at the tested pH 7. This is consistent with the theory that aromatic nature and conjugated double bonds in the substrate are important for removal and that electrostatic interactions also play a role. Microcystin-LR (MC-LR) are the most frequently reported cyanotoxin class to cause outbreaks of mass poisoning and MC-LR are cyclic heptapeptides produced nonribosomally by microcystin synthetases. In *Microcystis aeruginosa*, genes of microcystin synthetase have been identified and sequenced; this is a 55-kb gene cluster consisting of 10 open reading frames bidirectionally transcribed

from a central promoter of 732-bp located in an intergenic region between *mcyA* and *mcyD*. Two transcriptional start sites (*tsp*) for the bidirectional promoter region have been identified and appear to be dependent on light conditions. However, other start sites have been detected for *mcyA* and *mcyD* and putative internal promoters have also been determined for the genes *mcyE*, *mcyF*, *mcyG*, *mcyH*, *mcyI* and *mcyJ* employing RACE [54].

2.4 Presence of microcystins in aquatic systems

Once released into surrounding waters, microcystins go through a variety of biochemical and geochemical processes in aqueous environments. Five pathways contribute to microcystin detoxification [32]: (1) dilution by uncontaminated water masses, (2) thermal decomposition aided by temperature and pH, (3) photolysis, (4) biological degradation, and (5) adsorption on particulate materials. Thermal decomposition does not significantly contribute to the decomposition of microcystins in natural aquatic environments [53] since microcystins are non-volatile and relatively stable compounds due to their cyclic structure [35]. Microcystins are known to be resistant to pH extremes and temperatures up to 300 C° [33]. Microbial degradation has been a possible way to eliminate microcystins, but a lag period of several days to weeks was required before biodegradation was initiated [55]. The photolysis of microcystins by sunlight alone was very slow, though the presence of dissolved natural organic matter, such as cyanobacterial pigments and humic substances, enhanced the degradation, due to the formation of highly oxidizing species [56]. At least 30 days are needed to achieve 90% degradation of microcystin-LR by indirect photolysis in lake water [57]. Recent studies document that microcystins are strongly adsorbed on soils, sediments and clay particles in natural environments [58]. Clay minerals, in particular, adsorb microcystins effectively, and are proposed as a removal technology for microcystins from drinking water and for mitigation of toxins in natural waters [59]. For example [40] examined the effect of soil properties on the adsorption of hepatotoxins such as microcystin-LR and nodularin. They observed significant positive correlations between toxin adsorption and clay and silt contents of the soils [60] found that clays in marine sediment, such as kaolinite and montmorillonite, played an important role in removing microcystin-LR from water. Suspended particulate matter (SPM) from lake sediment also significantly adsorbed both microcystin-LR and -LW, likely due to hydrophobic interactions [61].

2.5 Liver toxicity of microcystin-LR

In general microcystin-LR is liver toxin. Most of the consideration about the toxicity of microcystin-LR is based on studies of mice and rats that received intra-peritoneal (IP) injections of microcystin LR, i.e. injections directly into the abdominal cavity. In these studies the injection of microcystins caused death within a few hours. Early manifestations of liver damage contain an increase in serum of liver enzymes, a sign of liver cell death, and increased liver weight. Liver damage and cell death can be seen microscopically in as little as 20 minutes following the injection of a lethal dose of microcystin LR. Within an hour, the liver cells (hepatocytes) die, losing their connection to each other and disrupting the normal architecture of the liver [55]. For example, two mice given oral doses of 16.8 and 20 mg/kg were dead within 160 minutes [59].

Microcystin-LR inhibits a class of enzymes known as protein phosphatases. This enzyme removes phosphate from a protein, a common step in many biochemical pathways. This inhibition, with the subsequent buildup of phosphorylated proteins, is believed to be a mechanism by which microcystin-LR destroy livers. Hepatocytes from animals treated with microcystins appear to die by a process of programmed cell death or cell suicide called apoptosis [21]. Cells undergoing apoptosis fade away in a characteristic fashion, cannibalizing their own cellular organelles [22]. There is some evidence that microcystin LR increases other proteins in pathways leading to apoptosis but this has not been as extensively studied as the inhibition of phosphatases [23]. Microcystins LA, RR and YR inhibit the same phosphatases and induce histological changes in rodent livers similar to microcystin LR [24]. Therefore, the toxicity criteria computed for microcystin LR are also used for microcystins LA, RR and YR.

2.6 Health-based criteria for safe exposure to microcystin

The International Agency for Research on Cancer (IARC), a branch of the WHO, prior to the 2006 IARC evaluation, the WHO conducted an evaluation of the Tolerable Daily Intake (TDI) level, based on a non-cancer endpoint [4]. This value, 0.04 micrograms per kilogram body weight ($\mu\text{g}/\text{kg}/\text{d}$), is based on the results of liver toxicity studies in mice [2, 5]. TDI is the maximum daily dose of microcystins that is considered safe. Using

this TDI, WHO also developed a drinking water concentration limit of 1.5 µg/L for microcystin-LR. They assumed that a 60 kg (132 lbs.) person drinks two liters of water each day and that 80% of the two liters is from a contaminated source. Their calculation was as follows: $0.04 \text{ µg microcystin/kg body weight/day} \times 60 \text{ kg person} / (2 \text{ L water/day} \times 0.80) = 1.5 \text{ µg/L}$.

The most recent publication [4] cites the 1998 provisional guideline of 1 µg/L based on the above equation and rounded to one significant digit (rounding down to be health-protective). The WHO also categorized swimming risk levels as mild, moderate, high, or very high based on the water concentration of microcystins. These water concentrations are related to whether a swimmer, weighing 60 kg and ingesting 100 ml of water, would exceed the TDI.

2.7 Domestic animal poisonings

The greater part of reported cyanotoxin poisonings have occurred in domestic animals that drink freshwater containing cyanobacterial blooms [3]. Worldwide, thousands of livestock fatalities and numerous poisonings in dogs have been linked to the ingestion of cyanobacteria [4]. Animal poisonings have even occurred under environmental conditions considered unfavorable to cyanobacteria bloom such as in cold lakes with low nutrient levels [6].

In North America, domestic animal poisonings have been linked to blooms of *Microcystis sp.* in California, Colorado, Georgia, Michigan, Mississippi, Oklahoma, Wisconsin, and Saskatchewan, Canada. Most of the poisonings were fatal and were associated with visible scum of cyanobacteria. Symptoms of microcystin poisoning in domestic animals include diarrhoe, vomiting, weakness and recumbency [62].

Unfortunately, some animals appear to be attracted to cyanobacteria in water and dried crusts of algae on top of the water [61]. Livestock and dogs have been observed to drink infested water while clean water was plainly accessible, and to keenly consume crust and mats. Lopez-Rodas and Costas [62] found that mice showed a clear preference for *Microcystis aeruginosa* scum (1,000 and 15,000 cells/ml) over clean drinking water. These mice did not prefer non-cyanobacterial phytoplankton over clean drinking water and did not differentiate between toxic and non-toxic strains of the cyanobacteria. These observations and experiments indicate that at least some animals preferentially consume

cyanobacteria. Domestic animals should be prevented from drinking or entering untested bloom waters and from eating crust or mats on the shoreline.

2.8 Effects of microcystins on fish and wildlife

Microcystin-LR is toxic to fish at concentrations as low as a few micrograms per liter ($\mu\text{g/L}$) or perhaps even fractional $\mu\text{g/L}$. Bearing in mind that microcystin-LR has been measured in concentrations up to 25,000 $\mu\text{g/L}$ in waters with cyanobacterial blooms, it is not surprising that potential impacts on fish are receiving increased attention. Fish typically either ingest cyanobacteria directly or in prey that have fed on cyanobacteria. To a lesser range, they can absorb the toxins directly from the water [62].

As with mammals, microcystins are actively taken up by the liver in fish where they disrupt normal cellular activity by inhibiting protein phosphatases. Inhibition of these enzymes in fish can in the end result in widespread cellular death and loss of liver structure [62]. Protein phosphatases are particularly important during fish embryonic development because they regulate critical developmental processes. Due to the limited capacity of fish to detoxify microcystins, they easily succumb to the toxic effects of increased microcystin concentrations [62].

Field observations of impacts on fish coincide with periods when blooms are plentiful. However, aquatic ecosystems are complex and it can be very difficult to distinguish the exact cause of the impacts. For example, fish kills following a bloom could be caused by microcystin-LR being released from dying cells, but are more likely to be due to decreased oxygen and pH levels caused by the decaying bloom [51]. As a result, the toxic effects of microcystins in fish have been studied experimentally using several different fish species and exposure routes.

Like small mammals, most studies on the immediate (acute) lethality of microcystins in fish have utilized IP injections of extracted microcystins to determine the dose that is lethal to half the test population (LD50). Reported LD50 values of microcystins in fish range from 20 to 1500 μg microcystin LR/kg body weight [50]. The large range of values could reflect variations between fish species, or differences in toxin extraction, purification, or measurement methods. As a group, mature fish are less sensitive to acute microcystin toxicity than mammals. Data from these acute studies are useful for making general comparisons between species. However, IP injections of microcystins are not analogous to field exposures. Since the toxin is absorbed faster and metabolized

differently when administered into the abdominal cavity (as with the IP route) as compared to oral administration. For example, IP injection of 50 µg MC/kg in carp killed all test fish while an oral dose of 250 µg MC/kg in similar carp resulted in no lethality and minimal liver damage. No oral LD50 values were found for microcystins in fish. When developing loach were immersed in solutions of isolated MC-LR (over multiple days), the median lethal concentrations (LC50) were 164.3 µg/L in embryos and 593.3 µg/L in small hatched juveniles [63].

Several studies have observed severe liver damage in fish following oral administration of microcystins, usually in the form of freeze-dried cyanobacterial cells. The sublethal microcystin concentrations shown below are commonly found in food items of fish during blooms. For example, a diet containing greater than 130 to 2,500 µg MC/kg diet wet weight (ww) for two or more weeks may result in sublethal effects in carp (based on 5 kg fish consuming 2% body weight/day). Microcystin concentrations in cyanobacterial blooms commonly reach 20,000 µg MC/kg algae and have been reported as high as 129,000 µg MC/kg algae,(ww) converted from dry weight. Mussels, snails and zooplankton collected from areas with blooms have contained microcystin concentrations of up to 2,500, 2,900 and 13,700 µg MC/kg body weight (bw), respectively. These estimates indicate that fish exposed to typical microcystin producing blooms may be experiencing sub lethal toxic effects (i.e., liver damage). This is in agreement with Carbis et al., where the majority of common carp sampled from a lake with 22,000 – 40,000 µg MC-LR/kg bloom material (ww, converted from dry) exhibited widespread liver damage consistent with microcystin toxicity[64,65].

Since the early 1900s, bird deaths have been linked to cyanobacterial blooms in Canada and the United States. Species of cyanobacterial blooms that produce microcystins have synchronized with the deaths of ducks, gulls, songbirds, pheasants and hawks, as well as several other bird species. The severity of such bird kills have ranged from a few individuals to several thousand birds per incident. In California, high mortality in birds wintering at the Salton Sea has been linked to microcystins [66]. Levels of microcystins found in many of the dead birds were similar to those in mice exposed to lethal levels of this toxin. Microcystin poisoning has also been linked to the mortality and illness of great blue heron from Chesapeake Bay [67].

In other countries, microcystins have also been specifically implicated in bird poisonings. In Japan, approximately 20 spot-billed ducks died at a pond containing a bloom of *M. aeruginosa* [68]. Bloom material contained high levels of microcystins and

produced acute toxicity in a mouse bioassay that was consistent with the effects of the toxin. Waterfowl and other animals died at a reservoir containing an extensive *Microcystis sp.* bloom in South Africa [69]. Examined individuals showed liver damage consistent with acute and chronic microcystin toxicity. Furthermore, water from the reservoir was used to recreate the same effects in experimental animals.

2.9 Detection of microcystin-LR

The problem of microcystin-contaminated water bodies is increasing due to the eutrophication of lakes and reservoirs, and also possibly to climate change. This has led to the establishing by The World Health Organization (WHO) a guideline for microcystin-LR in drinking water as 1.0 µg/L. Development of reliable methods suitable for monitoring microcystin-LR in environmental samples has been the quest of researchers. Variety and complexity of widely encountered microcystins stimulate further development of the procedures for greater analytical precision. Several analytical techniques were utilized recently for detection of Microcystin-LR. The most widespread analytical method for the determination of microcystin-LR in drinking or raw water is based on the high-performance liquid chromatography (HPLC) which is more precise but requires expensive equipment, complex procedures, and a long time frame. The other methods of liquid chromatography/mass spectrometry (LC/MC) thin-layer chromatography (TLC), and capillary electrophoresis (CE) [70] require time-consuming sample preparation procedures that usually need pre-concentration of samples prior to LC analysis; and a typical detection range of chromatographic techniques from 1pg/L to 1µg/L. A major problem in quantitative analysis of MCs is the lack of standards [71]. Enzyme-linked immunosorbant assay [ELISA] method have been widely employed to monitor microcystin-LR at levels below 1µg/L [72]. Protein phosphatase inhibition assays (PPIA) [73] may yield false positives if the enzyme is inhibited by other compounds present in the sample. Recently, a commercial lateral flow dipstick (Microcystin ImmunoStrip) method was introduced which is based on colloidal gold particles [74]. Surface Plasmon resonance (SPR) spectroscopy has become a widely used analytical technique which has led to the development of SPR based immunosensor for the determination of MC-LR [75]. Quartz Crystal Microbalance (QCM) method was developed in combination with Au nanoparticle amplified sandwiched immunoassay lowering the detection limit for microcystin-LR

(MCLR) down to 0.11pg/L [76]. Another detection method using a color-changeable polydiacetylene vesicle achieved the 1pgL-1 detection level. [77].

The current project focuses on further development of optical bio-sensing methods for detection of microcystins of both purified and natural algae produced form. The main method in this study is spectroscopic ellipsometry in total internal configuration (TIRE) [78]. This method offers 10 times higher sensitivity than conventional SPR and has been extensively used recently in our research group for different bio-sensing applications, i.e. detection of low molecular weight toxins (herbicides, mycotoxins, alkyphenols), immune analysis of Alzheimers disease markers, the study of DNA hybridization [54], and in the most recent study of protein-chaperon interaction [11]. The method of TIRE is suitable for the evaluation of the thickness of the molecular layer after adsorption and binding of different molecules (from a single spectroscopic scan) as well as for the study of kinetics of molecular adsorption and evaluation of the association (affinity) constants (from dynamic spectral measurements). Several other methods such as, UV-vis absorption and fluorescence spectroscopy, IFM, AFM, FT-IR and SEM are used as complementary techniques in this work .

2.10 Current treatment technologies for microcystin-LR

A number of treatment technologies have been investigated to inactivate, degrade, and remove microcystin-LR from drinking water. These include conventional technologies (e.g., coagulation, sand filtration, chlorination, and activated carbon adsorption) as well as advanced technologies (e.g. ozonation, Fenton oxidation, and UV photolysis). The removal of microcystin-LR by different processes is discussed below.

Coagulation, flocculation, and filtration are frequently used in drinking water treatment. These technologies are effective in removing particulate cyanobacterial cells, but not effective for dissolved toxins like microcystin-LR [59]scientests [53] used three different coagulants, including ferric sulphate, alum, and polyaluminium chloride, to remove microcystin-LR, but no toxin removal was observed [51] reported that chemical treatment and mechanical agitation may cause damage to cyanobacterial cells, and result in an additional release of the toxin. The management of the sludge containing cyanobacterial cells and toxins may be a serious concern in this process [59].

Direct rapid filtration was not effective in removing cyanobacterial cells, while slow sand filters can remove 99% of the cells [53]. In addition, slow sand filtration possibly develops a biofilm on the top of the filter, due to its lower loading rate, resulting in biodegradation of microcystins [59, [51] found that more than 90% of microcystins were removed during slow sand filtration, primarily due to the biodegradation on or inside the filter bed. However, plugging of the filter and toxin release from the lysed cyanobacterial cells entrained in filter beds are significant problems [59]. As research continue to search for procedures for removing microcystin-LR from drinking water.

CHAPTER 3

THE CONCEPT OF BIOSENSORS

Biosensor is described in this chapter in terms of bio-sensing theory, principles, background and applications. Affinity sensors, especially immunosensors, are explained in detail, including the production of antibodies and immobilization techniques.

3.1 Biosensors: definitions and classification

Biosensor can be defined as a self-contained analytical device that responds selectively and reversibly to the concentration or activity of chemical species in a biological sample. No mention is made here of a biologically active material involved in the device; thus any sensor physically or chemically operated in a biological sample can be considered as a biosensor. The first biosensor was the combination of Clark's amperometric oxygen electrode, serving as a transducer, and the enzyme glucose oxidase as a sensing element for glucose monitoring. In 1962 Clark and Lyons [79], took advantage of the fact that an analyte like glucose, could be enzymatically oxidized and accompanied by consumption of the reactant O_2 or the appearance of a product, H_2O_2 , which could be electrochemically monitored. During the following decade a lot of effort was devoted to obtaining bioconjugates for enzyme immunoassays. Various methods for enzyme immobilization were also described, including adsorption, entrapment in a gel lattice, covalent binding through activated groups on the support, or the use of a cross-linking reagent [80-82]. In 1967 Updike and Hicks [83] gave the name enzyme electrode to a device comprising a polyacrylamide gel with entrapped glucose oxidase coating an oxygen electrode for the determination of glucose. Besides amperometry, potentiometric electrodes were also proposed by Guilbault and Montalvo in 1969 [84]. Since the early 1970 various combinations of biological materials associated with different types of transducers gave birth to the concept of a biosensor. As a matter of fact, as shown in Figure 3.1, a biosensor associates a bioactive sensing layer with any suitable transducer giving a usable output signal. Biomolecular sensing can be defined as the possibility of detecting analytes of biological interest, like metabolites, but also includes drugs and toxins, using an affinity receptor like antibodies

which can be a natural system or an artificial one mimicking a natural one, able to recognize a target molecule in a complex medium containing thousands of others molecules.

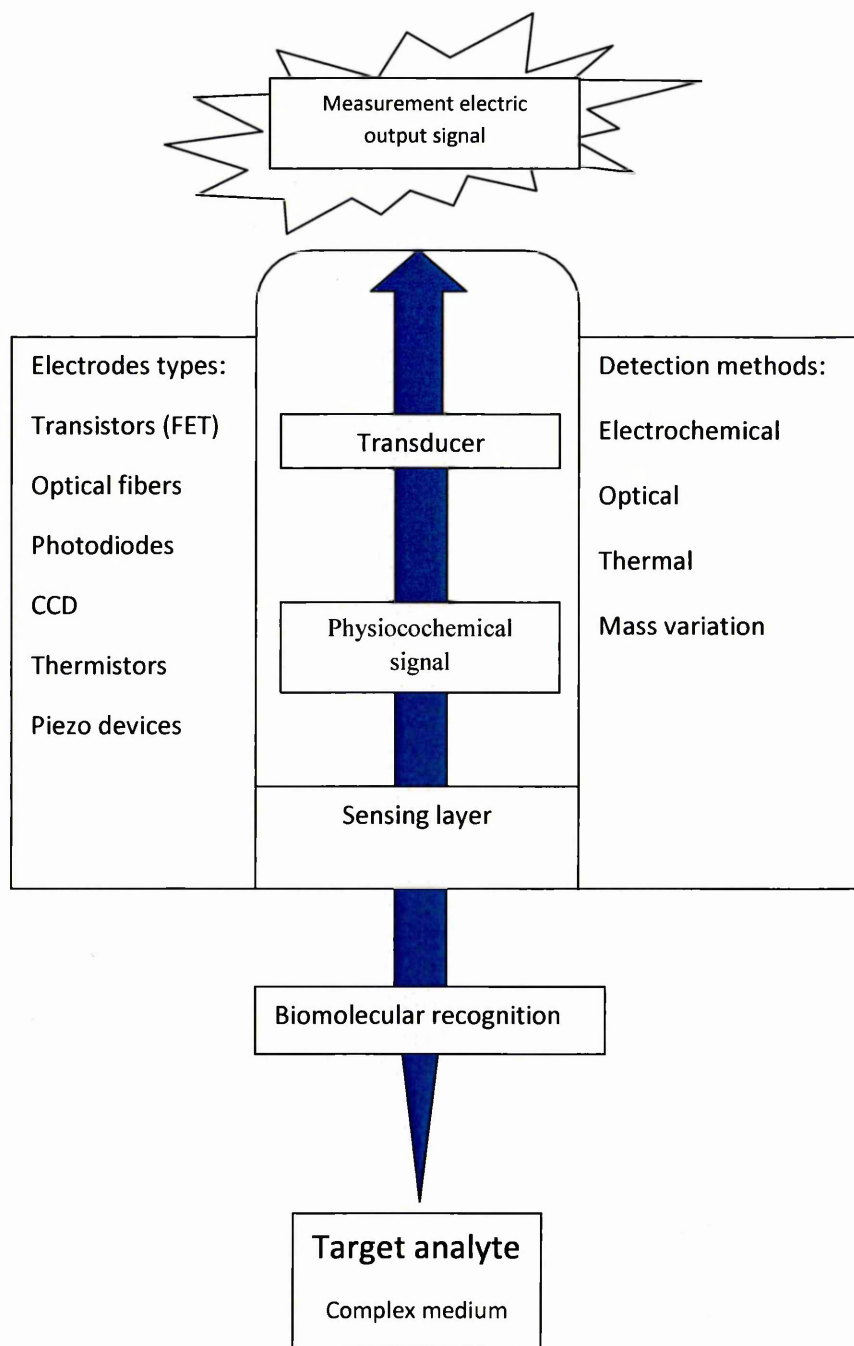


Figure 3.1 Configuration of a biosensor.

Generally, this device is electrical equipment with a transduction mode that can be electrochemical, thermal, optical, or based on mass variation. The selective molecular recognition of the target molecule can theoretically be achieved with different types of affinity systems, for example: enzyme for substrate, antibody for antigen, lectin - sugar interaction. Recently, arrays of different detector molecules have been applied in so called electronic nose devices, where the pattern of response from the detectors is used to fingerprint a substance.

3.1.1 Importance of the biological sensing system

Operating Conditions

It must be kept in mind that most of biological systems must be used under strictly defined conditions. For instance, most enzymes have an optimal pH range in which their activity is maximal; this pH zone must be compatible with the characteristics of the transducer. Except for rare enzymes capable of undergoing, for a short period, the temperatures higher than 100 °C, most biocatalysts must be used in a quite narrow range of temperatures (15-40) °C.

Immobilization of the biological system

The simplest way to retain bioactive molecules on the tip of a transducer is to trap them behind a perm-selective membrane (an ion-exchange material that allows ions of one electrical sign to enter and pass through). The availability of preactivated membranes suitable for the immediate preparation of any bioactive membrane thus appears as a real improvement.

A biosensor should respond selectively, continuously, rapidly, specifically, and ideally without an added reagent, and then different criteria must also be considered.

- Effect of the environment: the biosensing element must be either intimately connected to or integrated within a physicochemical transducer. The incompatibility of the biosensing reaction (pH for urease in the urea detector) and of detector itself (optical pNH₃ sensor for Penicillin uses Penicillinase to catalyse the transformation of Penicillin into Penicilloic acid, and this acid is detectable with a pH optical sensor). Micro-columns can sometimes be replaced by nylon coils, especially in luminescent reaction,

with the luminescence enzyme system bound onto the internal wall of the tube, allowing the reaction medium containing the sample to flow through.

- **Rapidity (Rapid response):** for enzyme electrodes a short response time may be between a few seconds and 30 sec, for instance. For immunosensors, 15 min is acceptable and considered to be short as compared to alternative techniques that are far more time consuming. For microbial sensors 20-30 min is a very short time, if we understand that biological oxygen demand (BOD) measurements, for instance, may last 5 days using conventional microbiological methods.
- **Reusability:** the cost and efficiency, when taking into account the preparation of the bioactive part, from a device in which reagents must be added for each measurement.

3.1.2 Biosensors world market

The need for sensitive, easy to use, and low cost sensor devices is a requirement for monitoring diseases in the early stages, for environmental control, for security, bio-defence and home diagnostic continues the growth trend up to increase in demands. Points of care diagnostics continue to be the largest market for biosensors. It has been estimated that global revenue from the biosensors market will continue to exhibit strong growth and will exceed USD 14 billion in the next seven years [85]. Other reports say that the USA and Europe dominate the global market for medical biosensors. While the Asian Pacific reached USD 794 million in 2012.

3.1.3 Labeled and label-free detection

Nowadays, the development of biosensors faces the challenges of detection of very low concentration (in fg to pg / ml range) of traditional analytes such as antibodies, peptides, DNA oligomers, and low molecular weight (300 - 100 Da) analytes such as toxins. Due to the difficulties of detecting biological analytes directly through their intrinsic properties such as size, mass, electrical impedance, or dielectric permittivity, labels that attach to one or more molecules have been used [85- 87]. A label, which is typically designed to be easily detected by its color or fluorescence acts as a surrogate to indicate the presence of the analyte. For example, fluorescent dyes conjugated with DNA or proteins can be used as a label when the fluorescence is excited with a laser [85]. The use of nanoparticles [88], enzymes [84], and radioactive labels [87, 89] are among the popular techniques to highlight biological interaction. In practical terms,

label- based assay possess several potential problems. There is a need to reduce the cost of raw materials (assay-related cost) and the complexity of assay while at the same time providing more quantitative information.

Label-free detection generally involves a transducer capable of measuring directly some physical properties of biological objects, for example DNA, peptides, proteins, cells, etc. Physical properties, such as mass, volume, viscoelasticity, dielectric permittivity, conductivity, etc., can be utilized to indicate the presence of these molecules. Label-free detection removes experimental uncertainty induced by the effect of the label or molecular conformation, blocking active sites, steric hindrance, or inability to find an appropriate label that functions equivalently for all molecules in the experiment. Label-free detection is able to reduce the time and cost required for the assay development while removing experimental artifacts from quenching and background fluorescence.

3.2 Immunosensores

An immunosensor is a device for the detection of an immune reaction, using antibodies as the bio-receptors. The use of antibodies as a recognition element is justified by their higher affinity, versatility and commercial availability [90].

Immunoassays are based on the interaction between the antigen (Ag) and its specific antibody (Ab) to form an antigen-antibody complex.



Equilibrium is reached, and equilibrium constant for the reaction is defined as:

$$K_A = [\text{AbAg}] / [\text{Ab}] [\text{Ag}] \quad (3.2)$$

This indicates that for a fixed concentration of antibody the ratio of bound to free antigen at equilibrium is quantitatively related to the total amount of antigen present. The reaction forms the basis of all immunoassays. When a fixed amount of labeled antigen is introduced into the assay the concentration of the unknown antigen can then be determined.

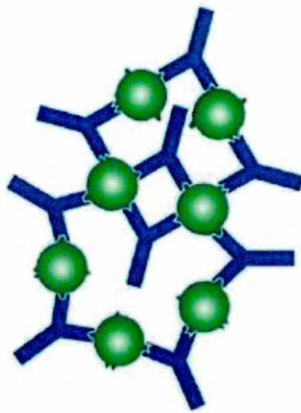
An antibody is typically an immunoglobulin, glycoprotein with a molecular weight of ~150,000 Daltons which is capable of specific binding with its antigen. The process of antibody - antigen binding is based on non-covalent interaction such as Van der Waals forces, Coulombic interaction, hydrophobic interaction, and hydrogen bonding [91].

This combination of interactions can make the antigen-antibody binding very specific. For instance, if two very similar antigens, A and B, are present where A has an additional hydrogen bond which B does not have, the strength of the interaction of A to the antigen compared to B can be 1,000 times greater. The affinity of monoclonal antibodies for their antigens is typically in the range of 10^6 - 10^8 mol /L.

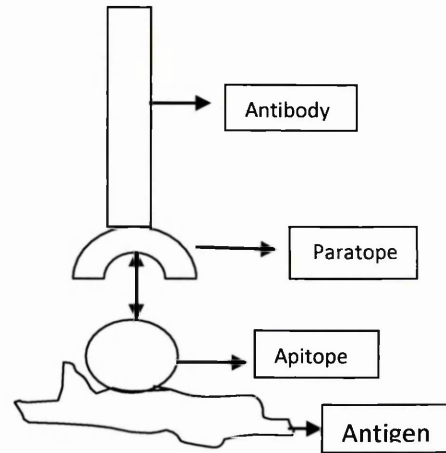
3.2.1 Avidity and affinity

Avidity and affinity are two parameters describing the strength of interaction between receptors and analytes. Affinity is the strength of the binding site of the antibody (Fab fragment or paratope) and the epitope of the antigen (antigen binding site). In other words affinity measures the strength of interaction between an epitope and an antibody's antigen binding site. The time taken for this to occur depends on the rate of diffusion, and is similar for every antibody. However high-affinity antibodies will bind a greater amount of antigen in a shorter period of time than low-affinity antibodies. K_A can therefore vary widely for antibodies from below 10^5 mol⁻¹ to above 10^{12} mol⁻¹, and can be affected by factors including pH, temperature and buffer composition. High-affinity antibodies will bind to antigen in a shorter period of time.

The affinity of monoclonal antibodies can be measured accurately because they are homogeneous and selective for a single epitope. Polyclonal antibodies are heterogeneous and will contain a mixture of antibodies of different affinities recognizing several epitopes, therefore only an average affinity can be determined. Avidity is a measure of the stability of a complex formed as a result of antigen-antibody binding (Fig. 3.2).



Avidity



Affinity

Figure 3.2. Illustrations for affinity, which is the strength of binding between the antibody and the antigen, and avidity describing multivalent interaction.

A measure of avidity includes the sum of the affinities for the multivalent interaction. In addition it measures the general strength of binding, which includes the structural arrangement of both molecules. Low affinity antibodies will bind weakly with the antigen and will dissociate easily, but high affinity ones will bind the antigen tightly and can remain bonded for longer.

3.2.2 Antibody - antigen interaction

Antibody-antigen reactions are widely used in medical diagnostics, environment analysis, forensic analysis, the food industry, etc. The use of antibody-antigen interaction in a biosensor approach seems to be suitable because of the following characteristics of antibodies [92, 93]:

- High specificity of antibody-antigen binding. A response to a specific antigen is specific for that antigen or a few closely related ones;
- The binding site of the antibody is derived from a huge number of potential combinations of 22 amino acid sequences which are able to bind a wide range of bio-molecules, cells, bacteria, and viruses;
- Demonstrating memory. The antibody "like remembers" if it has seen an antigen before and it reacts with it quicker and made stronger binding (K_A is larger);

- The antibody-antigen binding is non-covalent which allows for the recovery of the sensor by breaking the antibody-antigen complex;

Generally there are five classes of antibodies which excrete in serum, namely IgA, IgG, IgD, IgE, and IgM.

- **Immunoglobulin alpha (IgA)** can be found in mucosal areas of the body including the digestive, respiratory, and reproductive tracts. IgA is also present in saliva, tears, and breast milk,
- **Immunoglobulin delta (IgD)** appears in very small amounts in the blood, but is mostly found as receptors on B-cells.
- **Immunoglobulin epsilon (IgE)** is found in attached to mast cells and basophils, although eosinophils, monocytes, macrophages, and blood platelets also have IgE receptors.
- **Immunoglobulin gamma (IgG)** makes up about 75% of the antibodies found in the blood. It is the only antibody that can pass through the placenta from mother to fetus.
- **Immunoglobulin mu (IgM)** assist complement proteins to attack invaders by providing a bridge to which the proteins can attach themselves.

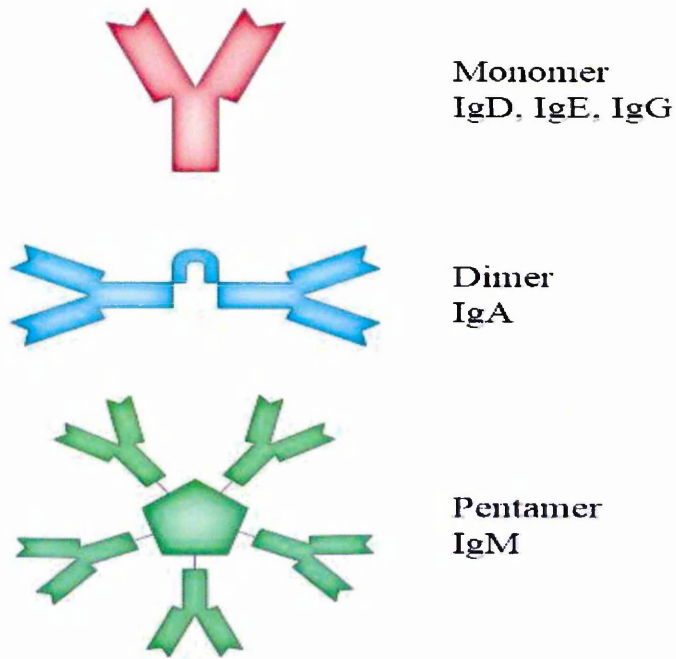


Figure 3.3. Diagram of the basic unit of immunoglobulin (antibody).

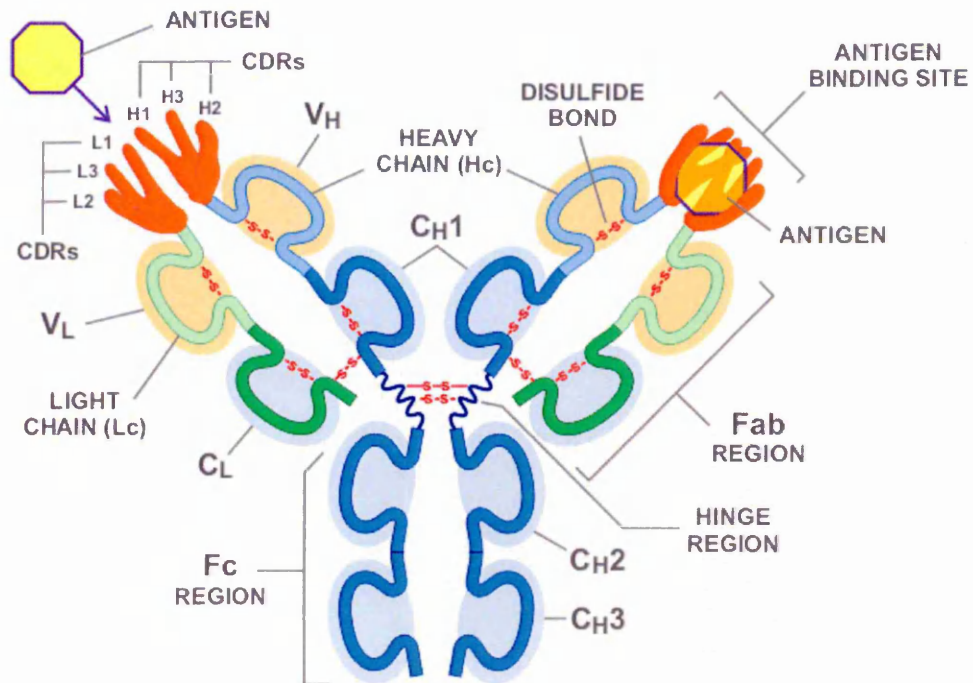


Figure 3.4 The antibody structure.

The main idea of detection of immune reactions is the use of antibodies as bio-receptors, which are capable of specific binding with their specific antigen. The process of antibody-antigen binding is based on non-covalent interactions [94-96], such as Van der

Waals forces, Coulombic interactions, hydrophobic interactions, and hydrogen bonding [97]. The combination of such interactions between few molecules can make the antigen-antibody binding very specific.

The antigen binding site of an antibody is situated at the top of each of the two outspread arms as shown in Fig. 3.4. Each site is distinguished by 6 loops called Complementary Determining Regions (CDR). Three are found on the heavy chain (H1, H2, and H3) and 3 on the light chain (L1, L2, and L3). These protein loops mirror, or complement, the shape of specific antigens. As a result, they determine to which specific antigens the antibody can and will bind.

Antibodies are typically generated in response to the challenge of an immunogen in the host animal, arising from separate cell lines which recognise various regions on the immunogen, termed polyclonal antibodies, while other antibodies are known as monoclonal antibodies [98, 99]. Both of these antibodies have certain advantages and limitations for use in immune-sensing. Studies have shown that immunoglobulin G (IgG), the most common human immunoglobulin, consists of two long "heavy" chains (A and B) and two short "light" chains (C and D). These are in the Y shape bonded together with disulfide bonds. There are several major areas of globular tertiary structure on the chains. The globular structure on the ends of the chains are variable and account for some of the differences in specificity for different antigens. There are also two carbohydrate chains in between the A and B chains. The antibody structure is slightly different, but still maintains the Y shape as shown in the Figure 3.4.

In order to be used in bio-sensing, antibodies must be immobilised on the surface of sensor (in our case, on the surface of gold). There are several immobilization techniques routinely used in different bio-sensing applications [56], they include covalent binding onto the intermediate layer of glutaraldehyde, encapsulation of proteins alginate gel or lipid Langmuir-Blodgett films, which provide a natural environment for proteins. Another immobilization approach which was widely used in our research group is based on electrostatic binding via the layers of polyelectrolytes [100]. This method proves strong binding of proteins (antibodies in our case) by electrostatic interaction as well as through the structural stability of proteins in polyelectrolyte membranes. Polyelectrolytes proved to be a natural environment for proteins and allow biomolecules to keep their functions for a considerably long time (up to several months) [98]. Polyelectrolytes are electrically charged polymers of either cationic or anionic

properties. Typical polyelectrolytes used are polycations - polyallylamine hydrochloride (PAH) and polyanion - polysterylsulfonate sodium salt (PSS). The chemical formulae of PAH and PSS are shown in Figure 3.5 (a, b). The above polyelectrolytes are water soluble: PAH dissociates on positively charged polymer due to NH_3^+ groups and counter ions Cl^- , while a PSS chain containing SO_3^- groups it has negatively charged polymer chain with Na^+ counter ions. A multilayered film can be built by alternative deposition of PAH and PSS layers as shown in Figure 3.5 (c). Proteins (IgG including) being either positively or negatively charged (depending on pH) can be adsorbed via the layer of oppositely charged polyelectrolytes [101] as shown in Fig. 3.5.

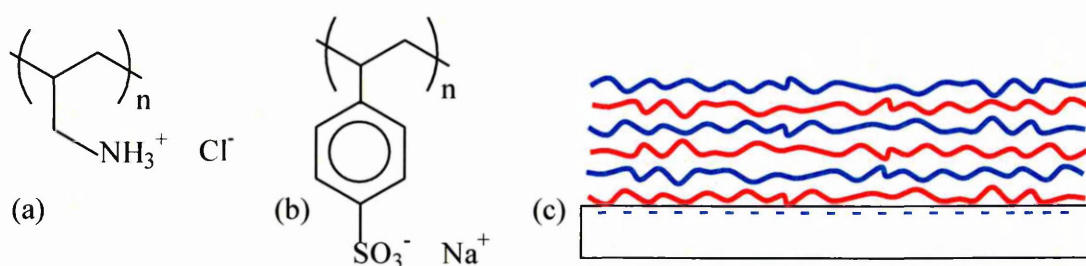


Figure 3.5. Chemical structures of (a) PAH and (b) PSS; (c) Multilayered film of alternated layers of PAH and PSS deposited on negatively charged surface.

3.2.3 Antibody immobilization

An antibody has four possible orientations on the solid surface as shown in Figure 3.6. Antibodies adsorbed electrostatically on the solid surface do not have preferential orientation and could end with Fc fragments directed upwards, downwards, or sideways, and therefore may not be available for binding antigens[102]. The desired “Fc upwards” orientation can be achieved using an interaction of the binding site in the second domain with protein A or protein G adsorbed electrostatically on the surface. The immunosensor response can be increased by up to 3 times as a result [103].

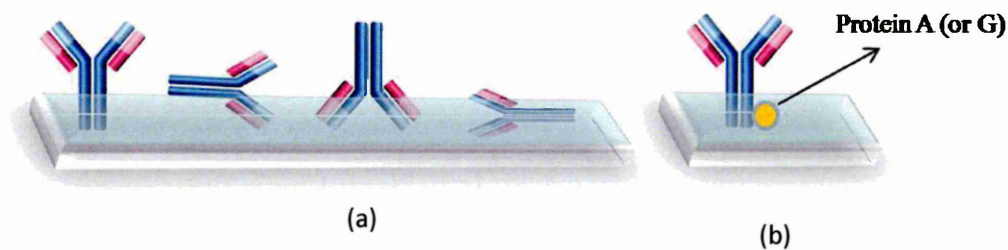


Figure 3.6. (a) Various orientations of antibodies on surface, (b) improvement of antibody orientation using proteins Protein A (or G).

The orientation of an antibody towards an antigen can be optimized by its binding to protein A or protein G at the Fc fragment of the antibody. The association of protein A (or G) and the antibody has three significant characteristics [104]:

- Binding sites of protein A or G and antibodies are located on the Fc fragment of the antibody; the association capacity of an antibody with an antigen cannot be changed;
- The affinity of protein A or G to antibody is so high; however, the association of protein A or G with an antibody will be lost in acidic solution;
- Protein A or G will resume its character readily.

3.3 Antibody production and purification

The production of antibodies begins with the preparation of antigen samples and their safe injection into laboratory or farm animals so as to increase the levels of antigen-specific antibodies in the serum, which can then be recovered from the animal. Polyclonal antibodies are recovered directly from serum. Monoclonal antibodies are produced by fusing antibody-secreting spleen cells from immunized mice with immortal myeloma cells to create monoclonal hybridoma cell lines that express the specific antibody in cell culture supernatant.

Antibody purification include isolation of the antibody from the serum (polyclonal antibody), ascites fluid or culture supernatant of a hybridoma cell line (monoclonal antibody). Purification methods range from the very basic to the highly specific:

- **Basic** : sedimentation of a subset of total serum proteins that contain immunoglobulins

- **Generic** : affinity purification of antibody classes (e.g., IgG) without regard to antigen specificity
- **Specific**: affinity purification of only those antibodies in a sample that bind to a specific antigen molecule.

Which level of purification is essential for obtaining usable antibodies depends on the intended application(s) for the antibody.

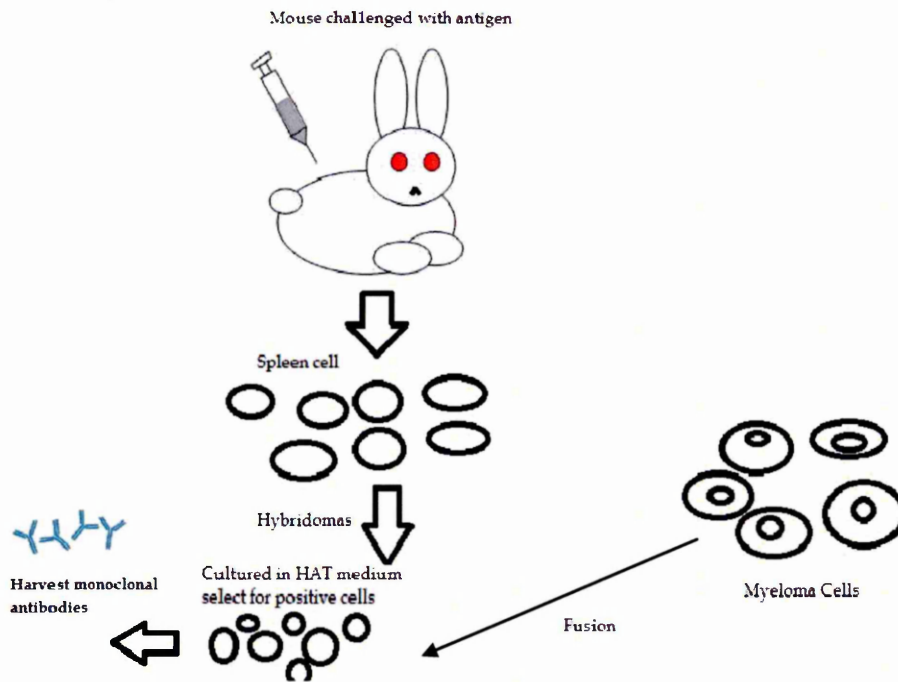


Figure 3.7. Production of antibodies.

3.4 Optical biosensors and detection of immune reaction

Optical biosensors are a large class of sensor devices which exploit some of the optical principles for the conversion of chemical (or bio-) reactions; they include light absorption, reflection, interference, diffraction, polarization, etc. Label-free optical biosensors involve detection of analytes in terms of measurements of changes in light intensity, peak wavelength, angle of light coupling or phase shift. In the case of field applications, biosensors based on the intensity changes may be preferred over other methodologies due to the inherent simplicity in instrumentation and hence overall cost of the sensing system. Most of the label-free optical bio sensing schemes that rely on light intensity measurements at a particular wavelength or over a broad spectral range are based on the detection of refractive index changes.

3.4.1 ELISA method

Enzyme-linked immunosorbent assay [105], is one of immunoassay technique using antibodies to apprehend an antigen and an enzyme, labelled antibody, to assessment the amount of antigen. The extension signal constructs upon the traditional horseradish peroxidase (HRP) enzymatic colorimetric detection to allow for an additional log of sensitivity. In ELISA, a dish with 96 wells (well-plate) is used, and wells are coated with antibodies. These antibodies are called “capture antibodies”, the role of which is to capture the target antigen molecules in the sample. Coating is carried out by adsorption on the surface of bottom area. The well-plate is made of polystyrene which is modified for very efficient adsorption. Because the concentration of antibodies is related to the efficiency of capturing antigen for brilliant sensitivity, antibody preparation is used as an IgG fraction, or non-specific antibody fraction obtained by an affinity chromatography rather than a crude gamma-globulin fraction prepared by ammonium sulfate fractionation. This metode takes a long time, about 2 hours or more, so the series of steps must occur as shown in Figure 3.8.

3.4.2 SPR (BIACORE)

There are growing concerns about applying optical biosensor knowledge, such as Surface Plasmon Resonance (SPR) based on Biacore tools, in drug discovery. SPR - based Biacore is one of the broadly used, real time checking systems and was shown to be a convenient system for wide a range of molecular sizes from small ligands to full cells. A biacore system can be effective in biomolecular interaction, selection processes, epitope mapping, kinetic analyses, screening processes and other applications. Biacore is an automated optical based detection system relying on SPR created by a swedish company, founded in 1984, which detects refractive index changes in close proximity to a metal surface. Upon immobilization of ligands on the sensors surface, the interfacial refractive index is altered, which will be detected and quantified by optical systems as the changes in the angle of reflectance [106]. Biacore needs a flow system and it is expensive.

These labeling methods are not favourable in some cases, because labeling materials may occupy the important binding sites or cause steric hindrance, resulting in false information about interactions. On the other hand, in some cases an additional step is required prior to the analysis of the interaction due to the difficulty of the labeling procedure. To overcome these limitations several techniques for monitoring

biomolecular interactions were developed in the past, which including saturation transfer difference nuclear magnetic resonance analysis which can provide the original information [107].

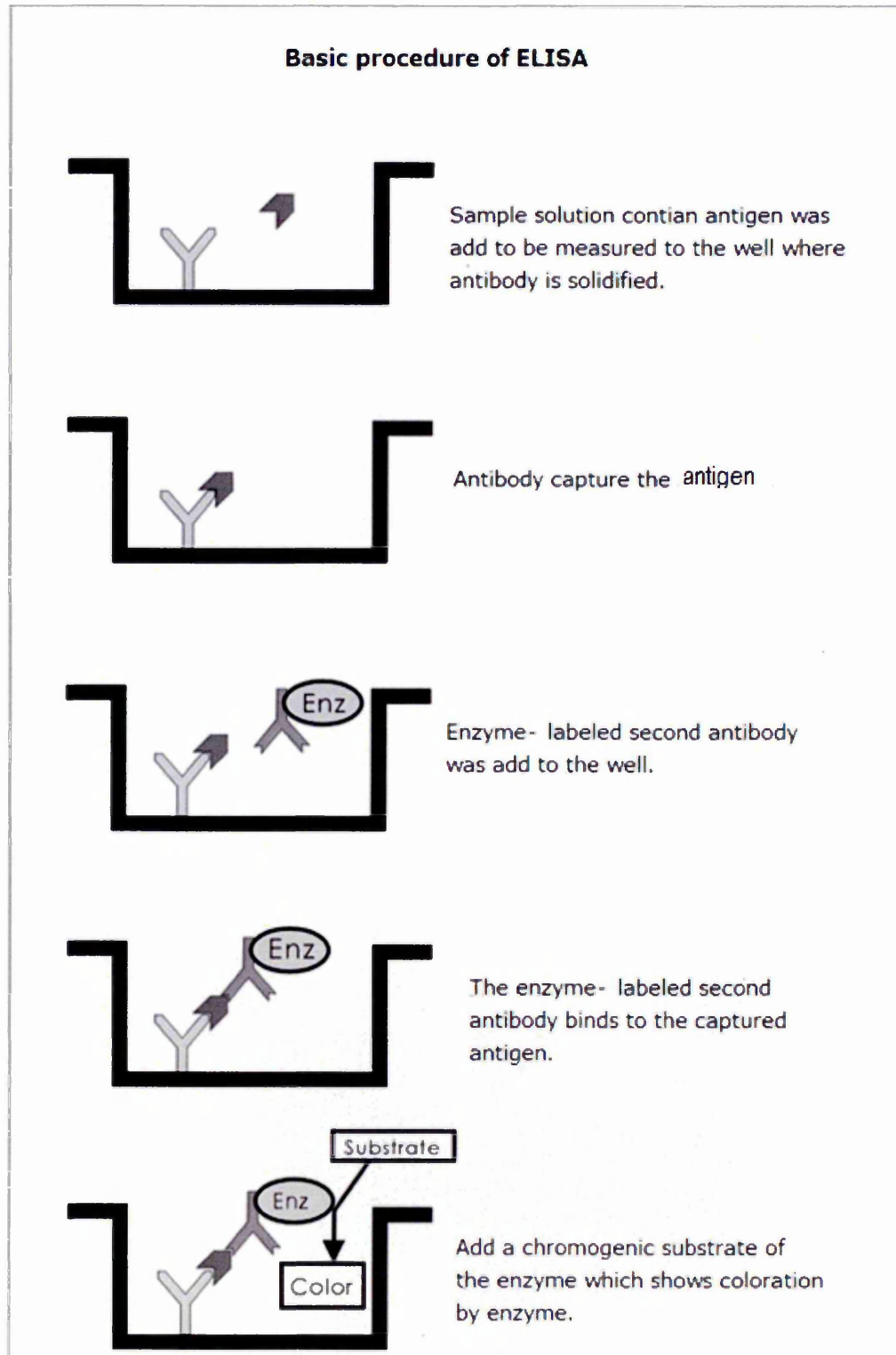


Figure 3.8 ELISA Method.

3.5 Summary

A biosensor is an analytical apparatus which converts a biological response into an electrical signal; there are many types of biosensors. In 1961 the first report on the immobilization of protein adsorption of invertase (an enzyme produced by yeast that catalyzes the hydrolysis of sucrose, forming glucose) on activated charcoal (Nelson and Griffin, 1922) involving the first glass pH electrode was undertaken. From this time many developments have occurred up to the present. Biosensor can be classified as:

- Receptor based biocatalytic-enzymes, cells, tissues biocomplexing-Ag/Ab-immunosensor Receptor/antagonists.
- Based on mode/transducers; electrochemical, optical, piezoelectric.
- Nanobiosensors, nanoparticles, nanotubes(CNTs), nanowires, and porous silicon.

The method of TIRE was used as the main experimental method in the study of microcystin-LR, and both of aflatoxin B₁, protein chaperone. UV-vis spectroscopy was selected as a secondary method to provide further analysis.

CHAPTER 4

OPTICAL IMMUNOSENSING METHODS: TOTAL INTERNAL REFLECTION ELLIPSOMETRY (TIRE)

This chapter outlines the basic theory of evanescent waves which is the chief mechanism for a number of optical sensors. The methods of Ellipsometry and Surface Plasmon Resonance (SPR) are described and the similarities between them highlighted. The background of the TIRE method (a combination of ellipsometry and SPR) is given.

4.1 Theoretical background of evanescent wave techniques

The optical procedure based on the evanescent field phenomenon combined with thin film technology gives some novel chances in the area of biosensing. Such methods are label-free and appropriate for express, in-situ, and in-field analysis. Typical parameters detected by this method are the intensity and/or phase shift of the reflected light.

Evanescent waves are an overall property of the wave-equation, and can in general occur in any context to which a wave-equation applies. They are formed at the boundary between two media with different wave motion properties, and are most intense within one third of a wavelength from the surface of formation. A typical example of evanescent wave is the electromagnetic wave propagating along the interface between two transparent media at the situations of total internal reflection [43]. As shown in Figure 4.1, the incident light entering the medium with lower refractive index ($n_1 > n_2$) experiences total internal reflection at the critical angle of θ_c which can be defined as

$$\sin\theta_c = \frac{n_2}{n_1} \quad (4.1)$$

As shown in Figure 4.1 (c) the evanescent field propagates along the interface. The amplitude of evanescent field decays exponentially in the direction z perpendicular to the interface

$$E = E_0 \exp(-\gamma z) \quad (4.2)$$

The existence of metal on (or near) the interface may play an important role in the propagation of the evanescent wave due to the interaction of the evanescent wave with free electrons in metal as shown in Figure 4.2.

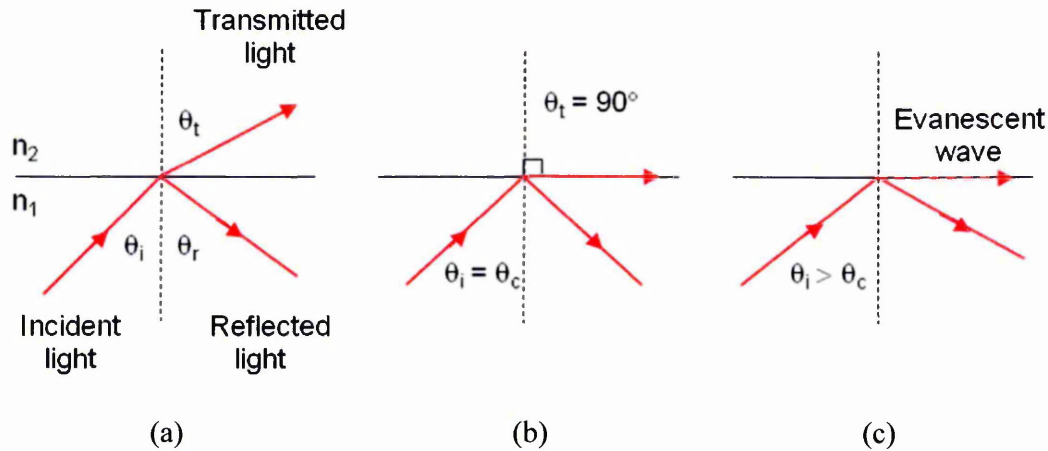


Figure 4.1 (a) Reflection and transmission of light at the n_1 - n_2 interface; (b) Total internal reflection, (c) The formation of evanescent wave.

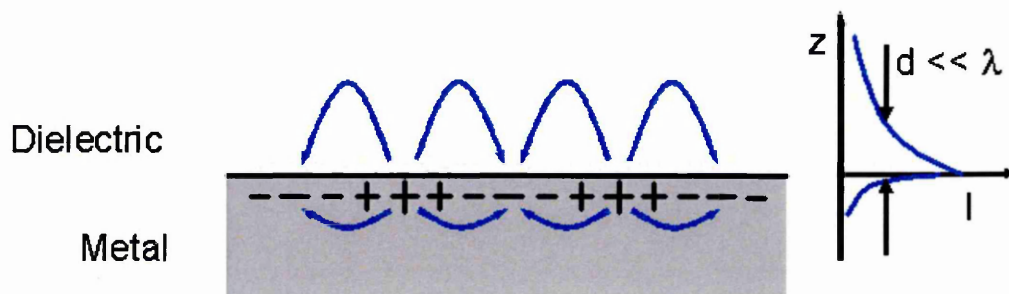


Figure 4.2 Schematic diagram of evanescent waves propagating along a metal-dielectric interface.

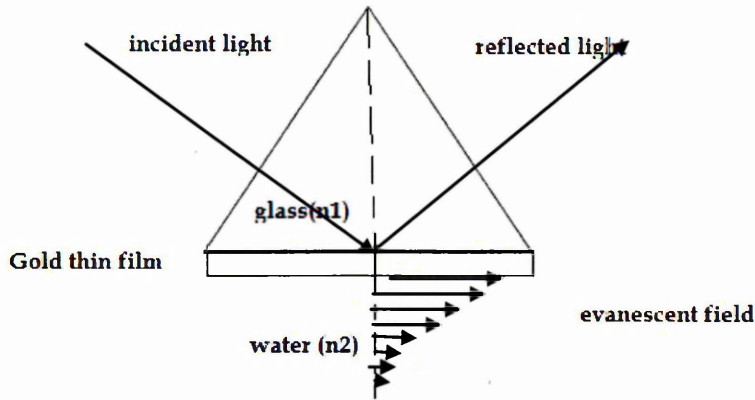


Figure 4.3 the formation of an evanescent wave at the boundary between two media ($n_1 > n_2$) while coupling the light through the prism at total internal reflection conditions.

One of the ways of creating an evanescent wave on the metal-dielectric interface is coupling the light through the prism at total reflection conditions, as illustrated by Figure 4.3.

4.1.1 Ellipsometry

Ellipsometry is an optical non-destructive procedure which provides an accurate description of thin films, surfaces and interfaces. Ellipsometry is mostly used to determine the thickness and optical constants (n , k) of thin films. The chief idea of ellipsometry is the detection of changes in polarization of light upon its reflection from examined surfaces as shown in Figure 4.4 [108].

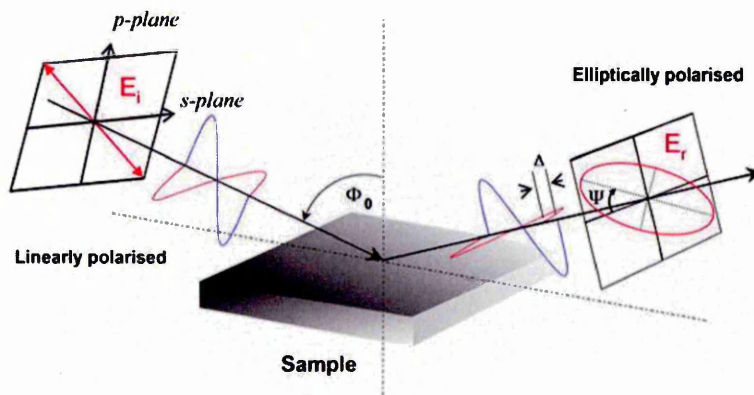


Figure 4.4 Changes in polarization of light reflected from the surface [108].

Ellipsometry does not really measure thickness or optical constants of the material but the angles of (ψ) and (Δ). The ellipsometric parameters ψ and Δ are defined, correspondingly, as a ratio of amplitudes and the phase shift between p- and s-components of the reflected electric vector:

$$\tan\Psi = \frac{r_p}{r_s}, \quad \Delta = \varphi_p - \varphi_s, \quad (4.3)$$

where p- and s- planes are defined in Fig. 4.1.

The parameters of thin films such as the thickness (d) and complex refractive index ($N = n - jk$) can be found by fitting the ellipsometry data. The calculation of ψ_{mod} and Δ_{mod} parameters (modelled) from given values of n , k and d (so-called forward ellipsometry problem) can be solved using the following equation [48, 49]:

$$\rho = \frac{r_p}{r_s} = \tan(\Psi) \exp(i\Delta), \quad (4.4)$$

in which the reflection coefficients of r_p and r_s are related to d , n , and k via Fresnel's formula [108].

In reality, however, we need to solve the reverse ellipsometry problem of finding d , n , and k from the experimental values of ψ_{exp} and Δ_{exp} . This could be achieved using one of the least-square techniques [109-111], where the forward problem is solved many times by varying initial parameters d , n , and k and minimizing the error function (MSE):

$$MSE = \frac{1}{2N - M} \sum_{i=1}^N \left[\left(\frac{\psi_i^{\text{mod}} - \psi_i^{\text{exp}}}{\sigma \psi_i^{\text{exp}}} + \frac{\Delta_i^{\text{mod}} - \Delta_i^{\text{exp}}}{\sigma \Delta_i^{\text{exp}}} \right)^2 \right] = \frac{1}{2N - M} X^2 \quad (4.5)$$

Where the summation goes over all the spectral points (N), and M is the target accuracy of the fit. A smaller MSE implies a better fit.

There are several types of ellipsometry instrumentation have been developed within the last four to five decades ranging from simple fixed angles, and single wavelength units to modern spectroscopic ellipsometric instruments. The most common types of automated spectroscopic ellipsometric instruments nowadays exploit the principles of either rotating optical elements (analyzer or compensator) or photoelastic modulators.

The J. A. Woollam M2000 spectroscopic ellipsometric instrument exploits the principle of a rotating compensator, which consists of a wide spectral range of light source (370 -

1000 nm), a polarizer, a rotating compensator, an analyzer and a photodetector, as shown in Figure 4.5.

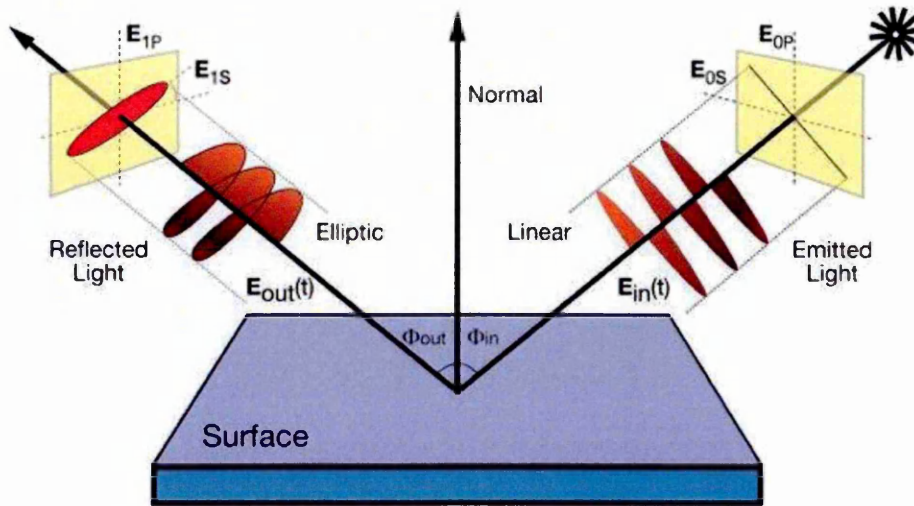


Figure 4.5 The schematic of rotating analyzer spectroscopic ellipsometry.

Ellipsometry has been known for decades as a method for optical characterization of materials. The instrumentation is under constant development, and modern spectroscopic instrumentation such as J.A. Woollam is capable of finding the thickness and dispersion characteristics $n(\lambda)$ and $k(\lambda)$ for complex materials (composite, multilayered, anisotropic, etc.). The sensitivity of ellipsometry is very high and sufficient for monitoring the variation of thickness (or refractive index) of molecular layers during adsorption or binding of molecules. However, the applications of ellipsometry for sensing are much more limited. The main problem of conventional ellipsometry is the fact that the light beam travels through the probing medium, so that variations of the refractive index of the medium, the absorption and the scattering of light (in the case of opaque or cloudy solutions) may affect the measurements. The cell is usually large (which is unsuitable for biosensing) and costly (because of the use of special non-polarized windows). Although J.A. Woollam has recently produced a reaction cell of about 0.5 ml in volume, there is another solution to that problem, which is outlined in the next paragraph.

4.1.2 Surface plasmon resonance (SPR)

The method of SPR uses properties of thin layers of gold (or other noble metals) on the surface of glass to absorb the light and excite electron waves (surface plasmon) on the gold surface. Traditional geometries of SPR (shown in Figure 4.6 involve the use of

glass prism, which allows coupling p-polarized into a thin metal films and the angle close to total internal reflection.

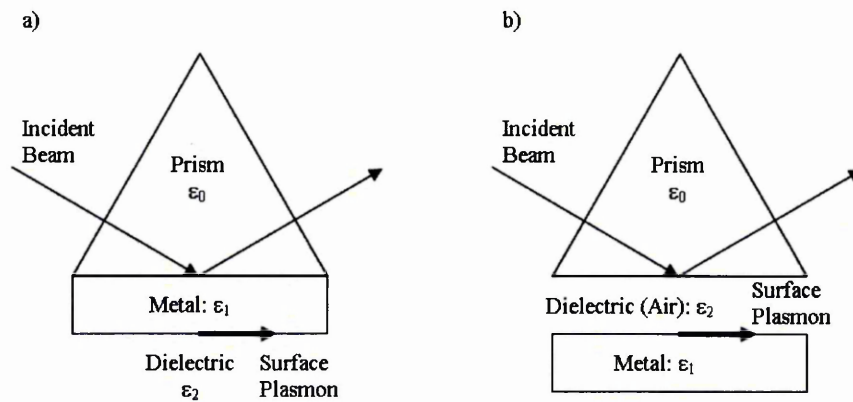


Figure 4.6 Kretschmann (a) and Otto (b) configurations of an Attenuated Total Reflection setup for coupling surface plasmons.

Usually, a monochromatic light (HeNe laser 633 nm) is used, and the variation of the component of k-vector in the interface plane (k_x) is achieved by changing the angle of incidence. In modern spectroscopic SPR instruments, however, the wavelength of the incident light is varied [112,113].

The evanescent wave propagating straight at the interface can interact with free electrons in the metal which is (20-40 nm in thickness). When the k_x vector of the evanescent field matches the k-vector of surface plasmons, the energy is transferred to surface plasmons and the reflected light intensity experienced a sharp dip (see Figure 4.8 b). This phenomenon happens only at a specific angle (or wavelength) of incident light and called surface plasmon resonance. The position of the resonance is highly dependent on optical properties of the metal layer used, such as Ag, Au, Cu. Different metals can be used in SPR, however gold was found to be the best practical solution because of its chemical stability and well-developed chemistry of immobilization of bio-molecules, as well as on the presence of adsorbed molecular layer on its surface. A typical SPR apparatus contains a cell on the side of the gold film which allows injection of various chemicals into it and thus performing different bio-chemical reactions (Fig. 4.7 a). For example, binding of a target analyte to a receptor on the gold surface produces a measurable shift of the SPR curve to the right (high angles) and can be easily detected as shown in Figure 4.7 b). The SPR shift could be calibrated in terms of the analyte concentration, and thus provide the result of the SPR bio-sensor. Otherwise,

the SPR shift could be fitted to Fresnel's theory and yields the sensor production in the units of either a refractive index or the thickness of adsorbed molecular layer.

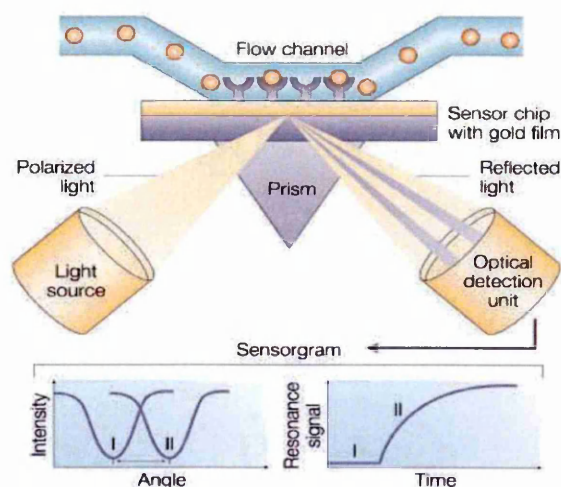


Figure 4.7 (a) Typical set-up of an SPR biosensor [46]; (b) the shift of SPR minimum upon binding of molecules; (c) kinetics of the SPR response.

Another analytical possibility lies in recording the reflected light intensity at a fixed angle of incidence or wavelength (see Fig 4.7 c). This allows the study of the kinetics of molecular adsorption (or binding) and then the evaluation of the affinity of biochemical reactions in real time, without the need for a molecular tag or label [114].

Optical biosensors that exploit the SPR principles have been widely used over the last two decades in the bio-analytical field. Advances in instrumentation and experimental design have led to the increasing application of SPR biosensors in many areas such as immunoanalysis, drug development, DNA analysis, medical diagnostics, environmental control, etc [112].

The SPR angle is dependent on numerous factors, including the characteristics of the metal film, the incident light, and the thickness and refractive index of the molecular layer making contact with the metal sensing surface [113]. As a result, spectra can be recorded on a metal surface with and without a coated molecular layer. Then, the shift in SPR angle between the two can be quantified and used to calculate the thickness or refractive index of the adhered molecules [112]. SPR has been established as an analytical tool in monitoring the thickness of a molecular layers [113]. The method was suitable for analysis of molecular monolayers or adsorbed molecules [114].

Beside its capability to determine the thickness of coated films, SPR has also emerged as a technology in the area of sensors (*e.g.*, for the detection of physical quantities, chemicals and biologics) [114]. Physical quantities (such as temperature and humidity) can be deduced from changes in refractive index. Chemical sensing can use changes in refractive index to measure concentrations of molecules adhering to the metal surface (as a result of chemical reactions). Biosensing can also use refractive index changes to deduce the happening of binding interactions (such as between antigens and antibodies). SPR also provide the significant advantage of being able to monitor reactions in real-time, without the need to go through the often complex process of labeling molecules with fluorescent or radioactive probes [115].

Like all surface analysis techniques, SPR has its restrictions in terms of sensitivity (the smallest amount of molecule detectable) [115], resolution (the smallest difference in SPR angle discernible), and sample characteristics (geometry, thickness, etc.). However, this technique still provides a remarkable diversity of capability for the description of reaction kinetics and thin film property, with a high degree of sensitivity, and in real-time, all important factors for a biomaterials scientist involved in the engineering, alteration and study of functionalized surfaces.

4.2 Total internal reflection ellipsometry (TIRE)

Ellipsometry is an analytical tool which is a well-established for thin film and surface characterization. With respect to organic material, spectroscopic ellipsometry has been extensively used in studying polymer thin films [116] self-assembled layers [117], LB films and liquid crystal [115]. A majority of these applications, however focus on the surface characterization. Ellipsometry is well known in thin film industry for in-situ monitoring of film deposition to control layer thickness, growth rate and layer quality.

Due to the high sensitivity to the thickness increment (around 0.01 nm) this method was recently adopted for the measurement of molecular layers absorbed on to solid surfaces which naturally leads to sensing applications. The advantages of the ellipsometry method in sensing application are [116]:

- The measurements are based on reflection of polarized light, no reference beam or label is needed.

- It is possible to measure very thin molecular layers (0.01 nm) adsorbed on the surface with fast response.
- Even higher sensitivity can be achieved using the parameter Δ (phase shift between p- and s components of polarized light).
- The method is capable of in-situ dynamic monitoring of both parameters Ψ and Δ in the course of bio-reactions such as affinity binding.
- Molecular multilayers representing consecutively adsorbed (bound) molecules can be studied using the advanced multilayer modelling facilities usually available in modern spectroscopic ellipsometry instruments.

The only drawback of the ellipsometry is an indirect method which needs an optical model for quantitative analysis and requires experienced personnel to do the fitting. On the other hand, modern ellipsometric instruments, such as J.A. Woollam's, provide a library of models and algorithms for different materials for thin film analysis.

Spectroscopic ellipsometry method has been reported in various bio-sensing applications including the detection of Hepatitis B, α -fetoprotein, and DNA hybridization. The detection limit of 0.1 ng/ml, 0.01 ng/ml and 10 mol/ml were achieved [112].

In bio-sensing applications the use of porous materials is a good approach, providing a large surface area for the immobilization of reagents. For this purpose, the ellipsometry method was successfully employed to study a porous surface of silicon [118] which was then suggested as a support for an enzyme based glucose sensor.

Other advances in spectroscopic ellipsometry for bio-sensing applications were achieved in its total internal reflection mode (TIRE). The idea of using ellipsometry in internal reflection mode was first realised experimentally by Wesphal [119], where the prism was used to couple the light beam into a thin metal film thus combining the ellipsometric principle of detection with the phenomenon of SPR. The increase in the sensitivity was achieved and the method was originally called Surface Plasmon Enhanced Ellipsometry. This method was further explored and theoretically explained by Arwin [120] and was given the current name of total internal reflection ellipsometry (TIRE). Further development of the method of TIRE was carried out by Nabok and his colleagues, the detailed modelling showed 10 fold gain of the sensitivity with the use of Δ spectra (as compared to Ψ spectra and traditional SPR measurements). The method of

TIRE was then successfully used in a number of bio-sensing applications and particularly in the detection of low molecular weight molecules such as pesticide like Simazine and Atrazine [121], T-2 mycotoxin [122] and nanylphenol [121].

The method of Total Internal Reflection Ellipsometry (TIRE) represents a very effective mixture of the spectroscopic ellipsometry instrumentation with the Kretschmann type SPR geometry of the experiment. Theoretically TIRE method was known long time ago, but its experimental investigation has been achieved relatively in recent years [115]. The method of TIRE was successful; at first, it was used for detection of low molecular weight toxins and later applied in many other bio-sensing application [116].

Our TIRE experimental set-up (shown in Figure 4.8) is based upon J.A. Woollam spectroscopic ellipsometer M200V with an addition of a 68° glass prism, a gold coated glass slide attached, and a 200 μ l cell with inlet and outlet allowing the injection of various liquids and thus performing various bio-reactions on the surface of gold.

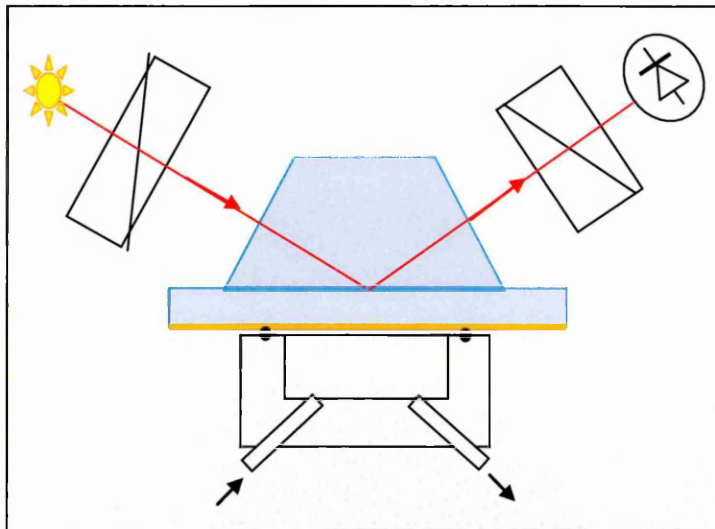


Figure 4.8 Experimental setup for surface Plasmon resonance enhanced ellipsometry.

The major benefit of TIRE is the use of two parameters ψ and Δ in contrast to only one parameter of reflected intensity in SPR. Figure 4.9 shows typical spectra of ψ and Δ recorded on the surface of bare gold. The spectrum of $\psi(\lambda)$ being the ratio of amplitudes of p- and s- components, resembles a typical SPR curve with the maximum and minimum equivalents, respectively, to total internal reflection and plasmon resonance

conditions. At the same time, the spectrum of $\Delta(\lambda)$ represents a novel quantity of phase shift which is not available in SPR.

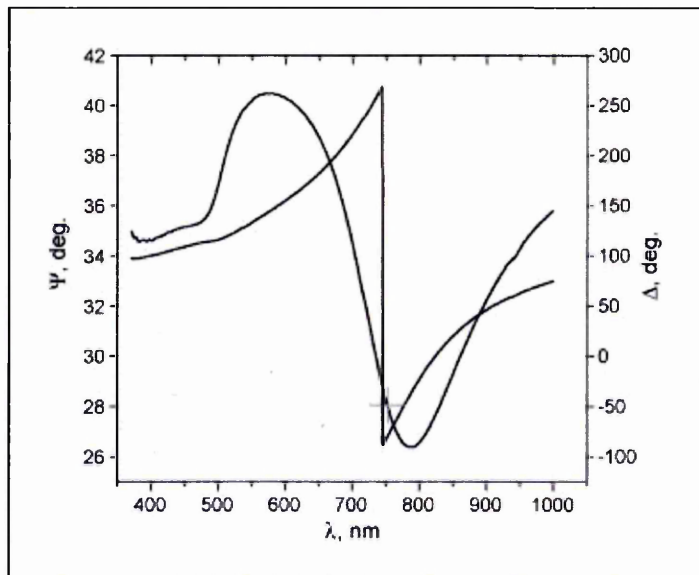


Figure 4.9 Typical TIRE spectra bare gold film on glass.

Both the modeling and experiments show about 10 times higher sensitivity of Δ (as compared to ψ) to small changes in optical parameters (thickness and refractive index) of thin films[115]. This means that the TIRE method (which could be called as phase SPR) is 10 times more sensitive than conventional SPR. Similarly to conventional SPR instrumentation, two types of measurements are available: single spectroscopic scans (for detection of the thickness of adsorbed molecular layers) and kinetic spectra measurement (for the study of reaction kinetics and subsequent affinity calculation).

The method of TIRE is an optical phase detection methods; the other possibilities are: (1) SPR interferometry which uses two polarizations (p- and s-) of light and first proposed by Kabashin and Nikitin, (2) and planar polarization interferometry [116]. The polarization interferometry is particularly attractive because of potential boost in sensitivity by two or three orders of magnitude due to a multiple reflection of light in the waveguide.

Considering the advantages of the TIRE method mentioned above along with the plus relative low cost of consumables and instrument running, the method of TIRE was selected as the main analytical technique for this PhD project.

4.2.1 TIRE experimental set up

The TIRE experiment set up was based on the basis of commercial M2000 J. A. Woollam Spectroscopic Ellipsometry operating in the 370 – 1000 nm spectral range and exploiting the rotating compensator principle (Fig.4.5 a)



Figure 4.10 (a) J.A. Woollam M2000 Ellipsometry (b) Newly designed TIRE cell

In order to use the instrument as a biosensor operating in liquid, a special small-volume TIRE cell was designed and machined from polytetrafluoroethylene (PTFE) material. The 200 μl volume of the cell substantially reduces consumption of bio-liquids, which is a very important factor in biosensing experiments. A silicon O-ring was used to seal the gold slide against the cell, as shown in Fig 4.5 (b).

The choice of a 68° glass prism which couples the light beam into a thin gold film was made to provide the condition of total internal reflection on a glass - water interface. A gold - coated glass slide was brought into optical contact with the prism via index matching liquid in order to avoid an air gap.

TIRE data processing requires building an optical model consistent to a sample. Dielectric functions of some layers (namely BK7 glass, gold, water) are known and can be selected from the WVASE software library [124]. Parameters of unknown layers(thickness and dispersal of n and k) can be found by fitting the experimental data to the

model layer which can be selected from the WVASE library. The most common model for the adsorbed molecular layers is the Cauchy model.

The measurement using on TIRE started with a single spectroscopic scan of the sample of a bare gold film in a standard Triz-HCl buffer for TIRE routine. The buffer solution (PH 8.0) to obtain the effective thickness and dispersion curves for optical parameters $n(\lambda)$ and $k(\lambda)$ of the Chromium - gold layer. The other layers of the model are ambient (BK7 glass), gold , and substrate (water) were used, where the parameters for glass and water are fixed but the thickness and optical constants of the metal layer are varied. The dispersion parameters of $n(\lambda)$ and $k(\lambda)$ for gold as well as the thickness of the evaporated gold layer were taken as initial guess values. The effective parameters for the Cr/ Au layer obtained by fitting for that particular sample were then used as fixed parameters for further fitting of data obtained from the same sample.

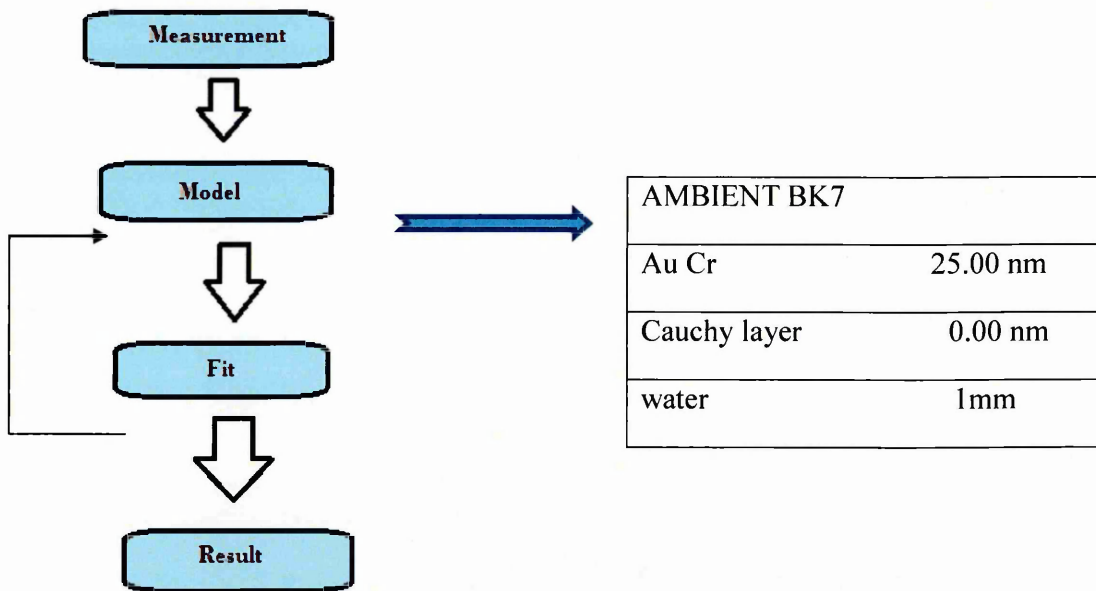


Figure 4.11 The flow-chart of data analysis in TIRE.

The process of fitting in ellipsometry requires a great deal of experience and the result depends on the selection of a physically adequate model as well as the choice of initial parameters and the fitting routine, the use of normal fit, global fit or spectral fit option, limiting the range of variable parameters are removing anomalous data points, etc.

In order to achieve reliable results, the fitting procedure needs to be repeated several times (preferably from different initial condition) until consistent values of thickness (d), refractive index (n) and extinction coefficient (k) are achieved. In some cases a good fit cannot be achieved due to the following reasons [125]:

- Inappropriate dielectric function selected in data analysis.
- The optical model in data analysis is not suitable.
- The measurements of (Ψ , Δ) spectra are inaccurate.
- The depolarization effect from the sample.

TIRE measurements usually consist of recording single spectroscopic scans in the same buffer solution after completing each step of adsorption (or binding). Parameters of adsorbed molecular layers (d , n , and k) were obtained by data-fitting to the four-layer model shown in Figure 4.11 and Table 4.1. In this model, the glass (prism and glass slide) acts as the ambient then the light goes through the Cr / Au film , the adsorbed molecular layer, and finally reaches the aqueous buffer solution in a cell which acts as a substrate. The molecular layer is modelled by the Cauchy dispersion function [125].

Table 4.1 Four-layer TIRE model.

No.	Layer	Parameters
3	BK7 glass(ambient)	$d \geq 1\text{mm}$, $n=1.515$ (at 633nm), $k=0$ n,k dispersion from WVASE32 library
2	Cr/Au	d is classically of 20 - 25 nm, $n = 0.359 \pm 0.078$, $k = 2.857 \pm 0.114$ at 633 nm
1	Adsorbed layer	Cauchy model: $A = 1.396$, $B = 0.01$, $C = 0$ $n = 1.42$, $k = 0$ at 633 nm
0	Water	n,k dispersions from WVASE32 library, $n = 1.33$ $k = 0$ at 633 nm.

The effective values of thickness and refractive index dispersion for Cr / Au were found earlier by fitting TIRE data to a bare gold surface. TIRE measurements were

always performed on the bare gold surface before deposition of a molecular layer. Then the obtained values of thickness (d), and the dispersion function for n and k were kept fixed in further TIRE fitting on this sample after deposition of molecular layers. Such a procedure had to be repeated for every new sample. For organic layers deposited on the sensing surface, the Cauchy dispersion function was used

$$n = A + \frac{B}{\lambda^2} + \frac{C}{\lambda^4}, \quad k = 0 \quad (4.6)$$

For organic material it is suitable to use the parameters of A, B and C during fitting and these were fixed at 1.396, 0.01 and 0 respectively, giving a value for n of about 1.42. A zero value for coefficient (k = 0) was used since all molecular layers were considered to be optically transparent in the spectral range used (270 - 1000 nm). The only variable parameter was the thickness, d. In such approximation, all changes (mostly spectral shift) in the TIRE spectra are associated with changes in film thickness.

The proposed approach in data analysis (fixing the values of n and k) is not strictly correct but was enforced by the natural limitation of both ellipsometry and SPR methods for thin dielectric films (thinner than 10 nm) [126]. Typical in bio-sensing it was assumed to fix the film thickness and relate all the changes to the refractive index. Recent experimental work has shown that the reflectivity increments caused by adsorption of different bio-molecules represent only 0.1 – 0.14 % of the refractive index, n, and therefore the spectral changes are associated mainly with thickness [127]. A similar value (n = 1.44) of the fixed refractive index was used in detection of E. coli phospholipids using Bruggeman effective medium approximation and resulting in the measurements of the effective thickness of lipids immobilized on silicon oxide [126].

4.2.2 Methodology of TIRE experiments

TIRE employs a prism coupler technique which combines the advantages of spectroscopic ellipsometry and the experimental convenience of Kretschmann SPR configuration. The angle of incidence selected should be close to the angle of total internal reflection, which needs to use a suitable prism, the typical ψ and Δ spectra from single spectroscopic measurements are shown in Fig. 4.12. The ψ spectrum resembles

typical SPR spectra with the maximal intensity corresponding to the conditions of total internal reflection while the minimum is due to the surface plasmon resonance. At the same time, the Δ spectrum experiences a sharp drop from 270° to 90° near the plasmon resonance. From the spectra given in Fig. 4.12, it is quite obvious that the parameter of Δ is more sensitive than ψ to small variations of the position of spectra cause by molecular binding.

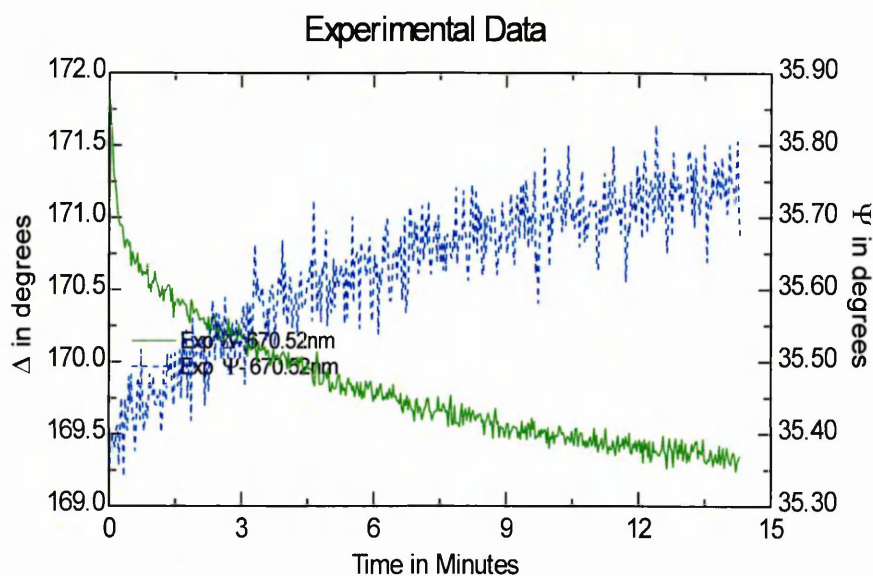


Figure 4.12 Typical time dependencies of ψ and Δ extracted from dynamic TIRE scan at selected wavelength.

Figure 4.12 shows typical dynamic spectra during immune reaction. From the large number of data recorded, only the spectra of ψ and Δ at certain wavelengths (near the plasmon resonance) were selected. For example, the selection of the wavelength at 600 nm in Fig. 4.12 gives rising ψ and decaying Δ signals. As one can see in Fig. 4.12, the Δ Kinetic curve is less noisy than the ψ one, and therefore $\Delta(t)$ characteristics were selected for further analysis of the molecular adsorption kinetics. Further analysis of the absorption (binding) kinetics was required for the evaluation of the affinity constants of the immune reaction studied [121].

4.2.3 TIRE kinetics analysis

TIRE dynamic spectral measurements are based on recording a number of spectra of both Ψ and Δ after a certain time interval, during the adsorption (binding) processes. The resulting time dependencies of Ψ and Δ at selected wavelengths (similar to that shown in Fig 4.12) are utilized for in-situ monitoring of all stages and molecular adsorption and biochemical reactions, such as immune reactions. TIRE dynamic spectral measurements followed by subsequent data processing allow the evaluation of the association and affinity constants of bio-reactions.

Adsorption of molecules to binding sites of concentration N on the surface is described by the following differential equation:

$$\frac{dn}{dt} = k_a C(N - n) - k_d n \quad (4.7)$$

Where k_a [$\text{Mol}^{-1} \text{s}^{-1}$], k_d [s^{-1}] are adsorption and desorption rates, respectively, C [Mol] is the concentration of analyte (antigen) in the environment (solution), n [Mol m^{-2}] is the concentration of adsorbed analyte on the surface, and N [Mol m^{-2}] is the concentration of binding sites (antibody) on the surface. $N - n$ is the concentration of available binding site on the surface. The solution of this equation is given as:

$$n = N \frac{k_a C}{k_a C + k_d} [1 - \exp(-(k_a C + k_d)t)] \quad (4.8)$$

It can be expressed as a sensor response, where the decaying exponential dependence for Δ is given as:

$$\Delta = \Delta_{\text{max}} \frac{k_a C}{k_a C + k_d} [1 - \exp(-(k_a C + k_d)t)] \quad (4.9)$$

The time constant in the above dependencies can be introduced as :

$$\tau = \frac{1}{k_a C + k_d} \quad (4.10)$$

The reciprocal value $S = \frac{1}{\tau} = k_a C + k_d$ depends linearly on the concentration of analyte. The rates of adsorption (k_a) and desorption (k_d) can therefore be evaluated as, respectively, a gradient and intercept of the graph S vs C . Then the association constant

can be found as a ratio of k_a and k_d ($K_A = \frac{k_a}{k_d}$) and the affinity constant K_D is the

reciprocal of K_A ($K_D = \frac{1}{K_A} = \frac{k_d}{k_a}$).

In order to find values for k_a or k_d , TIRE dynamic measurements have to be performed at different concentrations of analytes and the time constant (τ) has to be found by fitting every time dependence to the equation $\exp(-t / \tau) + b$. The reciprocal values

$S = \frac{1}{\tau} = k_a C + k_d$ have to be plotted against the concentration (C) of the analyte

(antigen). The linear fit of such dependence yields the values of k_a and k_d and consecutively K_A or K_D .

The correct analysis of the immune reaction kinetics has to be performed for different concentrations of antigen binding to originally empty binding sites for example antibodies freshly immobilized on the surface. In this work the adsorption steps started from the smallest concentration of analytes. This is much more practical but it has to be justified. If N_0 is the initial concentration of the binding sites (antibody) on the surface, the concentration of molecules adsorbed on the surface after first stage of adsorption is given as:

$$n_1 = N_0 \frac{k_a C_1}{k_a C_1 + k_d} [1 - \exp(-(k_a C + k_d)t)]. \quad (4.11)$$

Expanding eq (4.11) to a number of iterations, one can obtain that

$$N_i = N_{i-1} - n_{i\max}, \quad n_{i\max} = N_{i-1} \frac{k_a C_i}{k_a C_i + k_d} \quad (4.12)$$

until all binding sites are occupied and eventually $N_i = 0$. It is important to note that only the concentration of available binding sites on the surface (N_{i-1}) is varied during

such consecutive adsorption steps, while the time constant $\tau_i = \frac{1}{k_a C + k_d}$ remains the

same as in the case of single stage adsorption [121], and depends only on the parameters k_a , k_d and the concentration of antigens in solution (C_i). Thus we can conclude that the procedure of the evaluation of k_a and k_d from graph $1/\tau_i$ vs. C_i described in [128] is still valid in the case of consecutive adsorption. The above procedure was implemented for the immune analysis throughout the work and particularly for the detection of microcystin-LR.

CHAPTER 5

COMPLEMENTARY EXPERIMENTAL TECHNOLOGUES

This chapter outlines other experimental methods employed in this study, such as UV-vis. absorption spectroscopy as a complementary technique for the study of MC-LR cleansing. Other methods used for surface morphology analysis, include scanning electron microscopy (SEM), infinitive focus microscopy (IFM), Fourier transform infrared spectrometry (FT-IR) and hemocytometry. Langmuir–Blodgett film deposition was used to transfer cells onto solid substrates.

5.1 UV-visible absorption spectrophotometry

The UV-visible spectral region is divided into three sub-domains termed near UV (185-400 nm), visible (400-700 nm) and near infrared (700-1100 nm). Most commercial spectrophotometers cover the spectral range between 185 to 900 nm. The principles of absorption spectroscopy are related to the interaction of photons of the incident light beam with atoms and molecules in the sample. When a molecule interacts with a photon, this photon is absorbed and its energy is captured by one or more of outer electrons [129]. Consequently, such energy increase promotes electron transitions from the lower occupied molecular orbital (HOMO) to the higher unoccupied orbital (LUMO). The observed transitions involve electrons engaged in σ and π bonding orbital's as well as n (non-bonding) electron orbital's as shown in Fig. 5.1 below hypothetical energy diagram.

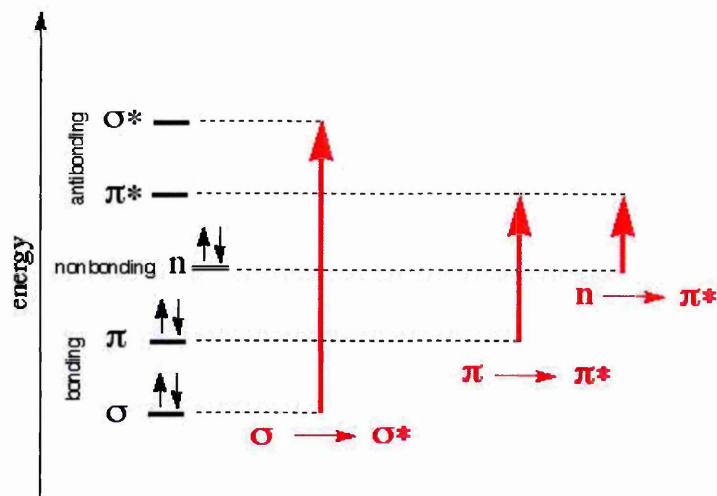


Figure 5.1 Electron transitions in organic materials stimulated by light.

A spectrophotometer is designed around three fundamental parts: the light source, the monochromator, and the detection system as shown in Figure 5.2 (a). These components are typically integrated in a unique framework to make a spectrometer [130,131].

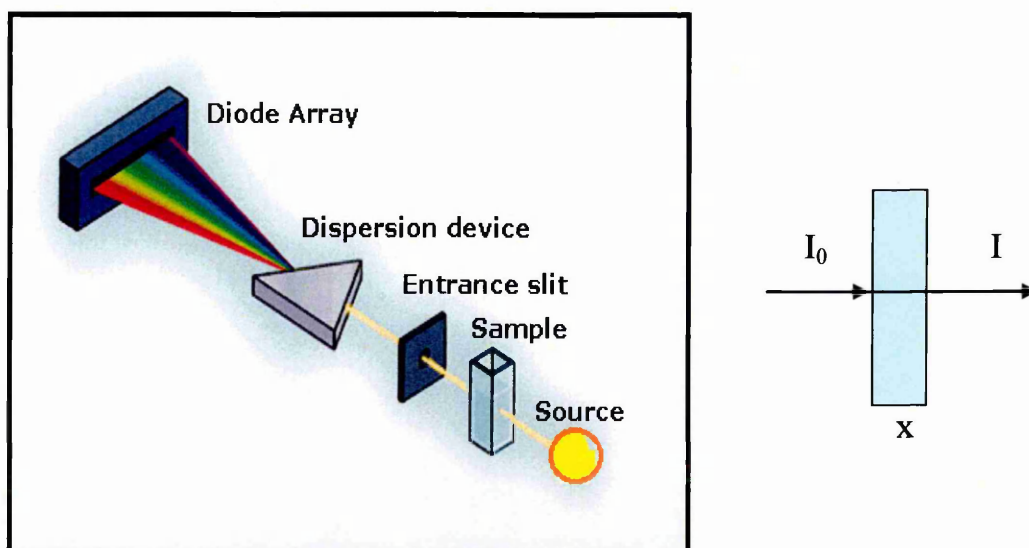


Figure 5.2. (a) Schematic diagram of UV-vis spectrophotometer[132]; (b) absorption of light by a sample (illustration to derivation of Beer-Lambert law).

As illustrated in Fig. 5.2 (b), the intensity of the incident light (I_0) and the intensity of light after passing through the sample (I) are related through the Beer-Lambert law:

$$I = I_0 \exp(-\alpha x), \quad (5.1)$$

where α is the absorption coefficient and x is the thickness of the sample.

In modern spectrophotometric instruments, the spectra of several parameters are available, for example transmission T (%):

$$T = I/I_0, \quad (5.2)$$

However the most common parameter to measure is the logarithmic unit which is called absorbance (Abs. or A) and defined as:

$$Abs. = \log_{10} \left(\frac{I_0}{I} \right). \quad (5.3)$$

Therefore, absorbance is linearly proportional to the absorption coefficient.

$$Abs. = \alpha x / 2.3 \quad (5.4)$$

In the case of light absorption by a liquid sample, the Beer-Lambert law and their absorbance can be related to the molar concentration (C) of a light absorbing medium:

$$I = I_0 \exp(-\alpha C x), \quad A = \log_{10} \left(\frac{I_0}{I} \right) = \alpha C x. \quad (5.5)$$

Other possibilities of light losses are reflection and scattering of light. Accounting for these two phenomena required some alterations in the eq (5.1). However in a simple case of transparent materials (with negligible absorption) and normal incidence (negligible reflection), the light losses can be associated with the light scattering only. These conditions are used in the measurement of optical density of some biological samples which are transparent in the visible spectral range but look cloudy” due to light scattering.

5.2 Scanning electron microscopy SEM

Scanning Electron Microscopy (SEM) uses a focused beam of high energy electrons to scan the sample surface [133]. Usually, a tungsten filament or a field emission gun are typically used as an electron source. The electron beam is accelerated by an electric field and focused by condenser electromagnetic lenses [134]. Another set of lenses performs the beam detour in a raster mode to scan the surface of the sample. The electrons reflected by the sample (primary electrons) or re-emitted by the sample (secondary electrons) are detected, and these signals are used to form an image of the sample. The operation principles of the SEM are shown pictorially in Fig.5.3.

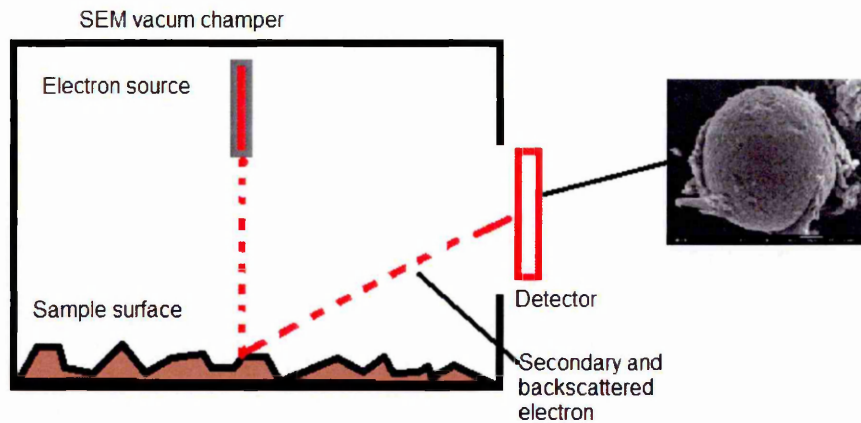


Figure 5.3 Operation principles of SEM.

The focused electron beam scans the sample surface. In standard imaging mode, backscattered and secondary electrons are detected and the measured signal is used to form a two-dimensional image. Because of high energy of incident electrons, the secondary electrons are usually emitted from deeper (core) electron levels; the electrons from high orbitals move down to fill the vacancies. The resulted X-ray emission can be used for elemental analysis (EDX) [135].

SEM is a very versatile analytical tool having up to nm-scale spatial resolution. The resulting SEM image shows a mixture of different types of image. Because the electron beam not only interacts with the sample surface but also penetrate inside the material, the measured signal is affected by the three-dimensional structure of the sample. This effect can be seen in Figure 5.3, which shows an SEM scan of concentrated ion beam-milled lamellae (h-bar type) for transmission electron microscopy (SEM) studies [136, 137]. The electron beam of the SEM needs to be operated in a vacuum. There have been attempts to lower the vacuum requirements in electron microscopy but usually there is a problem with the vacuum compatibility of biological samples. The SEM type FEI NOVA 200 NanoSEM was used in this study which has the following features:

- Field emission gun (FEG)
- High spatial resolutions of 1.5 – 2.0 nm (at 15 – 30 kV) or 2.5 – 5.0 nm (at 1 kV)
- The instrument operates in both high vacuum and low-pressure environments;
- Energy dispersive X-ray spectroscopy (EDX or EDS)

In the current project SEM was used for visualization of microparticles as explained in detail in Chapter 8.

5.3 Infinite focus microscopy (IFM)

The Infinite Focus Microscope (IFM) is a fast optical tool “non-touching” the sample with a vertical and side resolutions down to 10 nm and 400 nm, respectively, enabling to reconstruct a pseudo-3D image from a number of 2D images that have been captured between the lowest and highest focal planes. The instrument (Alicona) is capable of capturing images of samples with highly reflective surfaces and samples with a high surface roughness. The software for image analysis available in the IFM instrument allows presenting images in different shapes and formats and evaluates different parameters such as roughness [138].

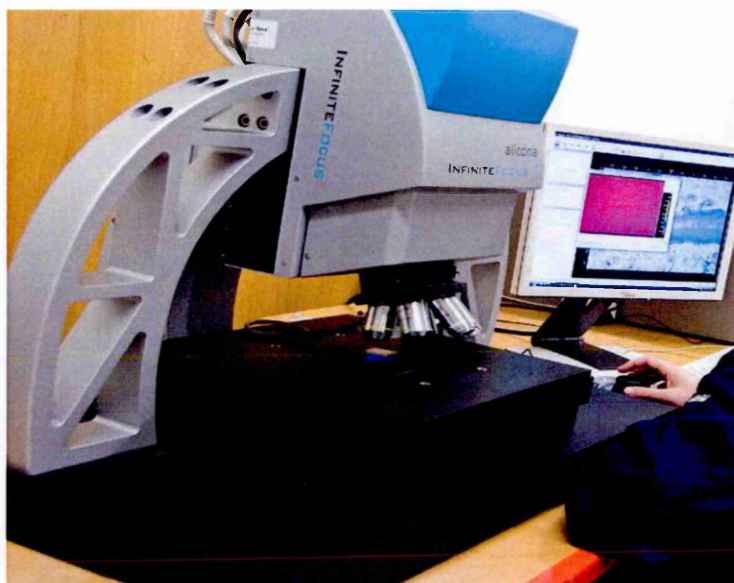


Figure 5.4 The view of IFM (Alicona) instrument.

5.4 Fourier transform infrared spectrometry (FT-IR)

Total Reflectance Fourier Transform Infra Red (ATR-FTIR) spectroscopy can be used to study quite small samples. This surface sensitive mechanism can provide information on coatings and laminates by presenting various sides of the sample to the beam, using ATR-FTIR to measure the adsorption of water and other solvents into polymer films

[139]. This process provides an abundance of information in addition to capturing the rate of diffusion of the solvent species and can contain information on polymer swelling and crystallinity and the interactions between the solvent and the polymer [140]. FTIR spectroscopy can monitor reactions of the amino acids, the ligands and specific water molecules in the active centre of a protein in the time range from nanoseconds to seconds, thereby providing a detailed understanding of the molecular reaction mechanism [141].

The principle of FT-IR is: Light emitted from the source across the spectrum, a monochromator separates the radiation into its various wavelengths. a slit selects the collection of wavelengths that glow through the sample at any given time. The sample absorbs light according to its chemical properties, a detector collects the radiation that passes through the sample, and puts out an electrical signal which is sent directly to an analog recorder. A link between the monochromator and the recorder allows recording energy as a function of frequency or wavelength, depending on how the recorder is calibrated as shown in Fig 5.5(a). There are many limitations:

- The monochromator/slit limits the amount of signal one can get at a particular resolution. To improve resolution, you must narrow the slit and decrease sensitivity.
- There is no simple way to run manifold scans to build up signal-to-noise ratios.
- The instrument must be repetitively calibrated.

While in FT a source, a sample and a detector the same, but everything else is different. All the source energy is sent through an interferometer and onto the sample. In every scan, all source radiation gets to the sample. The interferometer is a basically different piece of equipment than a monochromator. The light passes through a beamsplitter, which sends the light in two directions at right angles. One beam goes to a stationary mirror then back to the beamsplitter. The other goes to a moving mirror. The motion of the mirror makes the total path length variable versus that taken by the stationary-mirror beam. When the two meet up again at the beamsplitter, they recombine, but the difference in path lengths creates constructive and destructive interference, an interferogram. The recombined beam passes through the sample. The sample absorbs all the different wavelengths characteristic of its spectrum, and this subtracts specific wavelengths from the interferogram. The detector now reports variation in energy

versus time for all wavelengths simultaneously. A laser beam is superimposed to provide a reference for the instrument operation as shown in Fig. 5.5 (b).

The frequencies of electromagnetic radiation from source to proportionately slower oscillating signal. The sum of slower oscillating signals is passed to the computer which mathematically separates the signal into individual oscillations and calculates the oscillations of symmetric frequencies of observed radiation. This data is constantly recorded. The amplitude of each resolved oscillations is a function of intensity of radiation. A mathematical process called the Fourier Transform (FT) is used to convert time field spectrum to conventional frequency domain spectrum. Increasing the number of flat mirrored surfaces increases the number of reflections.

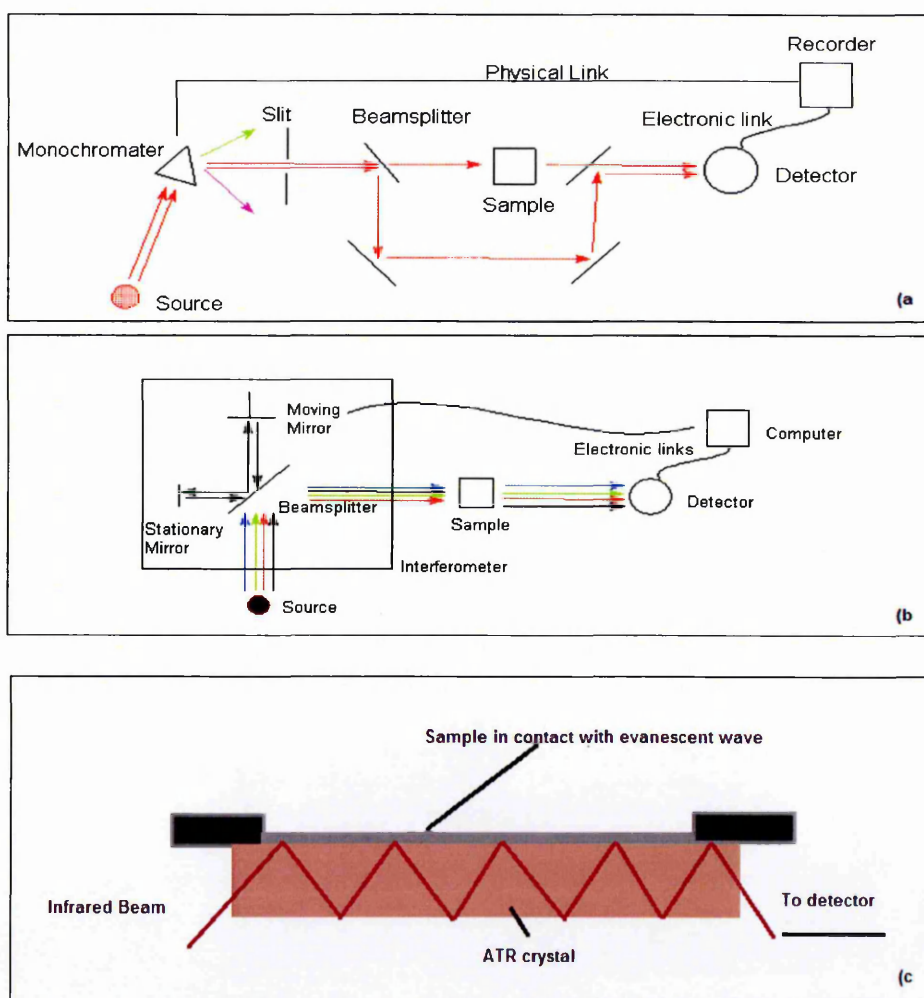


Figure 5.5 (a) the principles of a classical spectrometer,(b) FT instrument. (c)A multiple reflection ATR system in FT-IT measurements.

This tool was used in the current project to see the binding between microcystin-LR and the antibody MC10E7 as discussed in details in Chapter 7, also it was used to confirm that the core of microcapsules was removed as shown in Chapter 8.

5.5 Hemocytometry

Haemocytometry is the simplest and cheapest means of accurately determining the number of cells in a sample. It is based on the optical microscope and contains a Haemocytometer which is a specialised slide that has a counting chamber with a known volume of liquid. The haemocytometer consisting of a heavy glass slide with two counting chambers, each of which is divided into nine large 1 mm squares, on an etched and silvered surface separated by a trough. A coverslip sits on top of the raised supports of the 'H' shaped roughs enclosing both chambers. There is a 'V' or notch at either end where the cell suspension is loaded into the Haemocytometer. When loaded with the cell suspension it contains a defined volume of liquid [142]. The engraved grid on the surface of the counting chamber ensures that the number of particles in a defined volume of liquid is counted. The Haemocytometer is placed on the microscope stage and the cell suspension is counted. The diagram below shows the Haemocytometer slide under the microscope.

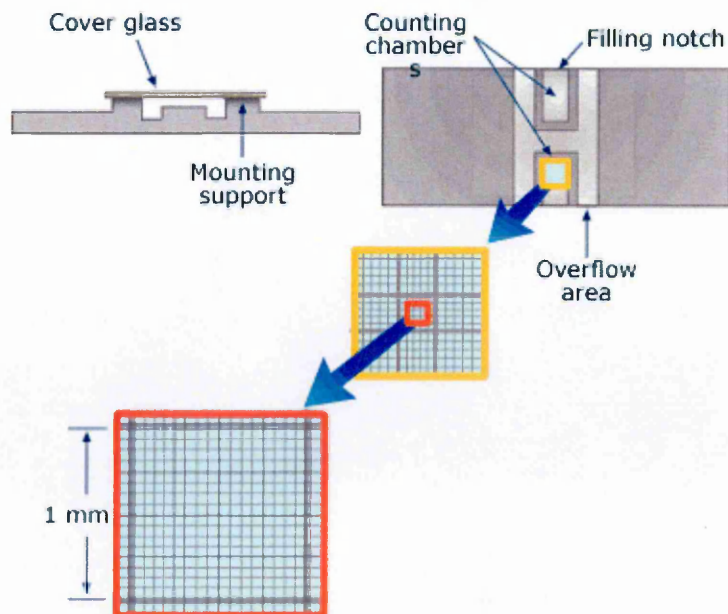


Figure 5.6 Haemocytometer slide and its cover.

One-half (ie. one chamber) of a Haemocytometer with Neubauer ruling

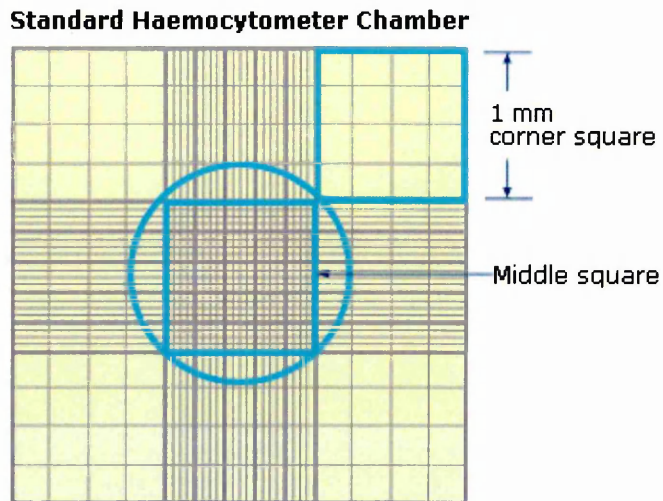


Figure 5.7 Standard Haemocytometer chamber.

Figure 5.6 shows one of the two chambers in the Haemocytometer. The entire chamber has nine $1.0 \text{ mm} \times 1.0 \text{ mm}$ large squares separated from one another by triple lines. The area of each is 1 mm^2 . Inside each of the larger corner 1 mm^2 squares are 16 small squares that serves as reference points to help avoid counting a given cell more than once. The central 1 mm^2 area is divided into 25 small squares, each 0.04 mm^2 and each of these is marked into a further 16 tiny squares.

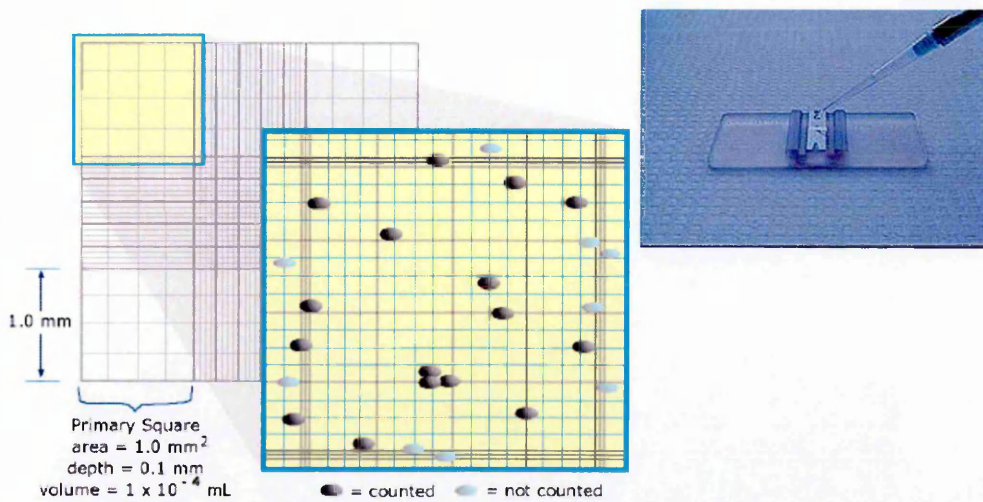


Figure 5.8 Example of using Haemocytometer for counting cells. Inset shows the sampling.

This slide was used to count microcystis aeruginosa cells to make standard curves for cells, as explain in Chapter 7.

5.6 Fluorescence microscopy

Is an optical microscopy that uses fluorescence and phosphorescence in addition to, reflection and absorption. A fluorescence microscope uses fluorescence to generate an image, used in biological research, environmental monitoring, public health and medicine [143]. One of the greatest advantages of Fluorescence Microscopy enables the viewer to obtain faster laboratory results that would not be seen with conventional optical microscopy. The sample is illuminated with light of a specific wavelength which is absorbed by the fluorophores and causes emission of longer wavelengths [144]. The illumination light is separated from the much weaker emitted fluorescence through the use of a spectral emission filter light source (xenon arc lamps or mercury-vapor lamps are common; more advanced forms are high-power LEDs and lasers). Prominent peaks of intensity occur at 313, 334, 365, 406, 435, 546, and 578 nanometers. It also contain a combination of dichroic mirrors and filters capable of exciting fluorescent chromophores and filtering out the excitation light from the viewed image. Chromophore or Fluorophore is a chemical component that can re-emit light upon light excitation [145]. Fluorophore usually contains several combined aromatic groups, or plane or cyclic molecules with several π bonds. They used in many case as a tracer in fluids, for example dyes for staining cells, tissues, or materials in different analytical methods. These covalently bonded to a macromolecule. In my project I used two types of dyes (SYTO-9 Green Fluorescence stain and Propidium iodide red Fluorescence stain). The fluorescence excitation maximum is 535 nm and the emission maximum is 617 nm for Propidium iodide red Fluorescence stain, is enhanced 20 to 30 fold. PI binding shifts the maximum fluorescence excitation by about 35 nm towards red while also shifting the maximum emission by about 15 nm towards blue. But for SYTO-9 Green Fluorescence stain the absorption is 485 nm and the emission is 501 nm.

At other wavelengths in the visible light region, the intensity is steady although not nearly so bright (but still useable in most applications). In considering illumination efficiency, mere lamp wattage is not the prime consideration. Instead, the critical parameter is the mean luminance must be considered, taking into account the source brightness, arc geometry, and the angular spread of emission. Sample stains by many

fluorescent stains have been designed for a range of biological molecules. Fluorescent microscopy is frequently used to image specific features of small samples such as microorganisms [146]. It is likewise used to visually improve 3-D features at small scales. This can be achieved by attaching fluorescent tags to anti-bodies that in turn attach to targeted features, or by staining in a less specific manner. When the reflected light and background fluorescence is filtered in this type of microscopy the targeted parts of a given sample can be imaged. This gives a detective the ability to visualize desired organelles or unique surface features of a sample of interest [147] as shown in Fig. 5.9.

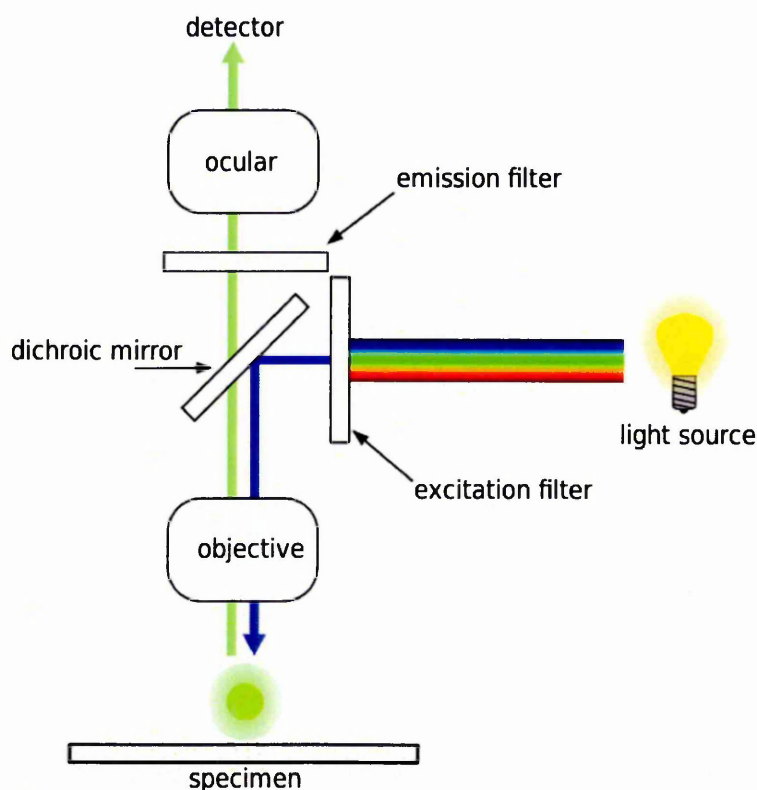


Figure 5.9 Schematic diagram of Fluorescence Microscope [143].

This microscopy was used in my project to capture image for microcapsules after they stained with fluorescence dye, these images are existing in chapter 8.

5.7 Langmuir–blodgett trough

Langmuir–Blodgett (LB) trough is laboratory equipment used to study monolayers of amphiphilic molecules on the surface of subphase (water). An amphiphilic molecule is one that contains both a hydrophobic and hydrophilic groups, and therefore exist on the air-water interface. The LB trough allows preparing a monolayer of amphiphilic

molecules on the surface of water, and then compress the monolayer thus modifying the molecular density or area per molecule [148]. This is accomplished by placing a subphase (typically water) in a trough, spreading a given amphiphile over the surface, and then compressing the molecular layer with barriers. The monolayer's effect on the surface pressure of the liquid is measured with a Wilhelmy plate. LB film can then be transferred to a solid substrate by dipping the substrate through the monolayer [149].

One of the important characteristics of monolayer is the surface pressure - area per molecule isotherm. A schematic diagram in Figure 5.10 shows the main elements of Langmuir trough which can be used to record surface pressure isotherms.

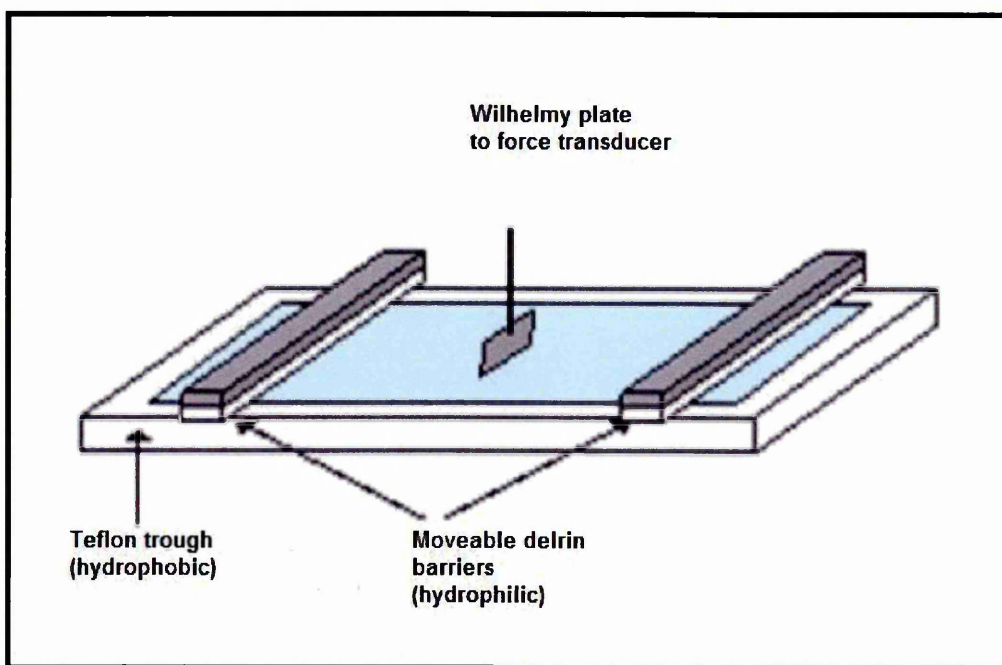


Figure 5.10 Schematic diagram of Langmuir trough for isotherm measurements [151].

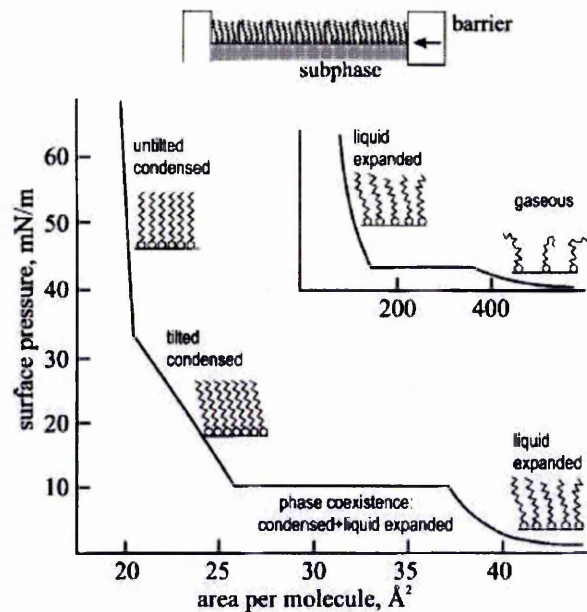


Figure 5.11 Schematic diagram of surface pressure – area per molecule isotherm indicating different stages of monolayer compression [154].

As shown in Fig 5.11, the region of constant slope in the isotherm indicates the homogeneous phase of the monolayer, while the change in the slope would indicate a phase transition. Detailed monolayer structure can be investigated further by other techniques including X-ray and neutron diffraction, ellipsometry, and nonlinear optical spectroscopy [150 - 153].

The work on protein chaperon, which is described in detail in Chapter 6, uses the NIMA-602 teflon LB trough of 172.0cm² in area equipped with two teflon barriers, Wilhelmy plate as a surface pressure sensor, and an dipping mechanism. The trough is interfaced to PC and controlled by dedicated NIMA software.

5.8 Edwards E360A evaporation unit

The Edwards E360A evaporation unit is commonly used in thin-film deposition (mostly metals). The metal evaporation unit is based on a vacuum system comprising a rotary pump (to create pre-vacuum in the range of 10⁻³ Torr) and the oil diffusion pump (to create high vacuum in the range of 10⁻⁶ Torr); the vacuum chamber in a shape of a glass dome is sealed against the stainless steel base via a rubber ring-seal.

Thermal evaporation of metals is achieved by passing high current through the filament made of materials with high melting point (W or Mo). A piece of metal to be evaporated (assumably having a melting point much lower that of the filament) is placed on a filament (typically having a boat-shape). After passing a sufficient current through the

filament, the heat produced causes the metal to melt and thus to evaporate into the space within a vacuum chamber. A number of substrates, which are fixed inside the chamber, will be coated with the layer of metal as a result. The control of metal deposition is achieved with a QCM sensor which is placed on the same distance from metal source as the substrates. The frequency fall of the quartz crystal in QCM sensor can be calibrated to a particular metal used, thus providing values of the evaporation rate in (nm/s) and the total layer thickness in (nm).

The evaporation unit has four compartments spaced at 90° on a turret, each containing an electrode; up to four filaments could be connected between these electrodes and the central one which is connected to the ground. By rotating the turret, these electrodes could be connected in turn to a power supply providing low voltage but high current (up to 100A). In that way, up to four metals could be evaporated one-by-one without breaking the vacuum in the chamber. The evaporation process can be terminated by either switching off power or by blocking the evaporation source with a shutter. In the current project, the Edwards E360A evaporation unit was used to deposit layers of Cr (2-3 nm) and Au (25-27 nm) on glass slides for TIRE measurements. The requirement of not breaking the vacuum between depositions of Cr and Au is crucial in order to achieve good adhesion of Au to glass, since a thin (2-3 nm) layer of Cr layer will be almost instantly oxidised in atmospheric conditions.

CHAPTER 6

FURTHER DEVELOPMENTS OF TIRE METHOD FOR OTHER APPLICATIONS

In addition to the main part of my study dedicated to the detection of microcystin-LR, a TIRE method was used successfully in other bio-sensing applications. My contribution to other research projects involved carrying out TIRE measurements and thus providing help to other researchers as well as learning TIRE method on the way. This chapter outlined the results obtained at the beginning of my PhD study.

6.1 Study of protein-protein interaction

A number of types of biological interactions were well-studied, namely immune reactions (i.e. binding of antigen to specific antibodies); enzyme reactions (decomposition of small molecules catalyzed by enzymes); hybridization of single DNA strands due to hydrogen bonding, etc., though the interaction of proteins in general is not well-studied and not completely understood. Time and again, we associate molecular binding, which does not have a simple explanation with so-called non-specific binding. In this chapter, we attempt to explain in more detail the interaction between chaperones and their specific receptors [157].

Chaperone proteins play an important role in cells protecting proteins from high temperatures and other cellular stresses, stabilizing protein structure and preventing them from aggregation and degradation. It was recently suggested that molecular chaperones, such as heat shock proteins Hsp 70 and Hsp 81, can form complexes with freshly translated proteins and thus prevent their aggregation [158]. In addition, the new finding of chaperone receptors in plants [159] indicates more specific participation of molecular chaperones in protein targeting. The study of the mechanisms of protein targeting may have a substantial impact in a number of applications including the origin of neurological diseases. It was shown recently that novel receptors OEP61 extracted from leaves are capable of specific binding of Hsp 70 while not binding Hsp 81 [160]. In this work, the interactions of chaperones with different receptors (including OEP61)

electrostatically immobilized on the surface was accessed with the TIRE measurements. Apart from confirming the binding properties of OEP61, this work showed a clear separation of specific and no-specific binding in terms of both the sensor response (i.e. thickness increment) and the binding affinity [161].

I was involved in a similar study of chaperone-receptor interaction, but this time with the use of receptors naturally embedded into chloroplast membrane. This work helped me to learn the techniques of electrostatic and LB deposition as well as to master the use of TIRE.

6.1.1 Study of chaperone interactions with receptors

This part of the experimental work is dedicated to detailed quantitative study of interaction between chaperone Hsp70 and Hsp90 with respective receptors present in the chloroplast membrane using the optical method of total internal reflection ellipsometry (TIRE).

6.1.2 Sample preparation

Monolayers of chloroplast were formed on the water surface in the Langmuir trough (NIMA mini-trough), compressed to a surface pressure of 20mN/m, and then transferred onto solid substrates (gold coated glass slides) using horizontal lifting method called as the Langmuir-Schaefer technique.(the chloroplast membranes were prepared by biological team Dr. Verena and Dr. ben).

Gold coated glass slides (1×1 inch) were prepared by thermal evaporation of Cr (3 nm thick) and Au (25-27nm) onto microscopic glass slides using an Edwards 360 unit and the a vacuum of about 10^{-6} Tor. In order to have the surface of gold positively charged, the samples were treated overnight in a 100mM methanol solution of Cystamine hydrochloride. After this treatment the samples were suitable for coating with chloroplast membranes having a negative charge on lipid bi-layers.

Typical surface pressure-area (Π -A) isotherm recorded during the compression of chloroplast monolayer is shown in Figure 6.1(a). The molecular weight and exact concentration of chloroplast cells in the buffer solution are not known, so that the area is presented in cm^2 units. The Π -A isotherm appeared to be reproducible with a small hysteresis caused by penetration of chloroplast in the water subphase. The deposition was carried out at a constant pressure of 20 mN/m, which was selected in the middle of

a linear section of Π -A isotherm. The recording of the surface pressure during deposition in Fig. 6.1(b) showed a repeatable pattern of increasing pressure during monolayer compression, disturbance at the moment of touch, followed by a sharp drop of pressure during the layer transfer, and then again the increase of Π to a target value

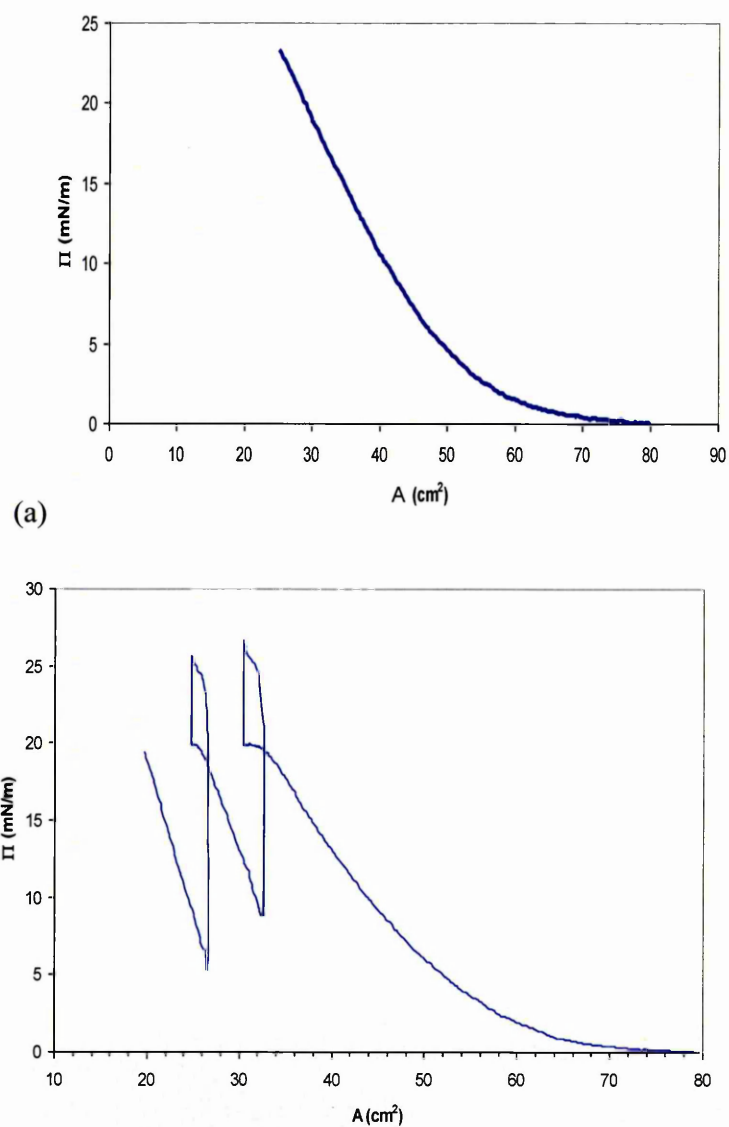


Figure 6.1 (a) Typical Π -A diagram of chloroplast membranes on a water surface, (b) Recording Π during Langmuir-Schaefer deposition of chloroplast.

of 20mN/m. The Π -A isotherm appeared to be shifted to a lower area values after each deposition step. The reduction in the area corresponds exactly to the area of the sample which indicates 100% transfer ratio.

6.1.3 TIRE measurements and data fitting

TIRE measurements were performed using the TIRE set up described earlier in chapter 4. Both static and dynamic TIRE measurements were carried out, to monitor, respectively, changes in the adsorbed layer thickness during binding chaperones to receptors, and to evaluate the association (or affinity) constant of binding chaperones to receptors. The Cr/Au coated glass slides with deposited chloroplast membranes were attached to the prism via an index matching fluid and with the gold-side sealed against the cell. The required liquids were injected into the cell using micro-syringe. First, the initial single spectroscopic scan was performed in a 100 mM Tris-HCl, pH 8.0 buffer solution. Then the solutions of chaperones in increasing concentrations (from 1 ng/ml to 100 $\mu\text{g/ml}$) were injected, and the dynamic TIRE spectra were recorded during the incubation time of 15 min. After each deposition the cell was rinsed by purging the 100mM Tris-HCl, pH 8 buffer solution through the cell (amounting to at least 20 cell volumes), then the single spectroscopic scans were recorded after each adsorption.

A typical series of TIRE spectra demonstrating binding of Hsp70 chaperones to OEP61 receptors naturally present in the chloroplast membranes are shown in Figure 6.2. The observed spectral shift is believed to be caused by the binding of Hsp70 chaperones.

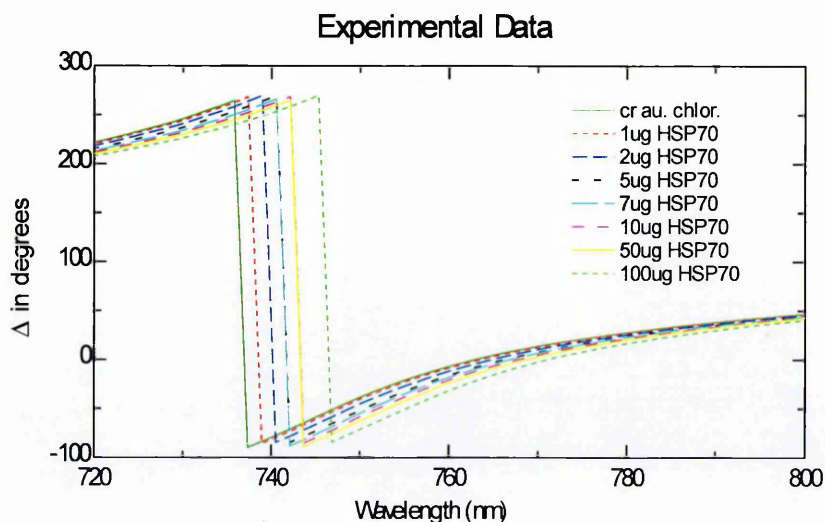


Figure 6.2 TIRE spectral shift caused by binding of Hsp70 chaperones.

- (1) The first layer is cr.au.chloroplast (2) 1 μg hsp70 (3) 2 μg HSP70 (4) 5 μg (5) 7 μg (6) 10 μg (7) 50 μg and (8) 100 μg . The spectral shift is go to the right.

The values of the thickness of the molecular layer were evaluated by fitting TIRE data using the software provided by J.A. Woollam Ltd [162]. A four-layer model built for the purpose of data fitting is shown in Table 6.1 below. This is an upside-down ellipsometry model typically used for TIRE data fitting in our previous work [163]. In this model, the glass (BK 7) serves as an ambient and the substrate is water; dispersion parameters for these two layers were taken from J.A. Woollam user library [164]. The Cr/Au metal film was described as a mixed layer, the effective parameters of which (d, n, and k) were found by fitting the TIRE data for uncoated Cr/Au films; then they obtained parameters were kept fixed during further fittings with the same sample. The molecular layer was described by the Cauchy model being typically used for transparent dielectric materials.

$$n = A + \frac{B}{\lambda^2} + \frac{C}{\lambda^4}, \quad k = 0, \quad (4.1)$$

where A, B, and C are constants and λ is the wavelength of light.

Table 6.1 Four-layer TIRE model.

Layer	Thickness (d), refractive index ($N = n - jk$)	Comments
BK7 glass	$d \geq 1\text{mm}$, $n=1.515$ (at 633nm), $k=0$ dispersion function $n(\lambda)$ for BK7 is from the user library of M2000 instrument.	parameters are fixed
Cr/Au	d is typically of 27 - 32 nm, Initial dispersion function for Au is from	Effective optical dispersion parameters $n(\lambda)$ for Cr/Au layer were found by fitting the data for bare Au surface; then d and $n(\lambda)$ were fixed in consecutive data fitting
Molecular layer	d is variable (subject to fitting); $n(\lambda)$ is described by Cauchy model from $n = A + \frac{B}{\lambda^2} + \frac{C}{\lambda^4}, \quad k = 0$	n is a fixed parameter ($n=1.42$ at 633 nm) with $A=1.39, B=0.01, C=0$
Water	$d \geq 1\text{mm}$, $n=1.33$ (at 633nm), $k=0$ dispersion function $n(\lambda)$ for water is from the user library of M2000 instrument.	Parameters are fixed

One of the characteristic features of ellipsometry and SPR is that the simultaneous evaluation of d and n of thin (less than 10 nm) dielectric films is impossible, so that either d or n must be assumed and fixed during the fitting. Here the refractive index is kept fixed and all the changes in the adsorbed layer are associated with the thickness. This is close to reality since all bio-organic substances have similar refractive indices of about 1.42 at 630 nm [165].

TIRE single spectra measurements were performed for binding different chaperones, e.g. Hsp 70 and Hsp 90 to chloroplast membranes, and the results of TIRE fitting are summarized in Figure 6.3 below.

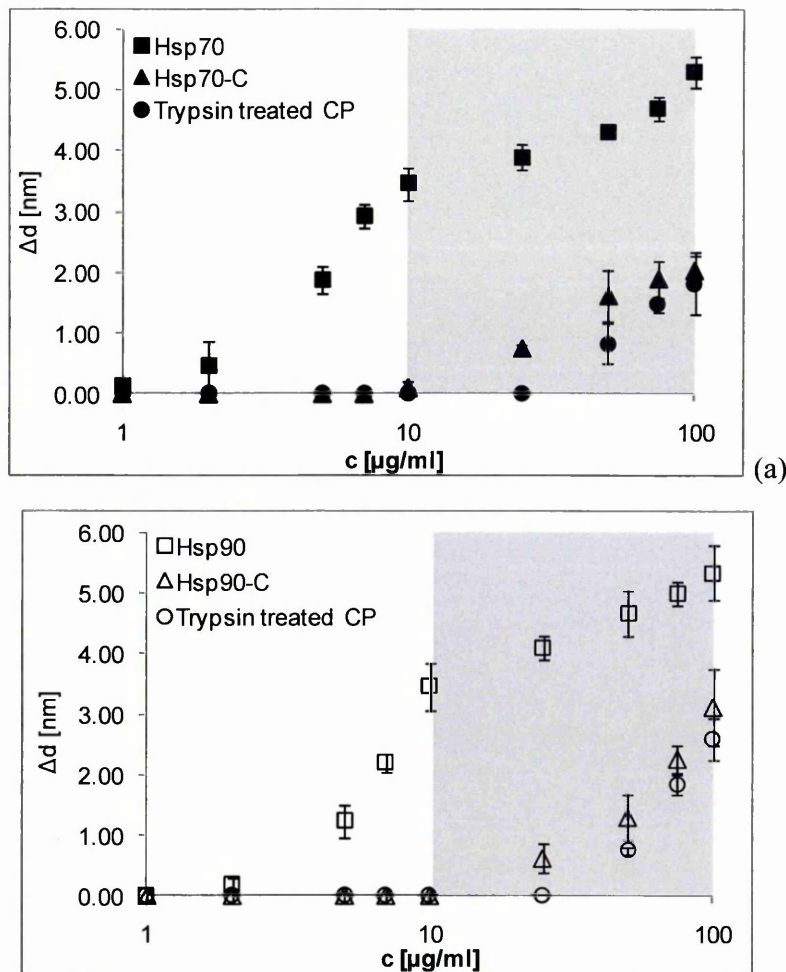


Figure 6.3 Calibration curves for Hsp70 (a) and Hsp90 (b) chaperones binding to receptors present in chloroplast membrane.

As one can see on Fig. 6.3 a, the calibration curve (layer thickness increment Δd vs. increasing chaperone concentrations) for Hsp70 (■) shows a typical rising with the concentration increasing up to saturation when all receptors are occupied. This is followed by a further increase of Δd which is an indication of non-specific binding. Similar features can be observed in Fig. 6.3 b for binding Hsp90 (□) chaperones to native chloroplast membranes. Two types of negative control: (i) truncated chaperone proteins (Hsp70-C and Hsp90-C; ▲ and Δ) and (ii) chloroplasts treated with the protease trypsin (● and ○) were performed in order to distinguish between specific and nonspecific binding. Grey background indicates the area of nonspecific binding, when the concentration of chaperons is higher that of the adsorbed receptors.

Both chaperones showed binding characteristics very similar to those observed earlier for binding chaperones to receptors immobilized on the surface electrostatically.

6.1.4 Analysis of chaperone binding kinetics

For the evaluation of the association (or affinity) constants a standard procedure of adsorption kinetics was used. The interaction between receptor and chaperone was monitored by observing changes in the sensor response. First, the time constants (τ) were determined from the time dependences of the ellipsometric parameter Δ recorded during dynamic TIRE measurements at different chaperone concentrations. Figure 6.4(a) shows typical time dependences of Δ recorded during the binding of Hsp70 and Hsp90 chaperones and the fitting to a first order exponential decay function $\Delta = \Delta_{\max} \exp(-t/\tau)$. Then the reciprocal values of the time constants ($1/\tau$) were plotted against the concentration of chaperones (C) as shown in Figure 6.4 (b) and fitted to a linear function $1/\tau = k_a C + k_d$. The rates of adsorption (k_a) and de-sorption (k_d), respectively, were calculated from the gradient and intercept of the above line; the association and affinity constants defined respectively as $K_A = k_a/k_d$ and $K_D = 1/K_A$ can therefore be evaluated. Data points in Figure 6.4(b) were obtained by averaging the results of several TIRE kinetic measurements. The obtained values of the gradient (k_a) and intercept (k_d) as well as the resulting values for K_A and K_D are given on respective graphs. The standard deviations were calculated as

$$\Delta K_A = \frac{k_a \Delta k_d - k_d \Delta k_a}{k_d^2}; \quad \Delta K_D = \frac{\Delta K_A}{K_A^2} \quad (6.1)$$

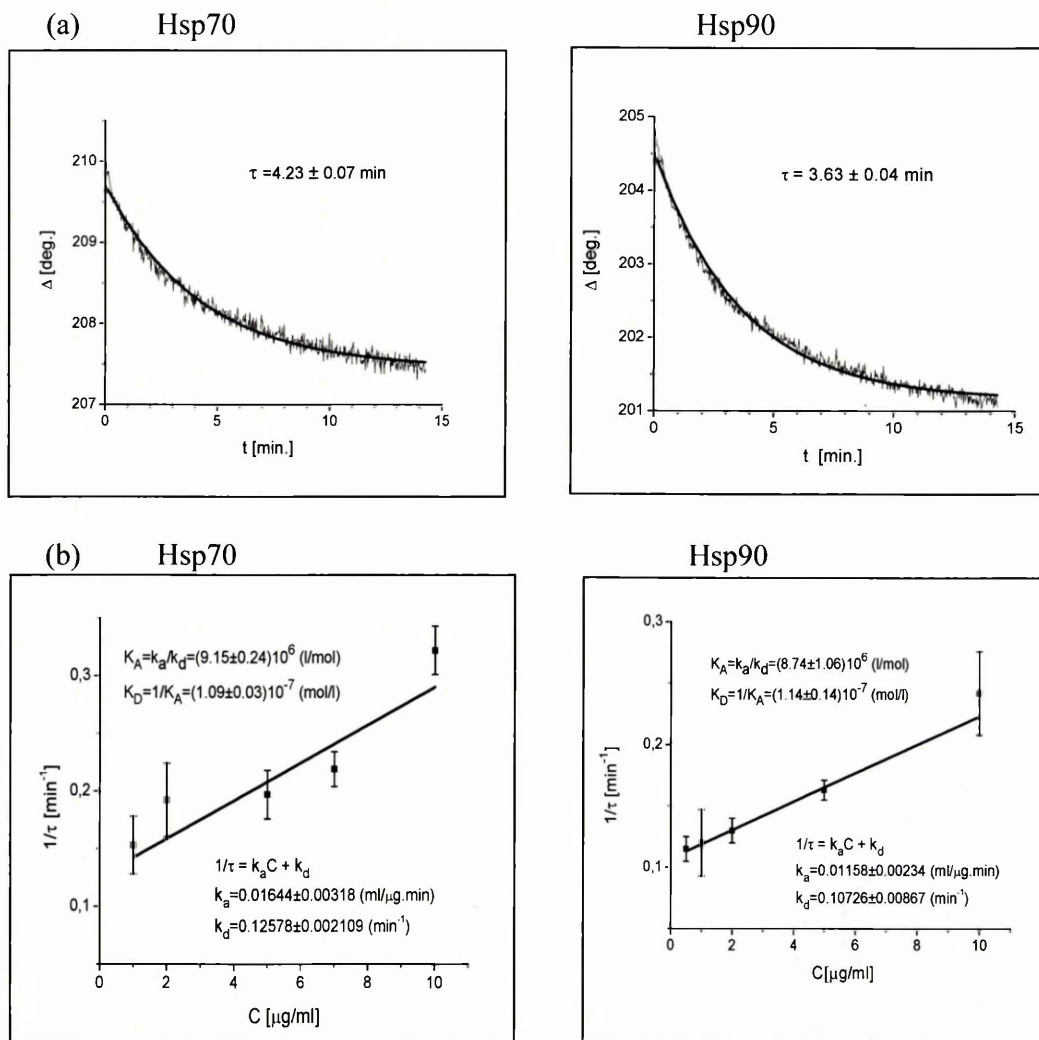


Figure 6.4 Dynamic TIRE measurements (a) and evaluation of the association constants (b) for binding chaperones Hsp70 and Hsp90.

The values of the association constant (K_A) were calculated for chaperone concentrations from 1 $\mu\text{g/ml}$ up to 10 $\mu\text{g/ml}$, representing the area of specific membrane binding (Fig.6.3). K_A values were determined as $(9.15 \pm 0.24) \times 10^6$ (l/mol) for Hsp70 and $(8.74 \pm 1.06) \times 10^6$ (l/mol) for Hsp90. For comparison Hsp70 and Hsp90 bind their co-chaperone the Hsp70-Hsp90-organising protein (Hop) with a K_A of 7.7×10^5 (l/mol) and 1.1×10^7 (l/mol), respectively providing further evidence that specific membrane interactions are being observed [38]. The K_A values are two to three orders of magnitude lower than the affinity constants previously calculated for chaperones with the recombinantly expressed receptors OEP61 and Toc64 which is probably due to the change to a more native environment and unspecific binding to proteins at the native membranes resulting in a higher dissociation rate.

6.2 Study of Aflatoxin B1 binding to polyelectrolyte capsules

This section is dedicated to the study of binding aflatoxin B1 (AFT B1) to polyelectrolyte microparticles functionalized with specific antibodies using UV-vis absorption spectroscopy. The purpose of this work was to establish a new technology of purification of substances containing Aflatoxin. Later this method was utilized for cleansing MC-LR.

6.2.1 Functionalization of microcapsules

The capsules were prepared by coating the MnCO_3 core particles of 4 μm in diameter (the core are from Dr. A. Nabok) by layers with PAH and PSS as described in Fig. 12 (Chapter 3). We used the particles (still retaining the core) with four PAA/PSS bi-layers, terminating in PAH layer. In this work the particles were functionalized with monoclonal antibodies specific to aflatoxin B1 (AFT B1). For this purpose the particle suspension was mixed in a 1:1 ratio with a 100 μg AflatoxinB1 solution for 15 minutes. Then the mixture was let to sediment for 30 min. After sedimentation of particles the liquid (above the sediment) was removed with a micropipette and the flask was topped up with water for rinsing purposes. The mixture was stirred for 5 min and let to sediment; after 30 min the liquid again was removed with a micropipette. Such a rinsing procedure was repeated three times ending with particles being coated with Protein A. In the next stage, particles were functionalized with antibodies following the procedure described above.

The resulting microcapsules functionalized with Protein A and Antibodies to AFT B1, were viewed with IFM and a typical image obtained is shown in Figure 6.5.

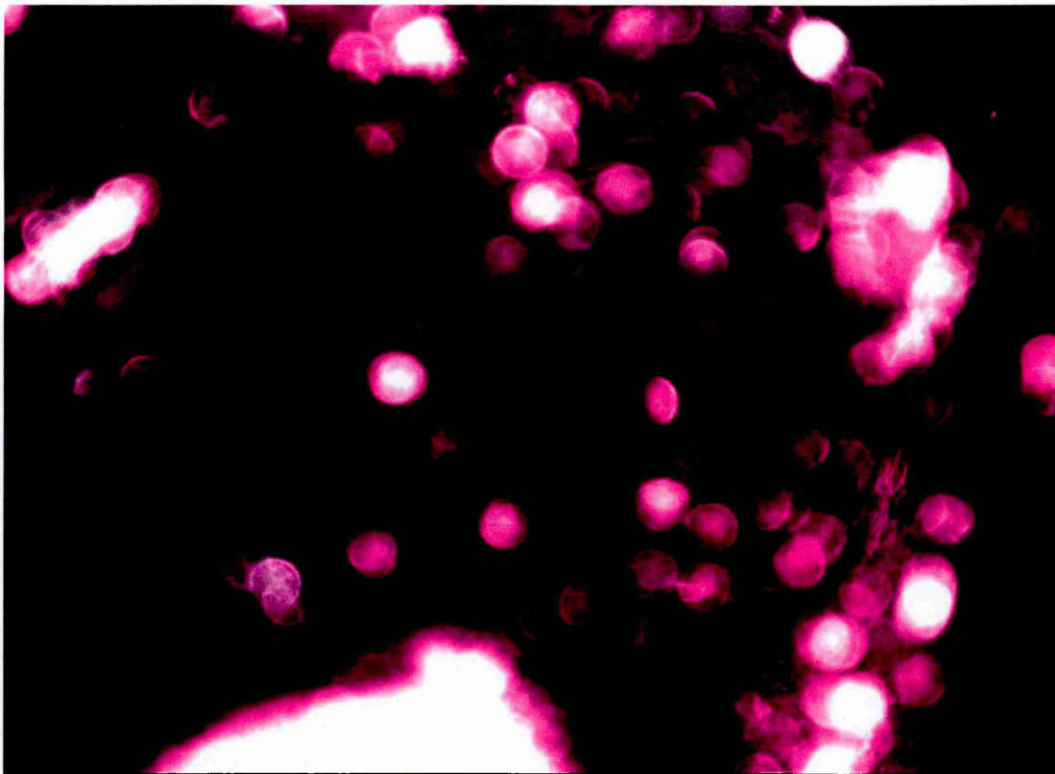


Figure 6.5 IFM image of microcapsules functionalized with antibodies to Aflatoxin B1.

SEM images were recorded for the same purpose and shown in Figure 6.6; the particles size was found to be about 5.15 μm in diameter.



Figure 6.6 SEM image of a microparticle with antibodies to Aflatoxin B1.

6.2.2 UV-vis absorption spectra study

In order to study the binding of AFT B1 to functionalized microparticles, a series of UV-vis absorption spectra were performed using Carry-50 (Varian) spectro-photometer. First, the spectrum of a quartz cuvette filled with de-ionized water was recorded as a reference (see horizontal line in Figure 6.7). Then, we recorded a spectrum of pure solution of AFT B1 which was prepared by diluting the original 10mg/ml stock solution of AFT B1 in methanol. Top curve represent the absorption spectra of 10 μ g/ml solution of AFT B1 having three characteristic absorption bands at about 224nm, 266nm, and 362nm. Since the band at 362 nm is the most intensive, we will monitor its amplitude after binding AFT B1 [166].

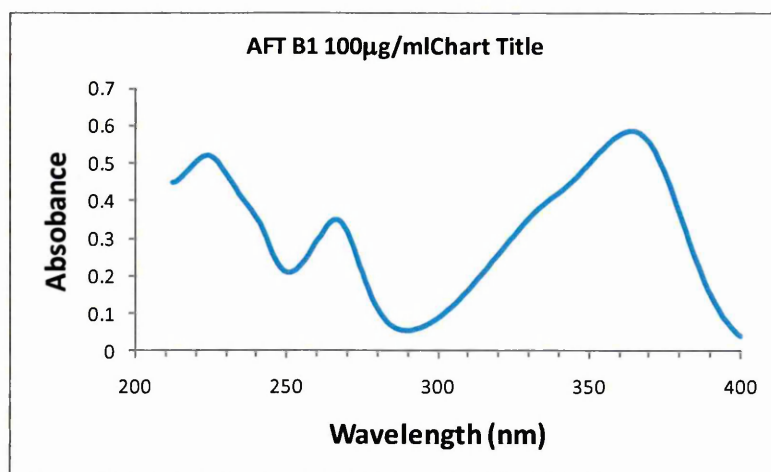


Figure 6.7 Uv-vis absorption spectra of 100 μ g/ml aqueous solution of AFT B1

The suspension of capsules modified with anti-AFT was mixed with a solution containing Aflatoxin B1. It was stirred for 5 minutes and left undisturbed for up to 30 minutes. The optical absorption spectra were recorded on samples of untreated solution of AflatoxinB1 as well as after treatment with microcapsules at various times. The results are shown in Figure 6.8.

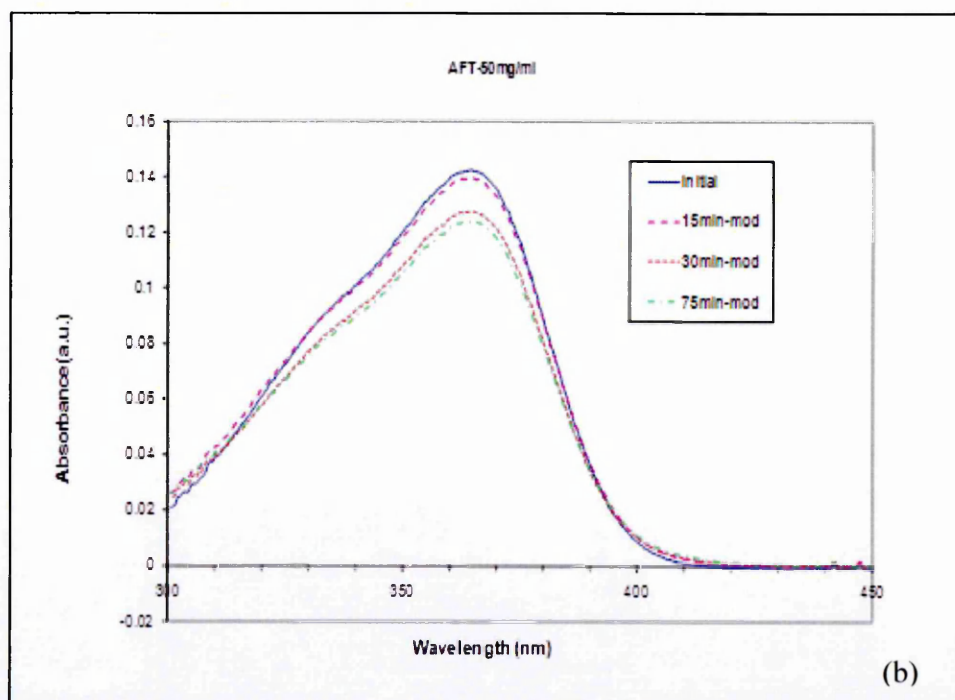
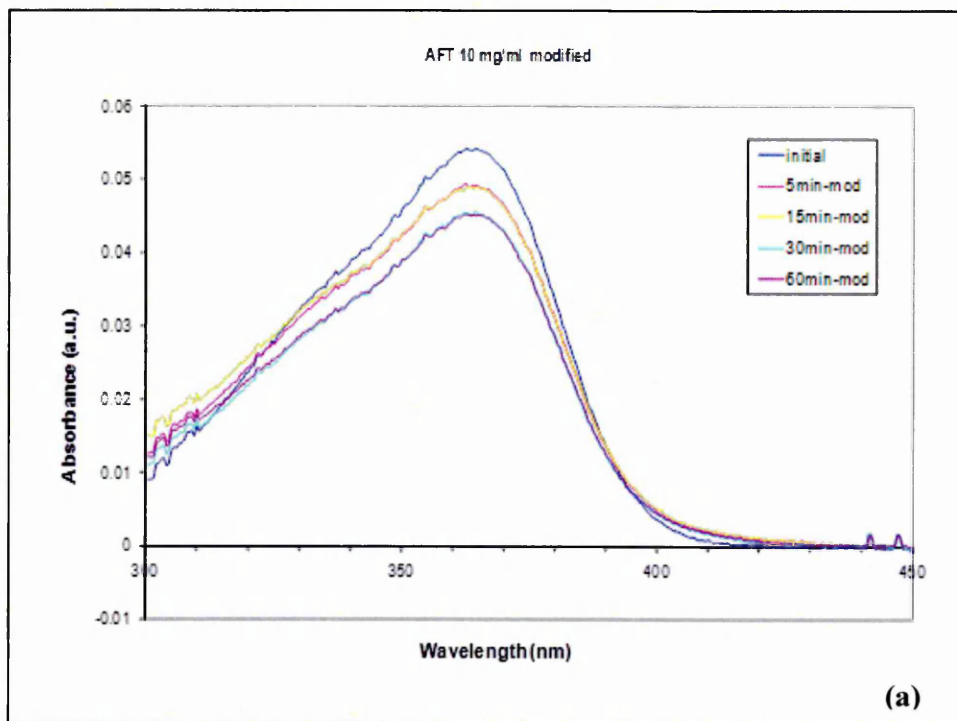


Figure 6.8 Spectra of AFT B1 solutions of (a) 20mg/ml and (b) 50 mg/ml concentrations, mixed with microparticles and incubated for a different periods of time;

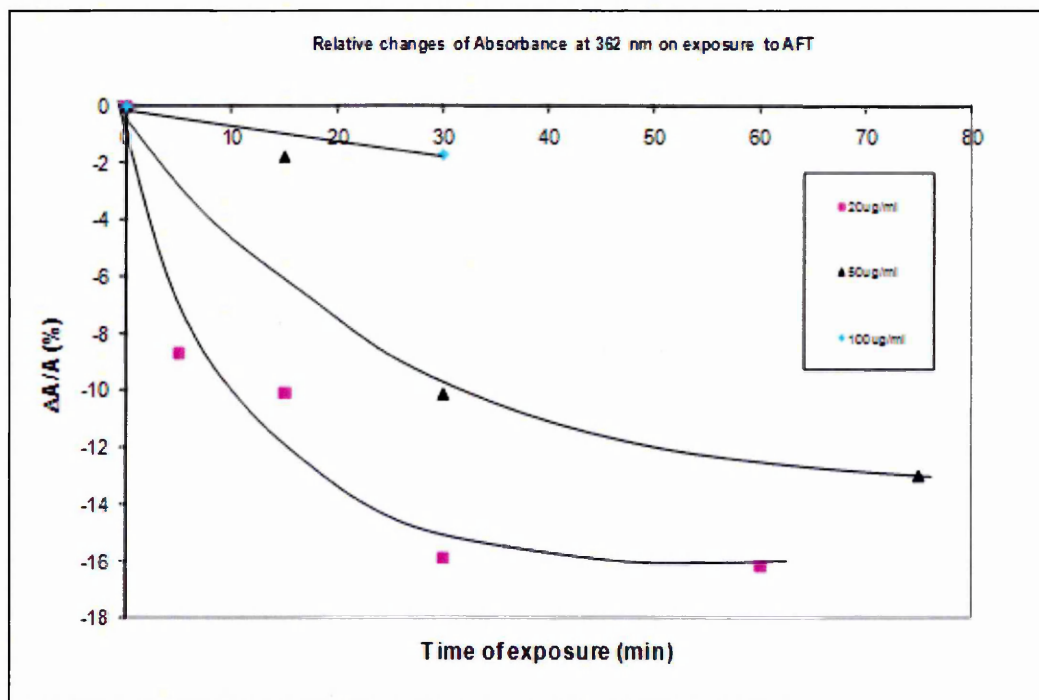


Fig. 6.9 The dependence of 362 nm band intensity of AFT B1 on the incubation time.

The results obtained clearly show the reduction of the 362 nm absorption band intensity in the course of the treatment of AFT B1 solution with functionalized micro-capsules. This can be explained by binding aflatoxin molecules to antibodies followed by sedimentation of heavy micro-particles. As a result the solution above the sediment contains less amount of aflatoxin. Obviously, solutions of higher concentration of AFT B1 are less affected by cleansing with capsules. Similar effect, i.e purification of the solution containing another mycotoxin, zearalenone, was observed earlier with the use of microcapsules functionalized with anti-zearalenone [167 - 169].

It is clear from the data presented in Fig.6.8 a,b that treatment of the AFT solution with micro particles functionalized with anti-AFT causes the reduction in the absorbance values; and that the larger incubation time results in more pronounced reduction in absorbance. The reduction in absorbance at the band maximum at 362 nm was investigated in more detail in Figure 6.9. A monotonous decrease of relative absorbance change ($\Delta A/A$) with a trend to saturation was observed at all concentrations of AFT studied. However, the concentration dependence was non-monotonous: a small absorbance increment was observed for 5 $\mu\text{g/ml}$ solution of AFT, and it reached the maximum at 10 $\mu\text{g/ml}$ and then started to fall again with a concentration increase to 25

and 50 µg/ml. The trend for a decrease in $\Delta A/A$ with an AFT concentration increase was caused by the saturation of absorption sites, i.e., antibodies, on the surface of the microparticles. A deviation from this trend at the lowest concentration of AFT of 5 µg/ml can be explained by the inaccuracy of spectral measurements such as noise and the deviation in the reference spectra. The maximal purification effect was achieved at the concentration of AFT of 10 µg/ml which corresponds roughly to the number of binding sites on the surface of microparticles. Knowing the molecular weight of AFT of 318.36 g/mol, the concentration of AFT molecules in its 10 µg/ml solution can be estimated as $N_{\text{AFT}}=2 \cdot 10^{16} \text{ cm}^{-3}$. The reduction of Abs on 16.2 % yields approximately $\Delta N_{\text{AFT}}=3 \cdot 10^{15} \cdot \text{cm}^{-3}$ for AFT molecules adsorbed on the microparticles. On the other hand, from the preparation of the microparticle suspension from initial the 0.6 mg/ml solution of 6 µm MnCO₃ core particles in water, the concentration of microparticles can be estimated as 10^7 cm^{-3} using the density of MnCO₃ in the range of 3.1–3.4 g/cm³ and taking into account about 30 % of material loss during multiple rinsings. Simple calculations of the number of binding sites (Nb.s.) for AFT on the surface of a microparticle having a radius $r=3 \text{ µm}$ can be calculate as:

$$N_{b.s.} = \frac{4\pi r^2}{2A_{\text{IgG}}} \approx 10^8 \quad (6.2)$$

It was assumed that the area occupied by an antibody on the surface $A_{\text{IgG}} \approx 20 \text{ nm}^2$, factor 2 in the determinant indicates two binding sites corresponding to two Fab fragments of IgG molecule. Therefore, the maximal absorption capacity of the microparticle suspension used can be estimated as 10^{15} cm^{-3} ; in other words, 1 ml of microparticle suspension is capable of absorbing 10^{15} molecules of AFT. This is quite close to the value of $\Delta N_{\text{AFT}}=3 \cdot 10^{15} \text{ cm}^{-3}$ which was found experimentally for 10 µg/ml AFT solution. Using similar calculations for all concentrations of AFT, the reduction in the absorbance can be estimated; the results of such calculations are summarized in Table 6.2. As can be seen, the reduction in $\Delta A/A$ was estimated reasonably accurately (particularly for low concentrations of 5 and 10 µg/ml) with a clear tendency for a decrease in the purification effect with the increase in AFT concentration. It is predicted that the purification of the sample with an AFT concentration of 50 µg/ml will be minimal (around 1 %).

Table 6.2 Calculation of absorbance reduction caused by adsorption of AFT on microparticules.

AFT concentration ($\mu\text{g/ml}$)	$N_{\text{AFT}} (\text{cm}^{-3})$	$-\Delta A/A(\%)$	$-\Delta A/A(\%)$ estimated
5	10^{16}	9.2	10.0
10	$2 \cdot 10^{16}$	16.2	5.0
25	$5 \cdot 10^{16}$	13	2.0
50	10^{17}	1.7	1.0

6.2.3 Conclusions

Polyelectrolyte microparticles retaining a MnCO_3 core and functionalized with antibodies specific to aflatoxin B1 were made and characterized with SEM. Protein deposited was clearly visible on SEM images. Reduction in the concentration of aflatoxin B1 in solution was achieved after treatment with microparticles functionalized with respective antibodies. These preliminary experiments proved the concept of using functionalized microparticles for detoxification of substances containing mycotoxins. Although can use these polyelectrolyte after they have functionalized with an antibody specific to microcystin-LR which is released by algae. Such a phenomenon can be utilized for the purification of substances contaminated with mycotoxins as well as other toxins including microcystin. As explained in Chapter 7.

Smaller-sized microparticles having a larger surface area could be more effective for the absorption of mycotoxins, in order to prove the principle; we deliberately used larger 4–6 μm particles which are heavier and thus sediment quickly. This research may lead to a number of possible applications of the new technology of mycotoxin scavenging in the areas of agriculture, food industry, environmental control, security, and biomedicine.

In summary, these studies of protein chaperon demonstrated that chloroplasts can be deposited on gold coated glass slides by Langmuir-Schaefer technique, whilst retaining functionality of the resident receptors. Binding of receptors to their specific protein partner can be directly monitored using TIRE, without the need for labels. Potentially,

molecular interactions with any other type of membrane, such as mitochondrial or ER membranes, could be analyzed using this combination of Langmuir-Schaefer films and spectroscopic ellipsometry and is the focus of ongoing work. As such, this technique opens many possibilities including the quantification of protein interactions involved in fundamental cellular processes, and rapid screening of drugs that target membrane proteins.

CHAPTER 7

TIRE DETECTION OF MICROCYSTIN-LR

7.1 Detection of microcystin-LR using TIRE

In this chapter experimental results on the detection of Microcystin LR (MC-LR) using direct immunoassay with specific MC10E7 monoclonal antibodies and TIRE detection are presented and discussed.

7.1.1 Samples preparation and TIRE measurements

The following chemicals were used in this work: The immune pair MC-LR and specific monoclonal antibodies MC10E7 (from Enzo Life Scientific) were used for both the immunoassay calibration and detection of natural MC-LR. For TIRE measurements antibodies were immobilized electrostatically on gold coated glass slides following the procedure described earlier in Chapter 4 and 6. The following sequence of adsorptions was used: the surface of Au layer was modified with the mercapto-ethyl sodium sulfonate ($\text{HS}-(\text{CH}_2)_2-\text{SO}_3^- \text{Na}^+$) to enhance the negative charge; the slides flooded with its 100mM solution in methanol overnight, then washed with methanol the next day. Then the poly-cationic layer of PAH was bound to the negatively charge substrate. Protein G molecules which are negatively charged in Triz-HCl buffer pH 8.0 were deposited on PAH, then MC10E7 antibodies were bound to Protein G via a binding site in the second domain and are ready to bind the antigen, i.e. MC-LR. Triz-HCl buffer PH 8.2 was used for rinsing the cell after molecular binding.

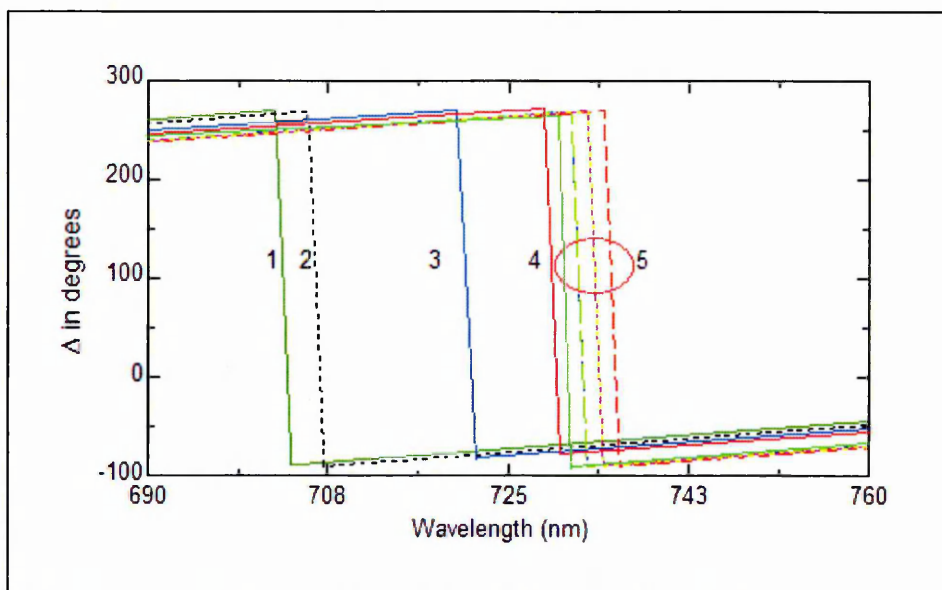
Two types of TIRE measurements were typically carried out: (i) dynamic TIRE measurements for monitoring chemical reactions (adsorption and immune binding, and (ii) single spectroscopic scans which were typically carried out in a standard Tris/HCl buffer (pH 8.0) after the completion of the every adsorption (or binding) stage. Dynamic spectral measurements were used for the study of kinetics of adsorption and binding and allowed the evaluation of the association constant of the immune reaction. While the spectra of ψ and Δ obtained from single spectroscopic scans were used for data fitting and subsequent evaluation of the thickness of adsorbed molecular layers. TIRE measurements and fitting procedure were described in detail previously [116,117].

7.1.2 TIRE study of the immune reaction between MC LR and antibody MC10E7

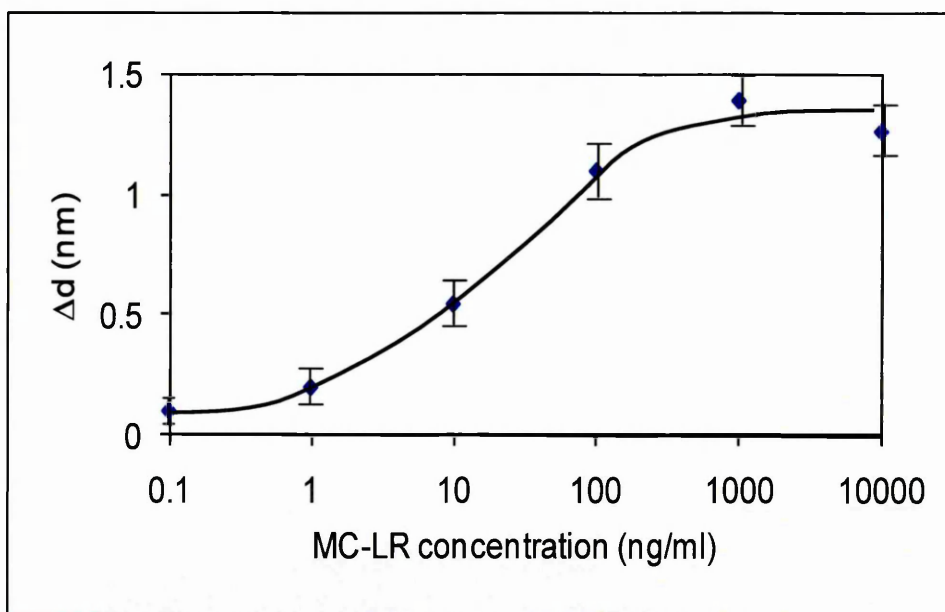
Figure 7.1a shows a typical series of (ψ) and (Δ) spectra recorded on the samples of gold treated with $\text{SH}-(\text{CH}_2)_2-\text{SO}_3^- \text{Na}^+$ (curve 1), then after electrostatic deposition of the PAH layer (curve 2), after the electrostatic deposition of Protein G (curve 3), and after the deposition of MC10E7 antibodies (curve 4). The remaining curves (5) correspond to the sequential binding of microcystin in different concentrations (starting from the smallest 0.1 ng/ml up to 10 $\mu\text{g/ml}$). All deposition and binding stages (1 – 4) were performed by injecting corresponding solutions into a TIRE cell of 0.2 ml in volume. Intermediate rinsing was performed between adsorption (binding) steps by purging 2 - 3 ml of water or buffer through its cell. In-situ dynamic spectral measurements were performed during all adsorption and binding steps. Single spectroscopic scans (shown in Fig. 7.1(a)) were performed in a standard Tris-HCl buffer solution (pH 8) after completion of all stages of adsorption (or binding).

It is clearly seen in Fig. 7.1a. that the spectral shift corresponds to the size (or rather molecular weight) of molecules attached: a small PAH polymer chain causes a small spectral shift, while the much larger molecules of protein G and MC10E7 antibodies yield larger spectral shift, Relatively small analyte molecules of MC-LR (molecular weight of less than 1000 Dalton) caused a measureable shift even at small concentrations of 1 ng/ml. More precise conclusions on MC LR binding can be made after fitting TIRE data to a model similar to that described earlier in Chapter 6.

Figure 7.1 b shows the results of ellipsometry data fitting, i.e. the dependence of the adsorbed thickness increment vs. concentration of microcystin. As one can see, the low detection limit of microcystin was between 0.1 and 1 ng/ml. The maximal thickness increment of about 1.2 nm is reasonable for a non-complete monolayer of MC-LR molecules of 3 nm. The study of binding kinetics yields the association constant K_A in the range of 10^7 l/mol, which is typical for the highly specific immune reaction between MC-LR and MC10E7 antibodies.



(a)



(b)

Figure 7.1,(a) Series of TIRE spectra recorded after each deposition step. (b) Calibration curve for MC-LR was measured through a series of dilutions beginning with 0.1 ng/ml up to 10000 ng/ml from commercial toxin, and this curve is used to indicate the concentration of natural toxin which extracted from algae.

Table 7.1 shows TIRE fitting data for immune reaction between microcystin-LR and antibody MC10E7. The Asterisk (*) sign indicates that the parameters were fixed during fitting. The values of n and k are given at the wavelength of 633 nm.

We evaluated the molecular layer thickness increment by doing data TIRE data fitting to the reflective system model consisting of glass (BK7) as an ambient, a Cr/Au metal layer, the deposited molecular layer, and aqueous solution. The data fitting procedure has been described in detail previously in Chapter 4 [116-117]. It is based on solving Fresnel equations and minimizing the error function between calculated and experimentally obtained ψ and Δ parameters at each spectral point using least-square techniques (least squares means that the overall solution minimizes the sum of the square of the errors made in the results of every single equation) [171,172-175]. The optical constants of glass and the aqueous buffer solution were kept constant; The thickness (d) and dispersions of n and k , being real and imaginary parts of complex refractive index $N = n - jk$, of the Cr/Au layer were fitted first before depositing molecular layers, and this was fixed at consecutive fitting. The adsorbed molecular layers were modeled by a Cauchy dispersion $n = A + B/\lambda^2 + C/\lambda^4$ typical for transparent ($k=0$) dielectric materials. Since all molecular layers used have similar refractive index ($n=1.42$ at 633 nm) [78, 116-117] it was fixed during the fitting and all changes in the adsorbed layers were associated with changes in the effective layer thickness (d).

Table 7.1 TIRE fitting results for immune reaction between microcystin-LR and antibody MC10E7. Asterics indicate parameters which were fixed during fitting.

Microcystin-LR accumulated concentration(ng/ml)	Δd (nm)	n, k (at $\lambda=633$ nm)
0.1	0.161	$n^* = 1.42, k=0$
1	0.189	$n^* = 1.42, k=0$
10	0.547	$n^* = 1.42, k=0$
100	1.11	$n^* = 1.42, k=0$
1000	1.212	$n^* = 1.42, k=0$

Protein G(65 kDa) and protein A(42 kDa) were used in our work. An intermediate layer of protein G molecules having a binding site within the Fc region of the IgG-type antibodies and also within the Fab region, were used to orient antibodies with their Fab fragments towards the solution as shown in Fig 7.1. The antibody MC10E7 have binding site also with protein A as shown in Fig. 7.2.

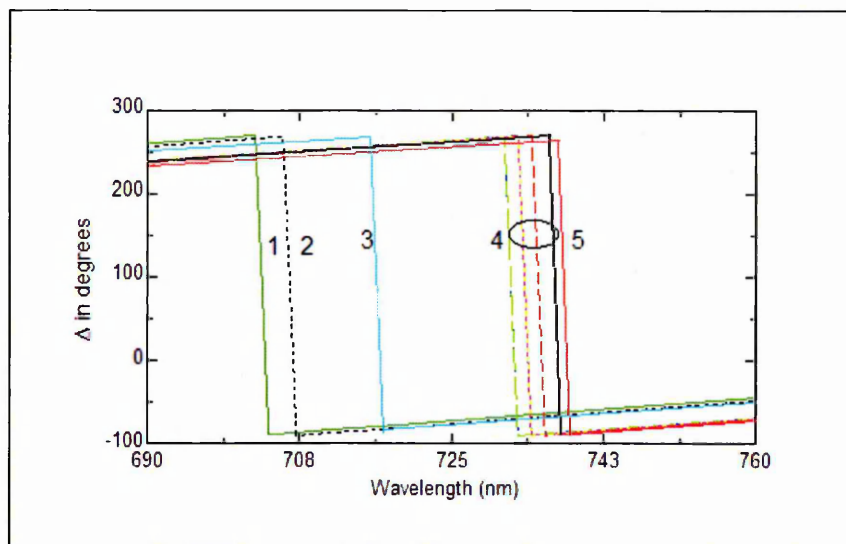


Figure 7.2 Spectral shift recorded after each deposition step, add protein A.

7.1.3 Study of MC-LR and MC10E7 binding kinetics

The time evolution, i.e. kinetics of Ψ and Δ , provide important information for instance analysis of the kinetics allows the researcher to calculate adsorption and desorption coefficients as well as the association constant of the reaction. The kinetics of binding of microcystin-LR to specific antibody MC10E7 were studied by measuring TIRE spectra every (1 to 20) second (depending on the duration of the kinetics scan) during the exposure to microcystin-LR solution which was typically for 15-20 min. The time dependences of either Ψ or Δ could be obtained at selected wavelengths. Time dependencies of Ψ and Δ at 633 nm of different concentration of microcystin-LR in the range 0.1 ng/ml to 1 μ g/ml were extracted from TIRE dynamic spectral measurements during binding of MC-LR to MC10E7 antibodies immobilised on the surface. Typical kinetic curves for 0.1 ng/ml MC-LR during binding are shown in Figure 7.4. It was demonstrated that a 15 min. incubation time was sufficient to reach the saturation at the lowest concentration of MC-LR.

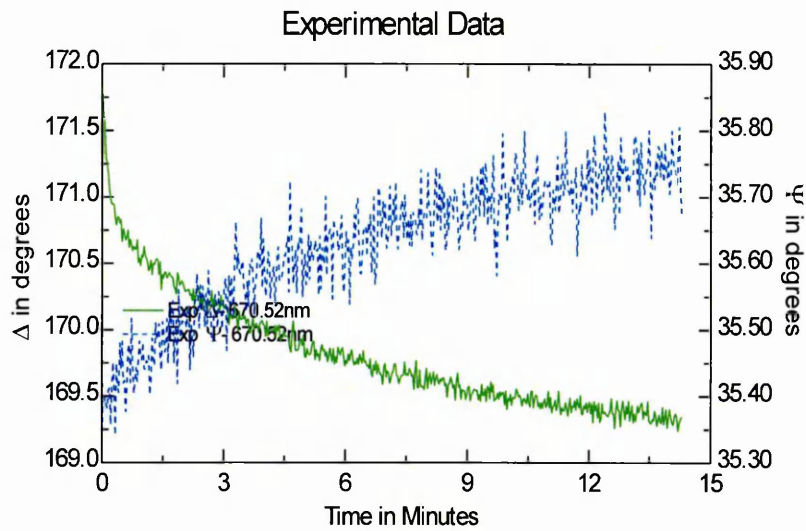


Figure 7.3 Typical dependencies of $\Psi(t)$ and $\Delta(t)$ Evaluation of the during MC-LR & MC10E7 binding.

Then the procedure for the evaluation of rates of adsorption (k_a) and desorption (k_d) of the immune reaction was applied [176-178]. The characteristic time constant (τ) of the immune reaction was evaluated by fitting the data to the exponential function of Δ .

The inverse value of the time constant was plotted against the concentration of the antigen in Figure 7.4, and the values of k_a and k_d were found, respectively, from the gradient and intercept of the linear graph. The values of k_a and k_d obtained from the graph allowed the calculation of the association and affinity constant as: $K_A = k_a/k_d$ and $K_D = 1/K_A$

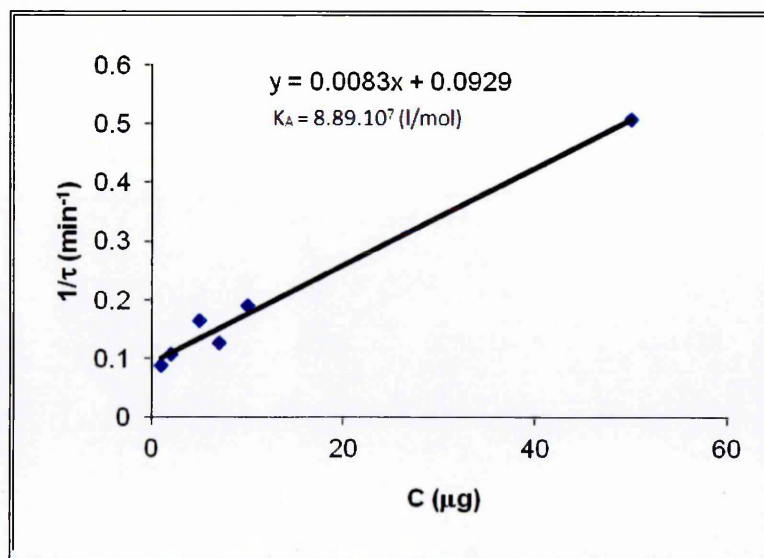


Figure 7.4 to the evaluation of the association constant K_A .

The linear equation for the graph in Fig. 7.4 is: $S = 0.0083 C - 0.0929$

After adjusting the units and given the molecular weight for MC-LR of 995.2 Da:

$$k_a = 0.0083 \left[\frac{ml}{ng \cdot min} \right] = 83 \cdot 10^{-5} \frac{10^{-3}}{10^{-9} \cdot 60} \left[\frac{l}{g \cdot s} \right] = 13.833 \left[\frac{l}{g \cdot s} \right]$$

$$k_a = 13.833 \cdot 995.2 = 13181.76 = 1318176 \cdot 10^{-7} \left[\frac{l}{g \cdot s} \right]$$

$$k_d = 0.0929 \left[\frac{1}{min} \right] = \frac{0.0929}{60} = 0.00154 \left[\frac{1}{s} \right]$$

The association constant is therefore equal to:

$$K_A = \frac{k_a}{k_d} \left[\frac{l \cdot s}{mol \cdot s} \right] = \frac{13181.76}{0.00154} = 8.89 \cdot 10^7 \left[\frac{l}{mol} \right]$$

And the affinity constant is equal to:

$$K_D = \frac{1}{K_A} = 1.1682 \cdot 10^{-7} \left[\frac{mol}{l} \right]$$

The obtained values of $K_A = 8.89 \cdot 10^7$ (l/mol) and $K_D = 1.1682 \cdot 10^{-7}$ (mol/l) are typical for a highly specific immune reaction with monoclonal antibodies.

Negative control

It is known that microcystin-LR has a negative charge. To ensure that MC-LR do not bind directly to PAH in the gaps between antibodies these potential binding sites were blocked with BSA (66.5 KDa). For that purpose the slides were treated for 2 hours in the 10 mg/ml solution of BSA in PBS (100 mg BSA was dissolved in 1000 ml of PBS); for maximal blocking efficiency pH was adjusted to 8.0 [179].

injection PAH, followed by protein A or G. Microcystin-LR didn't bind as shown in Figure 7.6, as MC-LR has specific binding site with the antibody MC10E7[180-183]. The study of binding kinetics yields, the association constant K_A in the range of 10^3 l/mol, as shown in Fig 7.5 without antibody meaning there is no binding as shown in Fig. 7.6 (a) and (b). And the spectral shift was appeared sm

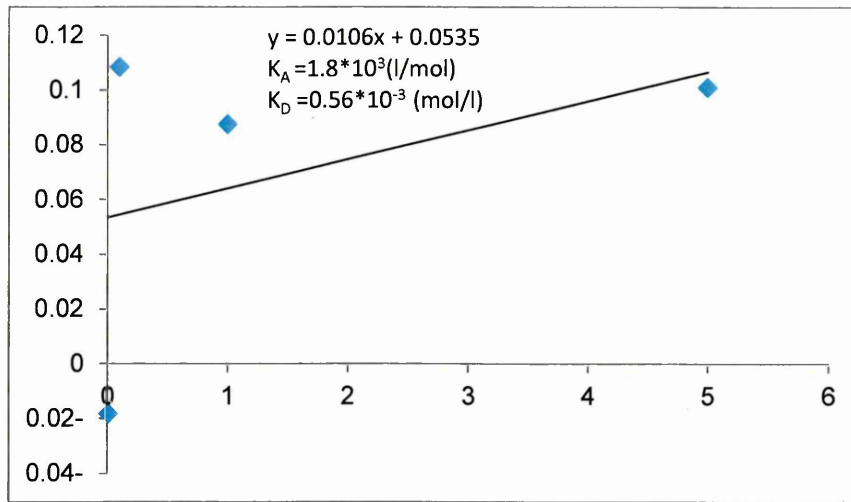


Figure 7.5 Binding kinetics yields the association constant K_A in the range of 10^3 l/mol, without antibody

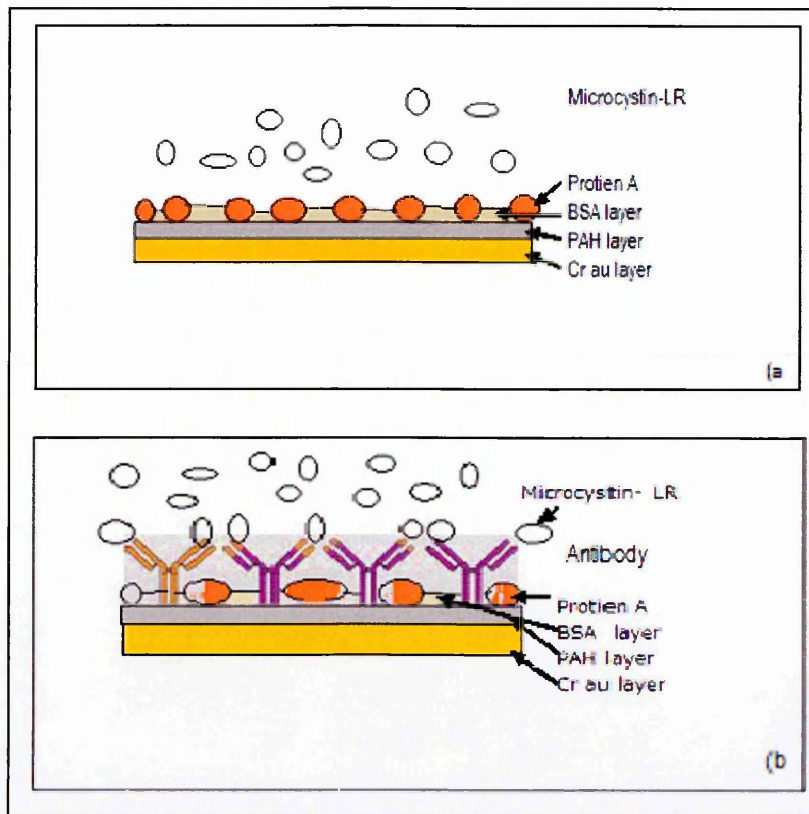


Figure 7.6 the negative test for blocking spaces between the antibody and protien A. In (a) there is no binding because there are no antibodies were immobilized, while in (b) there is binding occur.

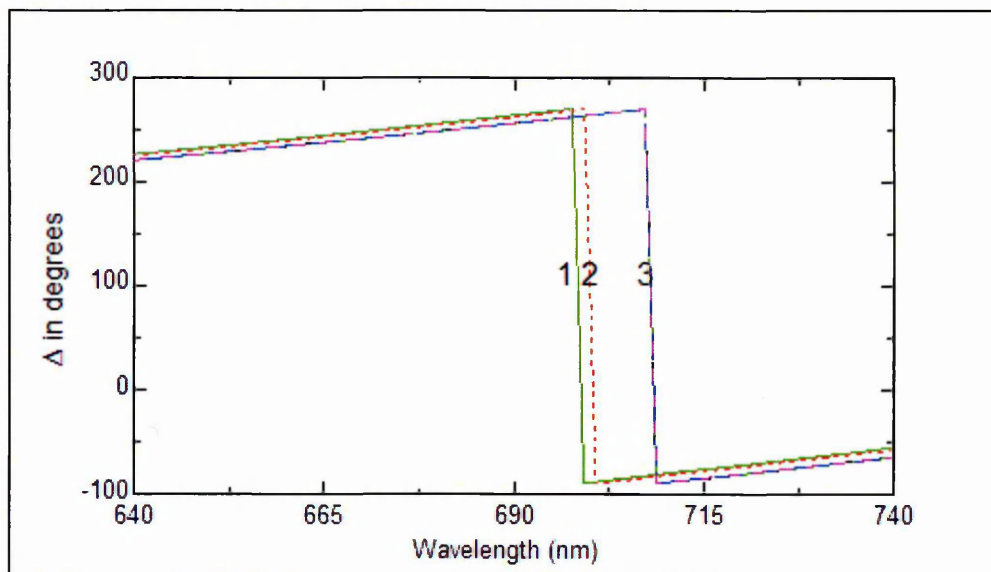
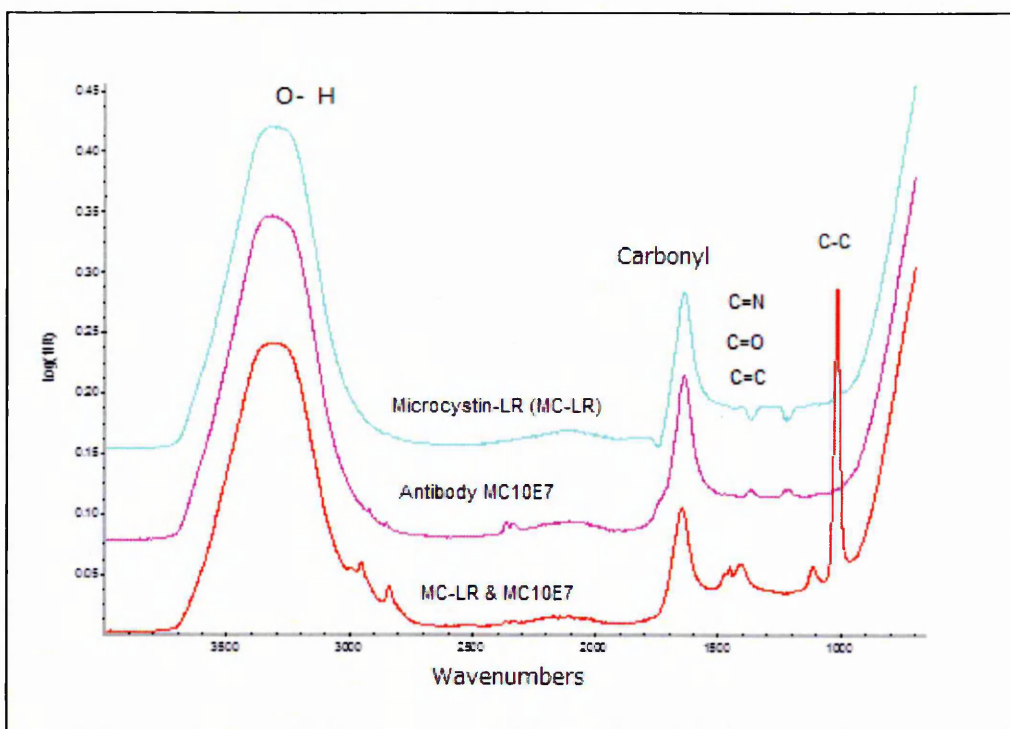


Figure 7.7 Spectral shift for negative control without antibody, layer (1) is CrAu, layer (2) is PAH, layer (3) Protein A, layer (4) BSA. There is no binding.

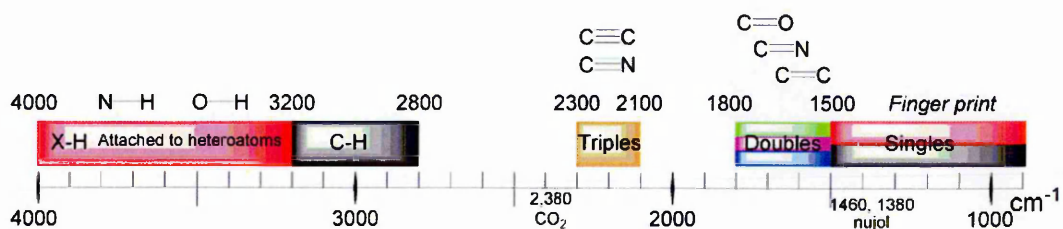
The spectral shift after deposition of the layers, shows no shift after (BSA layer).

7.2 Fourier transform infrared spectrometer (FT-IR) measurement

The interaction between microcystin-LR and the antibody MC10E7 was studied by FT-IR spectra. Microcystin-LR and its specific antibody were analysed for their infrared spectra. As shown in Figure 7.8 (a), the bands at 3300 cm^{-1} and 1600 cm^{-1} correspond to the stretching vibrations associated with $-\text{OH}$ and $-\text{NH}_2$ groups, and the bands near 1400 cm^{-1} and 1200 cm^{-1} are the stretching vibration of $-\text{NH}_2$ of microcystin-LR. The band at 1594 and 1378 cm^{-1} are due to the bending vibrations of $-\text{NH}_2$ and the stretching of $\text{C}-\text{N}$. In the spectra of MC-LR/antibody complex, the band at 1594 cm^{-1} , which belongs to the $-\text{NH}_2$ bending vibrations and a new band at 1000 cm^{-1} appeared which indicates the generation of some new chemical bonds. When comparing experimental spectra with (a) with the scheme of vibration bands (b) the band at 1000 cm^{-1} appears and the absorption intensity of the band at 1151 cm^{-1} increases which was most-likely caused by the binding between the antibody MC10E7 and microcystin-LR. The FT-IR spectra of the antibody and the toxin proved that interaction was strong, and is rich with many active functional groups, such as $-\text{OH}$ and $-\text{COO}^-$, which can spontaneously link to the active amino groups of the (antibody) [184-186].



(a)



(b)

Figure 7.8 (a) FT-IR spectra of 1 MC-LR, antibody MC10E7, and MC10E7/ MC-LR immune complex.(b) The scheme of molecular vibration in the system illustrating region of active functional group.

7.3 UV-visible spectral study of microcystin-LR

UV-visible absorption spectroscopy (Varian, Carry 50) was used to monitor the concentration of MC-LR in solutions. The UV spectrum for MC-LR showed a peak at 238–240 nm. The spectrum of a quartz cuvette filled with de-ionized water was recorded as a reference then, we recorded the spectrum of pure solution of MC-LR 5 $\mu\text{g/ml}$. Following the procedure developed earlier [184] micro-particles functionalized with MC10E7 antibodies were utilized for purification of solutions containing MC-LR.

In terms of spectroscopy, the solutions for MC-LR of different concentrations were mixed 1:1 with a suspension of functionalized microparticles and incubated for up to 1 hour. Heavy particles sediment on the bottom of sample tubes leaving purified solutions above. The results obtained clearly show the reduction of the 238 nm absorption band intensity in the course of the treatment of the MC-LR solution, with functionalized micro-capsules. This can be explained as a result of the binding of MC-LR molecules to antibodies followed by the sedimentation of heavy micro-particles as shown in Fig. 7.9.

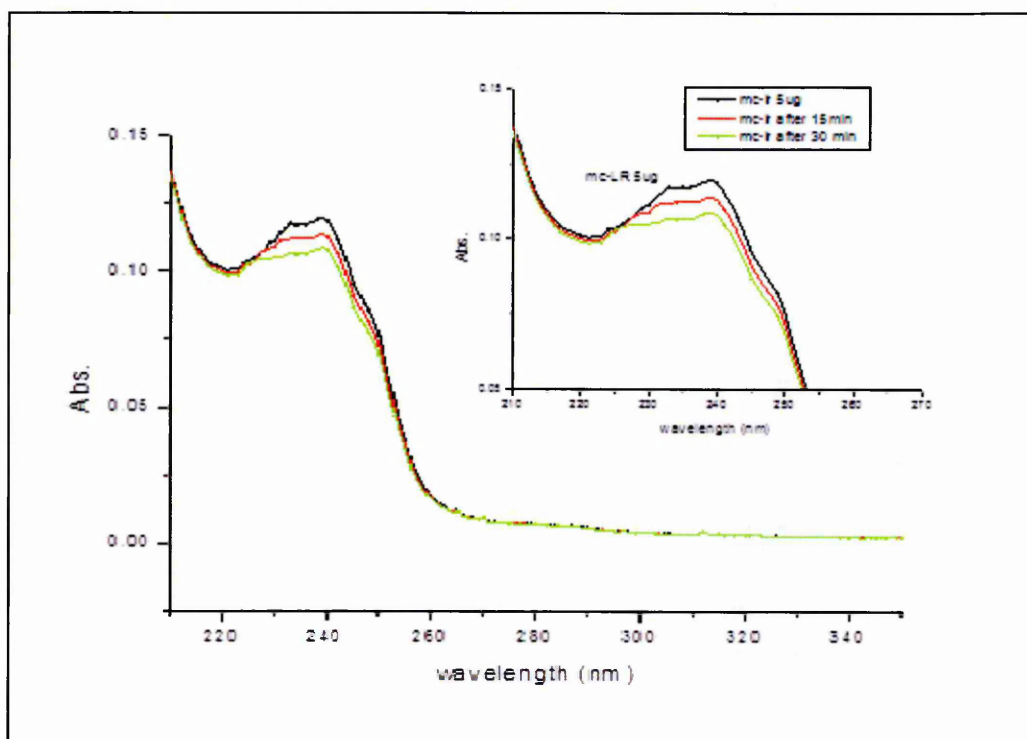


Figure 7.9 UV-vis spectra of MC-LR solution before and after treatment with functionalized micro particles.

7.4 Detection of MC-LR produced by cyanobacteria: effect of environmental factors in algae and toxin production

The methodology of optical detection of MC-LR was established previously using aqueous solutions spiked with known concentration of toxin. Now we have to apply the developed methodology were applied to the detection of MC-LR produced by algae [187]. It is known that Cyanobacteria growth and toxin release depend on a number of environmental factors, there is an enzyme in the cell of the *mcy* gene cluster coding for microcystin biosynthesis [188,189]. This enzyme is influenced by environmental conditions like light intensity, temperature, nutrients and salinity. The microcystis aeruginosa strain grows under different environmental conditions to determine the effect on the toxin produced. However, the control of the production of this enzyme is effecting in such a way as to reduce the microcystin-LR in water [189,190].

We examined growth rates, using isolated strains under various environmental conditions, such as water temperature, light intensity, salinity and nutrient concentration. The growth temperature is one of the most effective parameters in this field. The growth rate of *M. aeruginosa* was significantly higher growth under lower temperatures (20°C and 25°C). Reducing the growth temperature to the frozen range has been studied. Growth rate under various light intensities was determined. The toxin produced by this strain was extracted, in order to study the consequences of environmental conditions on the production of the toxin. It was found that the amount of toxin released by the effect of the nutrient was about 1.7 of the normal condition, which is much higher than normal by 14.6 µg/ml and approaching 40.5 µg / ml. The toxin concentration is still stable due to the increasing of salinity concentration but the growth rate dropped to be almost zero.

7.4.1 Selection of microorganism and growth of algae

Microcystin-LR (MC-LR) was produced naturally by the cyanobacteria strain microcystis aeruginosa (*M. aeruginosa*) strain PCC7820, purchased together with a Bold 3N growth medium (Bold Modified Basal Freshwater Nutrient, Solution 50 ×, liquid, plant cell culture tested). From the UTEX Culture Collection of the University of Texas at Austin, we chose the most common and commercially available bacteria,

microcystis aeruginosa, whose cell size is 2 μm , as, when it forms bloom it can be seen with the naked eye, and it is easier to grow in the lab than other strains. There is an enzyme protease found in the cell of the *mcy* gene cluster coding for microcystin biosynthesis, which is influenced by environmental conditions like light intensity, temperature, nutrients, and salinity [191]. *M. aeruginosa* algae was incubated in a shaker at 25°C for 12:12 hours of light (full sun)/dark cycle. Sufficient growth of a *Microcystis* strain appeared after two months; the initial cell count of the *Microcystis* strain at the beginning of the experiment was estimated at $15 \cdot 10^3$ cells/ml by using a haemocytometer. Growth for *M. aeruginosa* was carried out under different environmental conditions, i.e. light intensity, temperature, nutrient (NaNO_3 and K_2HPO_4) content, and salinity. MC-LR toxin was extracted by centrifuging *M. aeruginosa* cells cultures at 3000 rpm; then the liquid was passed through the 0.2 mm filter and left to sediment for two days. Both the *M. aeruginosa* cell count and the concentration MC-LR produced were monitored with optical density measurements (6715 JENWA), i.e. optical absorption at 600nm and 238nm, respectively. Haemocytometry and fluorescent microscopy were used to count *M. aeruginosa* cells in the culture. The water used was purified by distillation, producing water with 18.2 $\text{M}\Omega\text{cm}$ resistivity. The effect of the environmental conditions on both the *M. aeruginosa* strain growth and toxin release was studied by monitoring, respectively, with the optical density of *M. aeruginosa* culture at 600 nm (OD_{600}) and the concentration of microcystin LR produced by optical density (or optical absorbance) in the adsorption band of MC-LR at 238 nm (OD_{238}). The calibration curve in Figure 2a correlates the optical density of *M. aeruginosa* culture at 600nm (OD_{600}) with the direct cell counts obtained from haemocytometry and fluorescent microscopy measurements.

7.4.2 The growth in optimal condition

M. aeruginosa growth was determined by optical density at 600 nm, UV-visible spectroscopy and haematocytometer. After 1 month we obtained standard curves for cells and toxin as shown in Fig7.10. As one can see, the OD_{600} signal, and thus the bacteria count goes up almost linearly for up to 15 days followed by saturation and finally by its decline after 27 days of growth. Obviously, the concentration of MC-LR correlates with the *M. aeruginosa* cell count; the OD_{238} signal and thus the concentration of MC-LR, generally follow the same trend, though showing no decrease

in MC-LR concentration since the toxin produced was kept constant despite the bacteria declining [191].

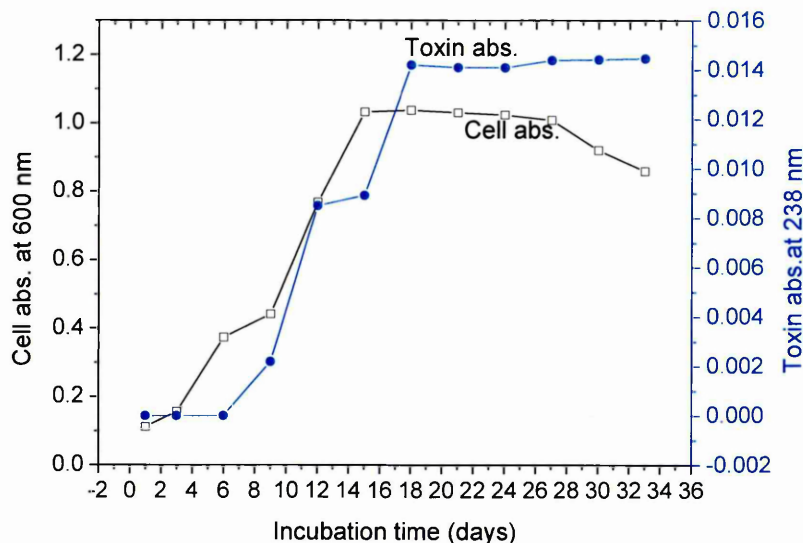


Figure 7.10 Optimal condition 25C & sun light

Optimal Condition for Cell Growth and Toxin production.

The calibration curve for MC-LR in Figure 7.11 was obtained by optical density measurements at 238nm (OD_{238}) of aqueous samples having a known concentration of MC-LR. The data points for naturally produced toxins were placed on this graph and thus allowed for an evaluation of the concentration of MC-LR produced by *M. aeruginosa*.

Calibration curves for *M. aeruginosa* cells and MC-LR toxin

Calibration of optical density for *M. aeruginosa* cells has been done performing both haemocytometry and OD 600 measurements on bacteria cells culture taken every three days during bacteria growth. The methodology of such measurements is described earlier in Chapter 5. The data are shown in Figure 7.11.

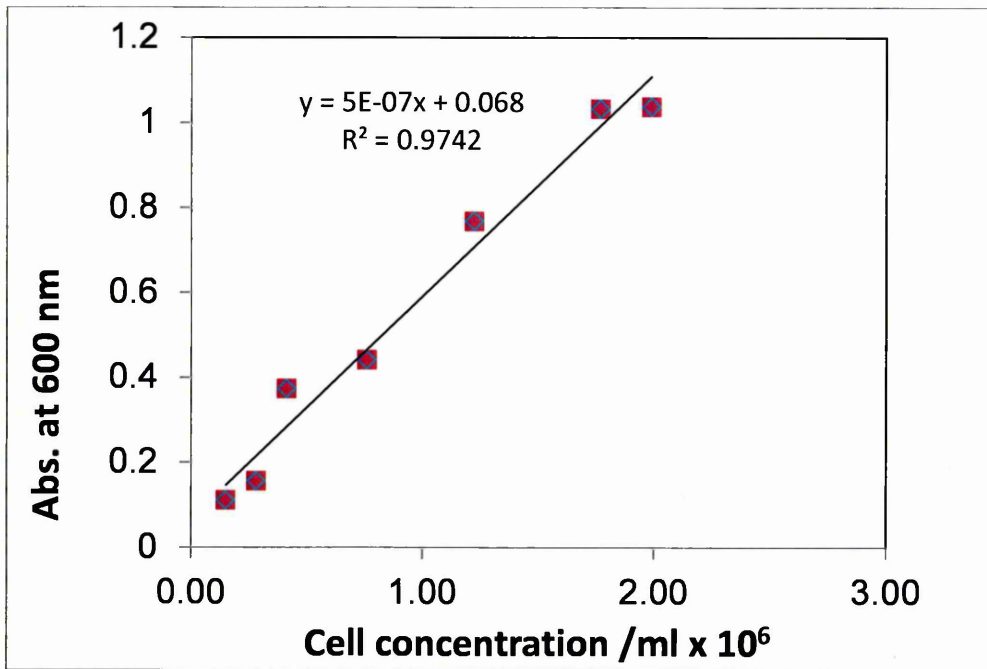


Figure 7.11 Calibration curve for microcystis aeruginosa cells.

Standard curves (type of graphs used to determine unknown sample properties) was created to determine the concentration of MC-LR which produced by *microcystis aeruginosa* after grown it in the lab. Using known concentrations of commercial toxin. The peak of MC-LR in UV-vis at 238 nm as shown in Fig. 7.12, and measured in OD, after adjusting the wavelength to 238 nm, and graphed also measured in UV-vis. And graphed as shown in Fig. 7.13 and 7.14. Standard curve allowed determining the concentration of unknown sample by interpolation on the graph.

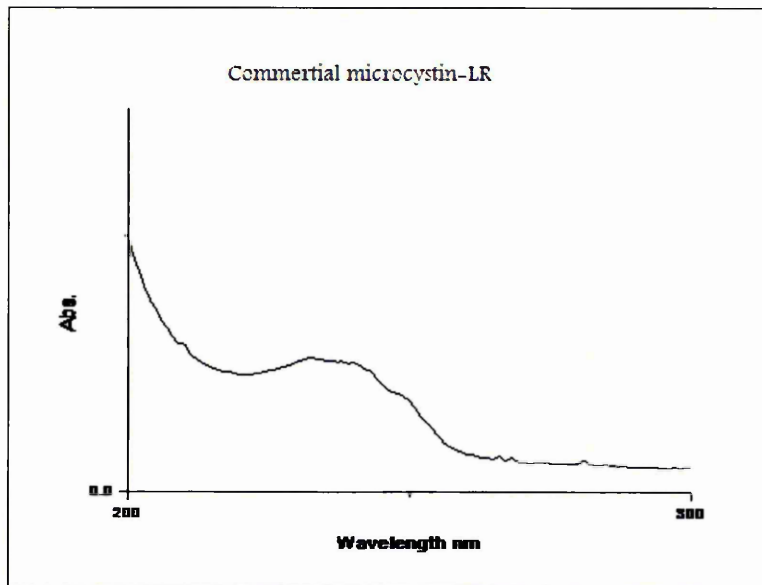


Figure 7.12 Peak of commercial toxin in UV-vis at 238 nm.

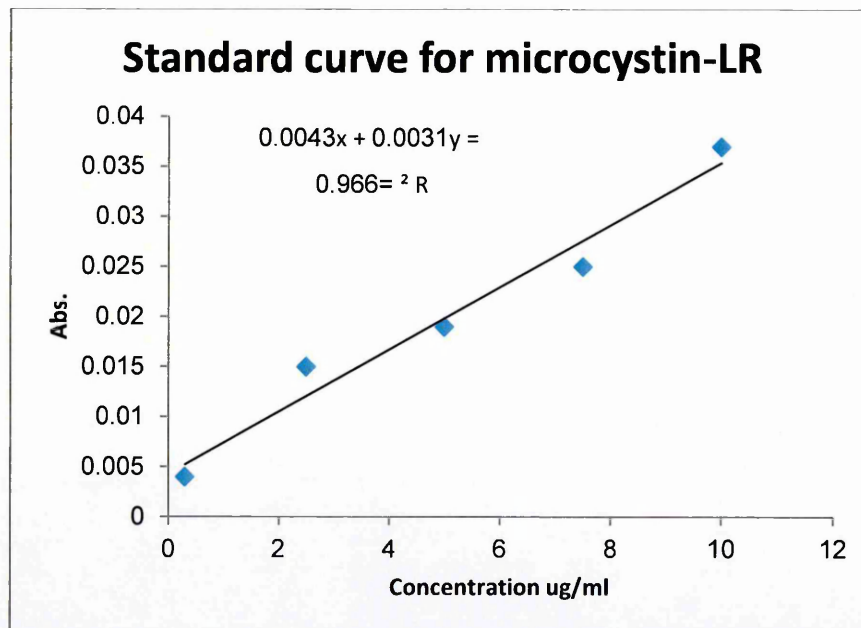


Figure 7.13 Calibration curves for toxin (microcystin-LR) in OD.

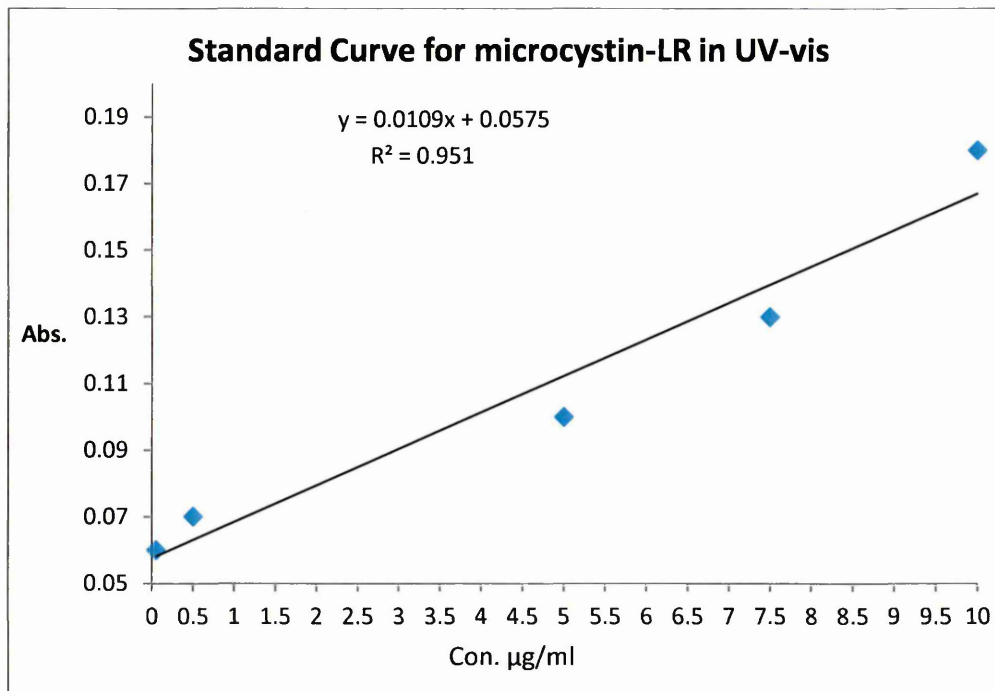


Figure 7.14 Calibration curves for microcystin-LR by the UV-vis.

7.4.3 Growth of *microcystis aeruginosa* under increased and decreased nutrient levels in broth and change environmental condition

The medium which *Microcystis aeruginosa* was grown in Bold 3N medium [192]. The following stock solutions were made per 250 ml of deionized water [NaNO_3 7.5 ml (Fisher BP 360-500), $\text{CaCl}_2 \cdot 2\text{H}_2\text{O}$ (Sigma C-3881), 2.5 ml, $\text{MgSO}_4 \cdot 7\text{H}_2\text{O}$ (Sigma 230391), K_2HPO_4 (Sigma P 3786) 2.5 ml, K_2HPO_4 (Sigma P 0662) 2.5 ml, NaCl (Fisher S271-500) 250 ml, P-IV Metal solution 1.5 ml, Soilwater: GR+Medium 10 ml, Vitamin B_{12} 0.25 ml. The media was autoclaved in a Steam Autoclave at 121C° (250F)/15 psi (103.4 kPa) [the SI unit for pressure is the Pascal (Pa), equal to one newton per square metre (N/m^2)].The algae cultured in Bold 3N medium after added 5ml from [NaNO_3

and K_2HPO_4 (Sigma P 3786). Additional amount of nutrients ($NaNO_3$ and K_2HPO_4) increased the bacteria growth rate, thus leading to larger concentrations of MC-LR extracted ($40.5 \mu\text{g/ml}$) while removing the above salts ($NaNO_3$ and K_2HPO_4) from the growing medium resulted in less bacteria growth rate and thus a smaller MC-LR concentration of $7.55 \mu\text{g/ml}$ as shown in Fig.7.15. The effect of environmental factors on cell growth is show in Fig. 7.16, and microcystin LR release is summarized in Figure 7.15.

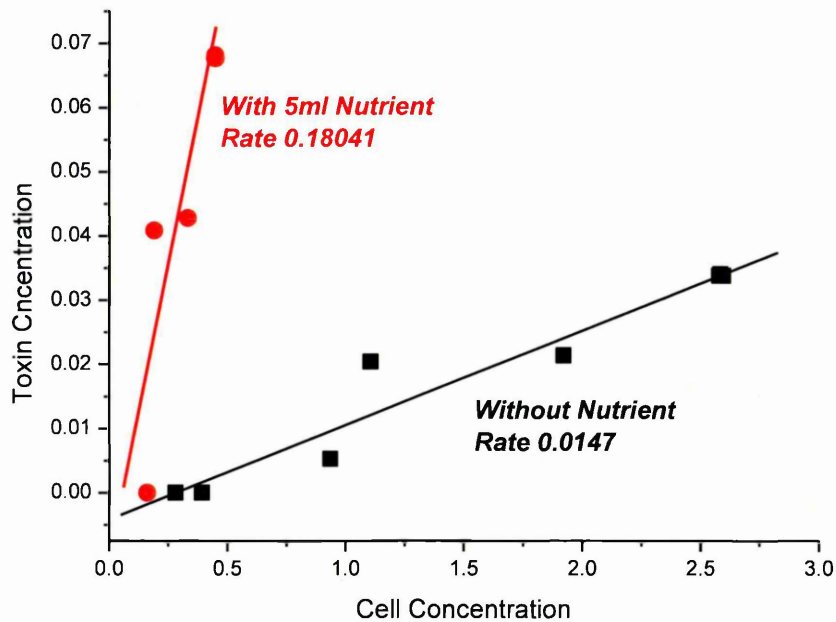


Figure 7.15 MC-LR release after *microcystis aeruginosa* grown in cultures with increase and decrease nutrient.

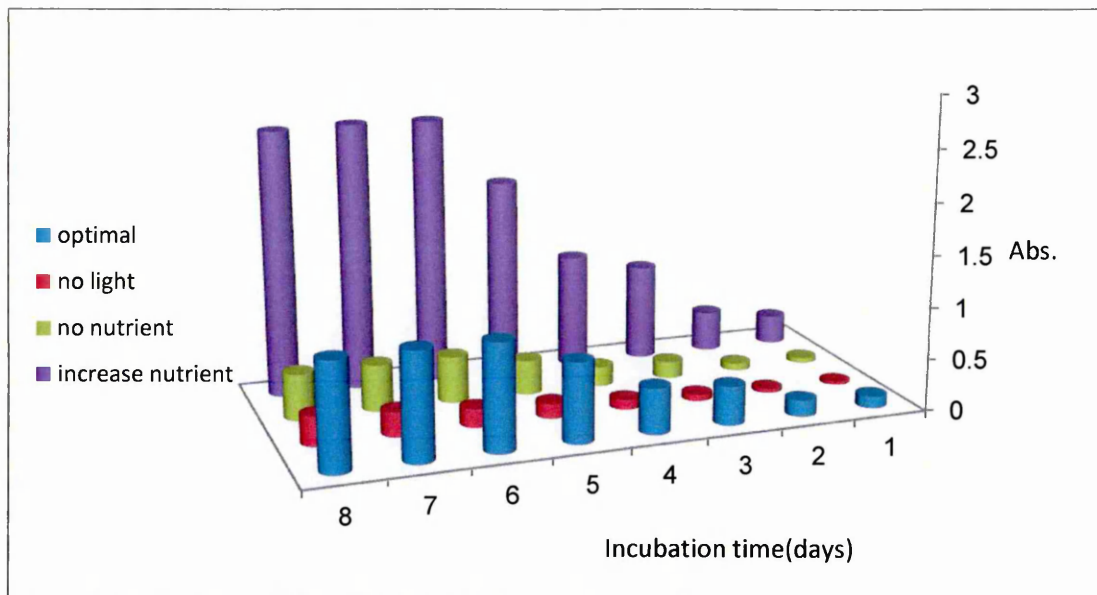


Figure 7.16 Cell growths with change in environmental conditions.

The light considered critical for *microcystis aeruginosa* growth and its ability to produce the MC-LR toxin, The light intensity had a significant effect on the bacteria growth rate and therefore on the concentration of MC-LR produced; without illumination, the MC-LR concentration dropped down to 2.7 μ g/ml as explained in Fig. 7.17. Temperature had a significant effect on growth of *M. aeruginosa*, nevertheless there was a twofold interaction with light intensity [193]. Under high light intensity (sun light) growth increased with increased temperature, under low light intensity, growth decreased with increased temperature.

Fig. 7.17 presents the data for different samples produced in different environmental conditions in co-ordinates concentration of MC-LR (μ g/ml) vs Bacteria cell count per ml; this allows the evaluation of the rates of MC-LR to be released by *M. aeruginosa*. For example, in normal conditions each *M. aeruginosa* cell releases 1.64 pg of MC-LR toxin, which is equivalent to approximately 10^9 molecules of MC-LR.

Bacteria growth rate was examined under various environmental conditions such as temperature, light intensity, salinity, and nutrient concentrations. The growth rate of *M. aeruginosa* was significantly higher at temperature of (20 °C - 25 °C). Sunlight and nutrient content also had a positive effect on bacteria growth. Combined data for MC-LR and bacteria concentration in Fig.7.17 illustrates the bacteria efficiency of toxin production depending on temperature, light and nutrient content [194].

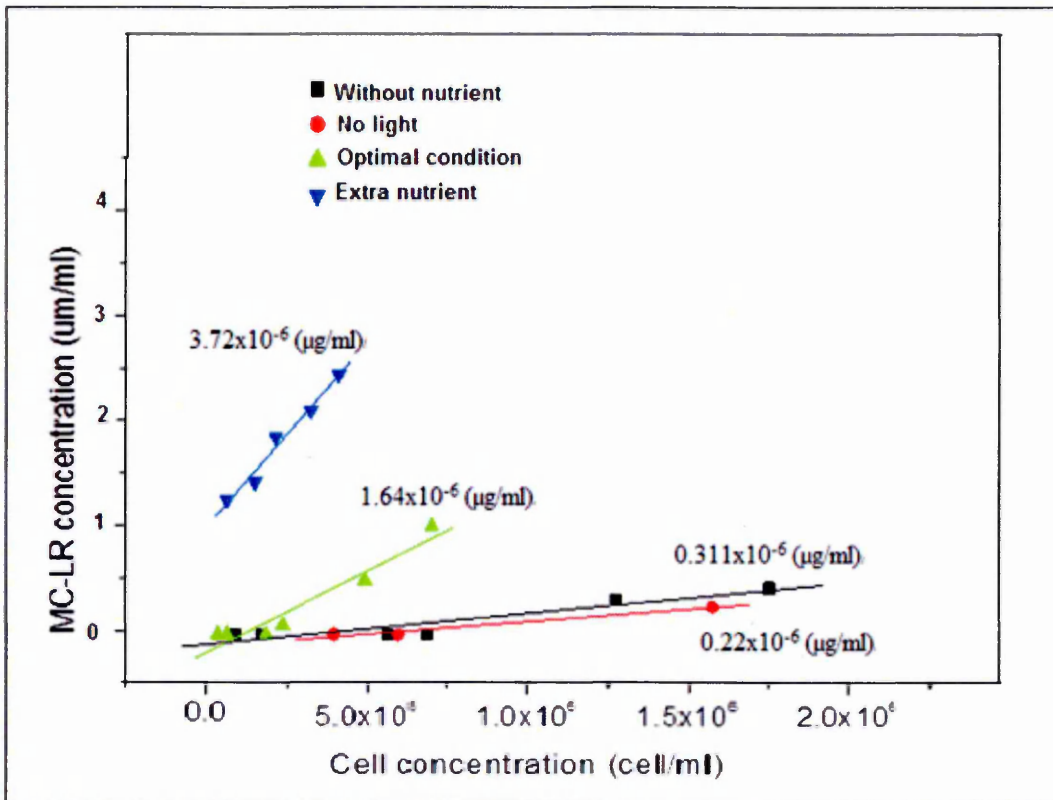


Figure 7.17 Effect of environmental conditions on MC-LR released by *M. aeruginosa*.

7.4.4 Extraction of MC-LR

M. aeruginosa cells cultures were centrifuged at a speed of 3000 rpm. Then the liquid was passed through the 0.2 mm filter and left to sediment for two days. The concentration of toxin was accessed by UV-visible absorption spectroscopy measurements [195,196]. The peak at 238 nm corresponds to MC-LR as shown in Fig. 7.16 for toxin produced in culture with optimal condition and toxin from culture have increase nutrient.

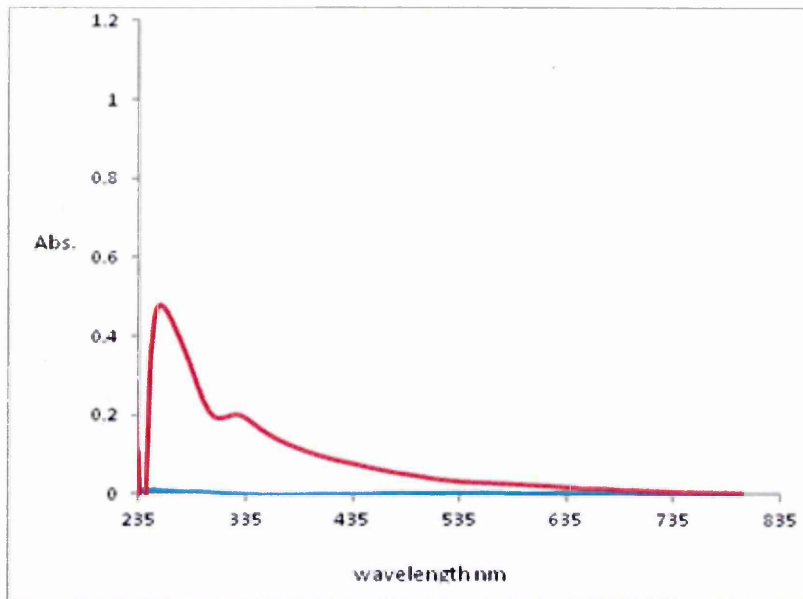


Figure 7.18 Natural MC-LR 40.5 µg/ml extracted from culture grown with increase in nutrient.

To calculate the toxin concentration which extract from culture of *microcystis aeruginosa* which grew under optimal condition found the peak 0.34 Abs at 238 nm wavelength as shown in Fig.7.16, by calculate the equation of the standard curve below :

$$y = 0.0109x + 0.0575$$

$$0.34 = 0.0109x + 0.0575$$

$$X = -0.34 + 0.0575 / 0.0109$$

X = 25.9 ug/ml is in optimal condition. In table 7.2 toxin concentration was calculated for different cultures.

Table 7.2 concentration of microcystin-LR released by *microcystis aeruginosa* under different environmental conditions.

Environmental condition which growth rate happens under it.	The peak of natural MC-LR. in UV-vis.	MC-LR concentration.
Optimal condition	0.34	25.9
Increase nutrient	0.5	40.5
Absent nutrient	0.14	7.55
Absent light	0.0873	2.7

In Fig 7.19 many images were taken to *microcystis aeruginosa* after grown in petridish and cultures, the image which take by SEM the cell were coated by gold, while the image which taken by Florescence microscopy the cells were stained by SYTO-9 Green Florescence stain.

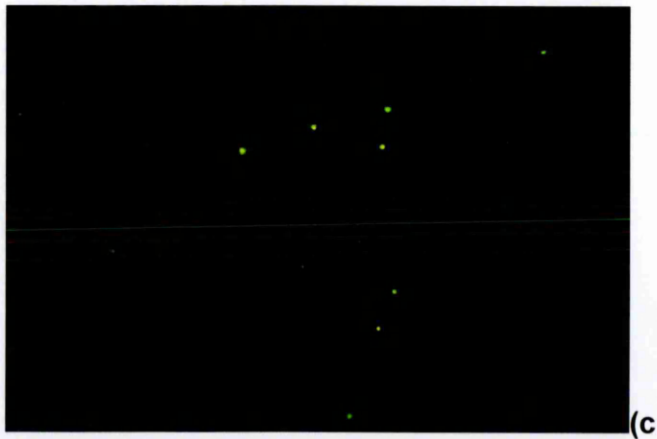
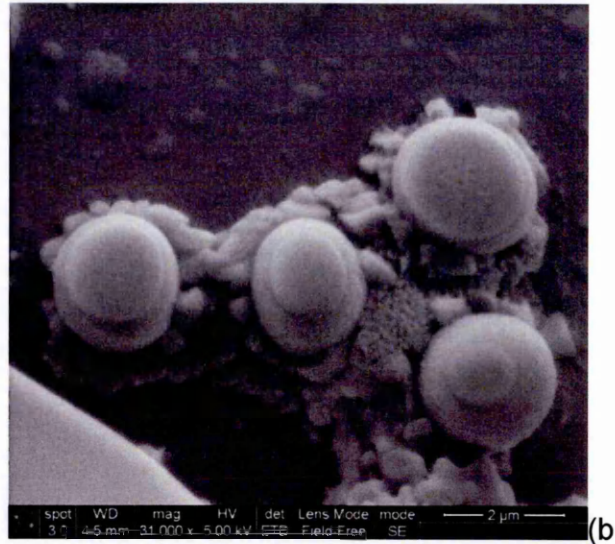
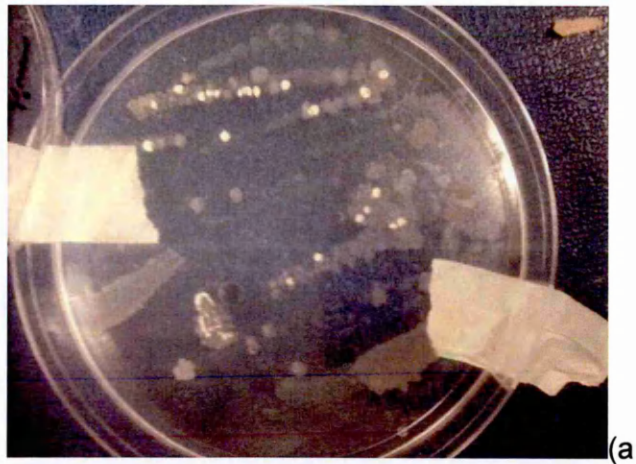


Figure 7.19(a) *Microcystis aeruginosa* growth in optimal condition,(b) *Microcystis aeruginosa* cells in SEM, and (c)*Microcystis aeruginosa* under Florescence microscopy 100x.

7.4.5 Effect of salinity on algae growth

Cultures of *Microcystis aeruginosa* were grown in a Bold 3N medium. The following stock solutions were first made per 250 ml of deionized water [NaNO_3 7.5 ml (Fisher BP 360-500), $\text{CaCl}_2 \cdot 2\text{H}_2\text{O}$ (Sigma C-3881), 2.5 ml, $\text{MgSO}_4 \cdot 7\text{H}_2\text{O}$ (Sigma 230391), K_2HPO_4 (Sigma P 3786) 2.5 ml, K_2HPO_4 (Sigma P 0662) 2.5 ml, NaCl (Fisher S271-500) 250 ml, P-IV Metal solution 1.5 ml, Soilwater: GR+Medium 10 ml, Vitamin B₁₂ 0.25 ml. The media was autoclaved at 15 psi for 15 minutes. For the salinity using 100ml flasks, 5 separate samples of media were prepared. Treatments from 0M, 0.625M, 0.125M, 0.250M, 0.5M, 1M. Sodium Chloride (NaCl) was prepared from the dissolved 5.84 g in 100 ml (1M) and a series of dilution were made and added to the media (1 ml) in every flask. The Optical Density OD meter was used to control the measurement. The toxic strain of *Microcystis aeruginosa* used was UTEX 2385 (from the Culture Collection of Algae at the University of Texas), it was necessary to wear gloves. Salinity is determined from empirical relationships between temperature and the conductivity ratio of a sample to the International Association for the Physical Sciences of the Ocean (IAPSO) Standard Seawater. Comparison of results with other laboratories required all researchers to use the IAPSO Standard Seawater for calibration[197-206].

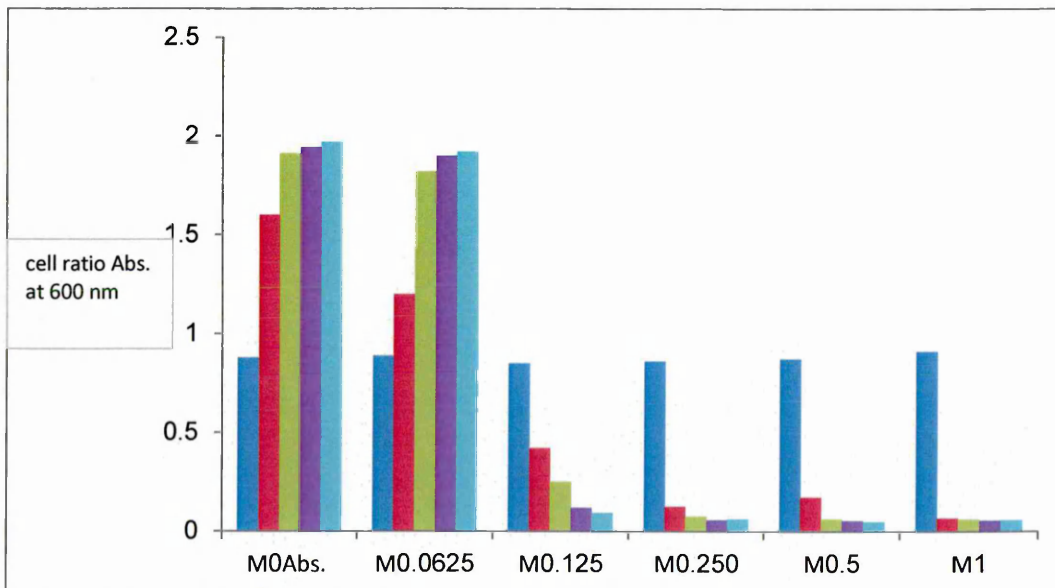


Figure 7.20 Effect of salinity on rate growth of *Microcystis aeruginosa*.

The salinity of growth of the medium (Bold 3N) for *Microcystis aeruginosa* was modified by adding NaCl salt up to a 1M concentration. The effect of salinity on the growth of *M. aeruginosa* was evaluated over one month of incubation using *in vivo* fluorescence to estimate cell density. The data in Fig. 7.20 shows that the increase in NaCl concentration caused substantial reduction of *M. aeruginosa* bacteria concentration. At the same time the concentration of MC-LR toxin which was already produced had not affected.

To convert the molarity to PPM the equation below was used:

$$PPM = \frac{\text{weight of solute}(g)}{\text{volum of solution}(ml)}$$

$$\text{ppm} = 5.84g / 100 \text{ ml} = 58400 \text{ ppm}$$

or

$$PPM = M * M \text{ wt} * 1000$$

Dilution from 1M to 0.0625 M was carried out and converted to PPM by the equation below:

$$PPM = 1 * 58.4 * 1000 = 58400 \text{ PPM}$$

$$0.5 * 58.4 * 1000 = 29200 \text{ ppm}$$

$$0.250 * 58.4 * 1000 = 14600 \text{ ppm}$$

$$0.125 * 58.4 * 1000 = 7300 \text{ ppm}$$

$$0.0625 * 58.4 * 1000 = 3650 \text{ ppm}$$

The algae were still alive, and released toxin in the presence of salt at 3650 ppm.

7.5 TIRE detection of naturally produced toxin (microcystin-LR)

The important thing is that in our work the antibody which we chose must work with the natural toxin, so for this purpose the TIRE method was carried out with natural toxin. A series of dilutions was made from natural MC-LR which began with (1:20 to 1:2000), as shown in Fig 7.21, and the TIRE measurements as shown in Fig 7.22, were done as explained in Chapter 4 and 6.

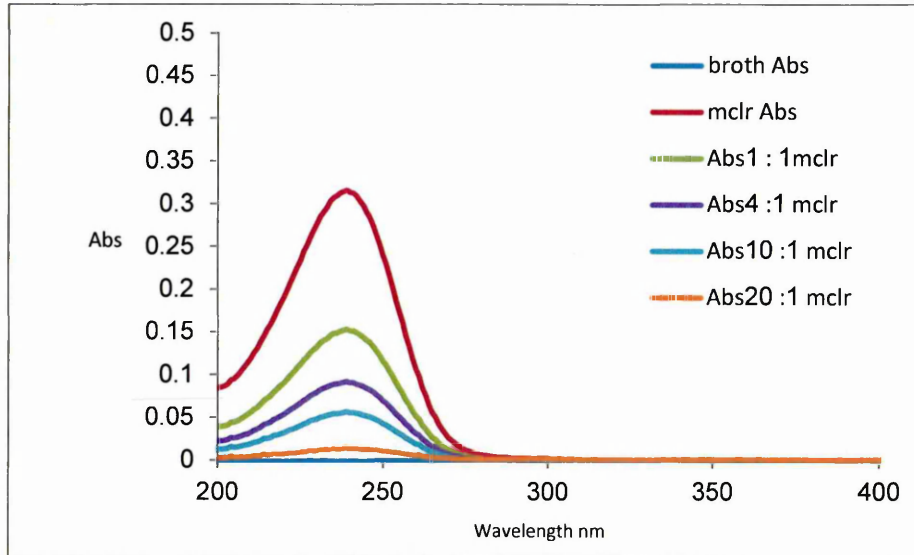


Figure 7.21 a series of dilutions was made from natural MC-LR.

Table 7.3 shows TIRE fitting data for immune reaction between natural microcystin-LR and antibody MC10E7. The (*) sign indicates that the parameters were fixed during fitting. The values of n and k are given at the wavelength of 633 nm.

We evaluated the molecular layer thickness increment by doing data TIRE fitting to the reflective system model consisting of glass (BK7) as an ambient, a Cr/Au metal layer, the deposited molecular layer, and aqueous solution. The data fitting procedure has been described in detail previously in Chapter 4.

In Fig 7.22 the K_A for natural toxin in the range (10^7 1/mol) this mean strong binding between natural toxin and the antibody, and the calibration curve which obtained from TIRE measurements is shown in Fig 7.23 indicated that the data fitting for both commercial and MC-LR produced by *M. aeruginosa* were nearly the same.

Table 7.3 the increase in thickness for natural MC-LR.

Natural microcystin-LR dilutions	d (nm)	$\Delta d(\text{nm})$	n, k (at $\lambda=700$ nm)
1:2000	1.513	0.314	$n^* = 1.42, k=0$
1:1000	1.827	0.883	$n^* = 1.42, k=0$
1:200	2.396	1.367	$n^* = 1.42, k=0$
1:100	2.880	1.407	$n^* = 1.42, k=0$
1:20	2.920	1.828	$n^* = 1.42, k=0$

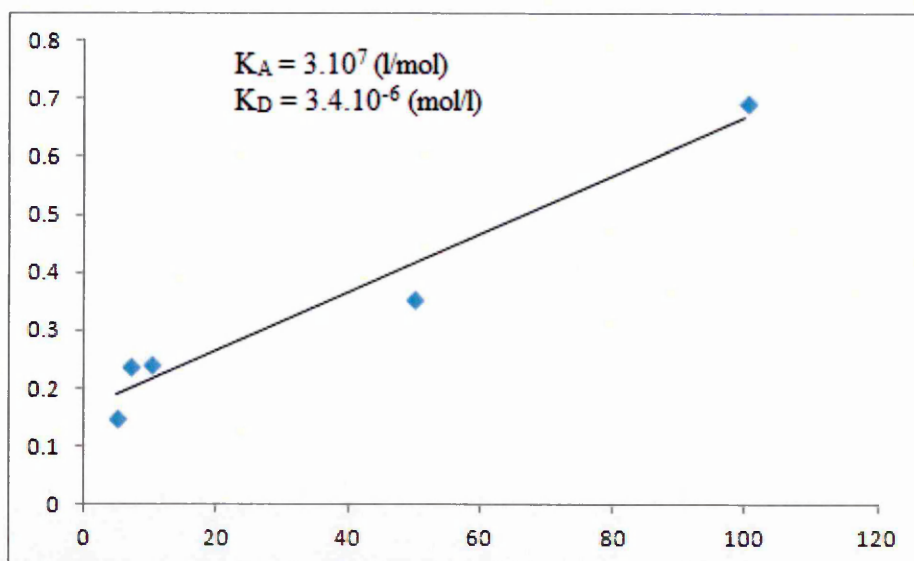


Figure 7.22 kinetic reactions between natural MC-LR and antibody MC10E7.

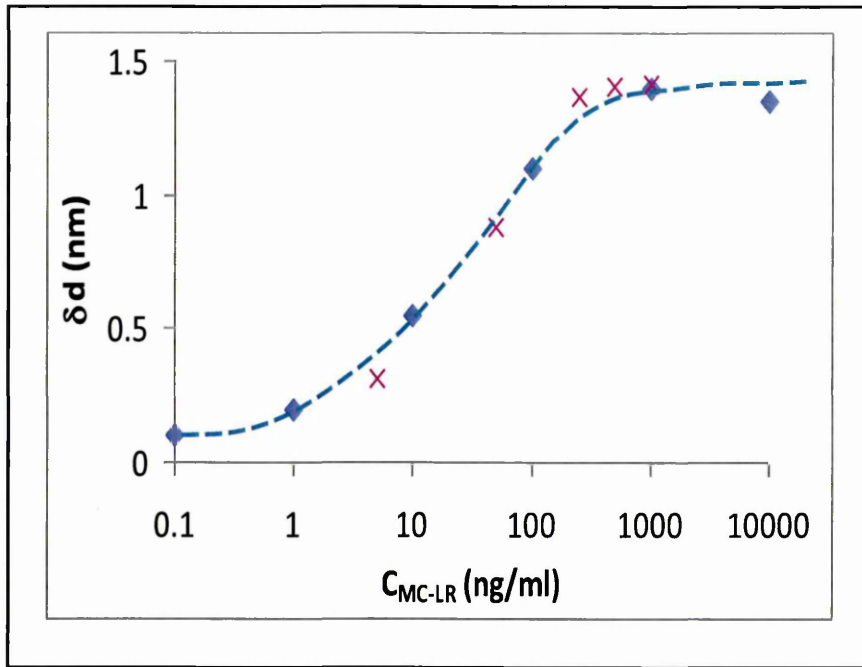


Figure 7.23 Calibration curve obtained from TIRE measurements and data fitting for commercial MC-LR (blue diamond data points and blue dotted line). The data points for MC-LR produced by *M. aeruginosa* are shown as red crosses.

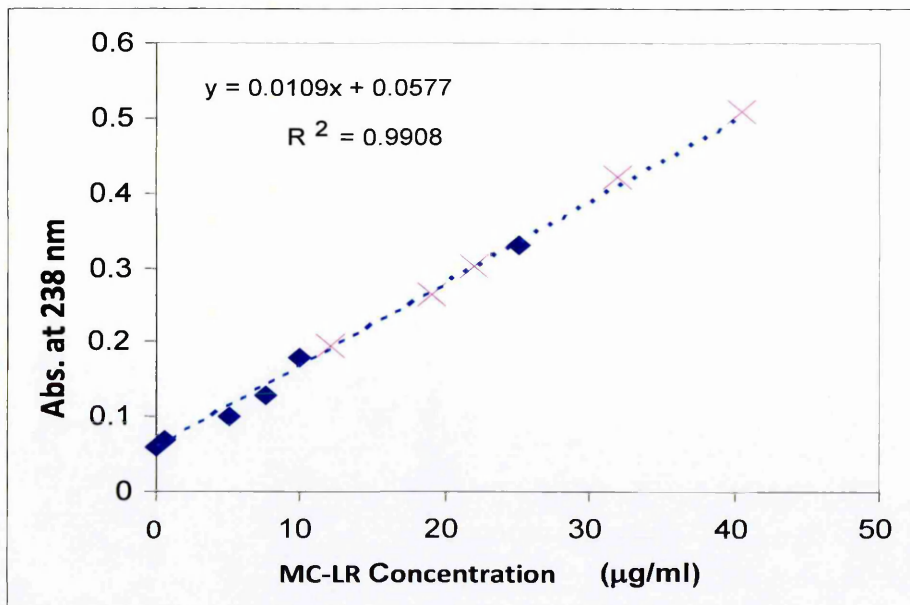


Figure 7.24 Correlation between the optical density (absorbance) and the concentration of MC-LR.

Fig. 7.24 was obtained by optical density measurements at 238nm (OD238) of aqueous samples having a known concentration of MC-LR. The data points for naturally produced toxin were placed on that graph and thus allowed to evaluate the concentration of MC-LR produced by *M. aeruginosa*.

7.6 Microcystin-LR removal with functionalized polyelectrolyte micro-particles

The technology of layer-by-layer (LbL) electrostatic [199], deposition has generated numerous applications in the formation of multilayer assemblies on solid surfaces. One of the applications is related to the fabrication of nano-engineered capsules which is based on the LbL coating of inorganic micro-particles with layers of oppositely charged polyelectrolytes, such as PAH and PSS, and was used after being functionalized with antibody MC10E7, this method will be discussed in detail in Chapter 8.

7.7 Conclusion

Detection of microcystin-LR was successfully achieved by optical methods of total internal reflection ellipsometry, UV-visible and FT-IR spectroscopies either in purified form (available commercially) or using naturally MC-LR produced by algae. The method of TIRE was particularly promising because of its high sensitivity below the limit of 1ng/ml established by the WHO.

The roles of environmental factors such as temperature, light, nutrients, and salinity, on the production of MC-LR by *microcystis aeruginosa* were studied. The production rate of MC-LR of 1.64 pg per bacteria cell was found at optimal conditions bacteria growth (20-25 C°), light-dark natural cycles, and balanced nutrients). Extra nutrients increase rate of generation of MC-LR, while the presence of NaCl reduced substantially bacteria growth and therefore the production of MC-LR.

CHAPTER 8

THE USE OF FUNCTIONALIZED MICRO-PARTICLES AS AN ABSORBENT FOR MICROCYSTIN-LR

In this chapter the use of nanotechnology in cleaning samples containing MC-LR by using functionalized polyelectrolyte micro-particles is described in more detail, the modification of micro-capsules with antibody MC10E7 which has specific binding to microcystin-LR, manufacturing hollow microcapsules to fill with dyes or living cells (antibodies or antigens) and a comparison between the reaction of micro-capsules with natural and commercial toxins (with microcystin-LR).

8.1 Microencapsulation

Our approach for material encapsulation is to use a novel class of carriers which are multilayered polyelectrolyte microcapsules that have recently been fabricated to encapsulate different molecules including drugs, by using polymers that are ecological or that can respond and release their load in response to well-defined reason. Microencapsulation is the process by which individual particles or droplets of solid or liquid material (the core) are surrounded or coated with a continuous film of polymeric material (the shell) to produce capsules in the micrometre to millimetre range, there are known as microcapsules. The concept of microencapsulation was first established by Chang in the 1960s by encapsulating proteins into stable microcapsules with semipermeable polymer membranes. After that, microencapsulation technology for the immobilization of a variety of biologically active species such as enzymes and living cells, have been advanced and used in biotechnologies for developing bioreactors, biosensors, and hybrid bio-artificial organs. Researchers have used many techniques to manufacture micro-capsules such as pan coating, air suspension coating, centrifugal extraction, spray drying and others. One of these methods is the polyelectrolyte capsules which were used in my project, and are described in more detail in the following section.

8.2 Polyelectrolyte microcapsules

The technology of layer-by-layer (LbL) electrostatic deposition has found numerous applications in the formation of multilayer assemblies on solid surfaces. The polymers adsorbed from an aqueous solution open the possibility of incorporating biological macromolecules such as proteins or nucleic acids in their active state which may even be interesting for biosensing applications. The fabrication of nano-engineered capsules was introduced at the Max Planck Institute; this method is based on the layer-by-layer (LbL) adsorption of oppositely charged macromolecules, whereby each one of the wall components adds functionality to the multilayered capsules

The idea of fabrication of polyelectrolyte capsules is very simple and lies in the coating of the inorganic core particles with the layers of PAH and PSS [199]. The process of building such polyelectrolyte capsules is schematically shown in Figure 8.1

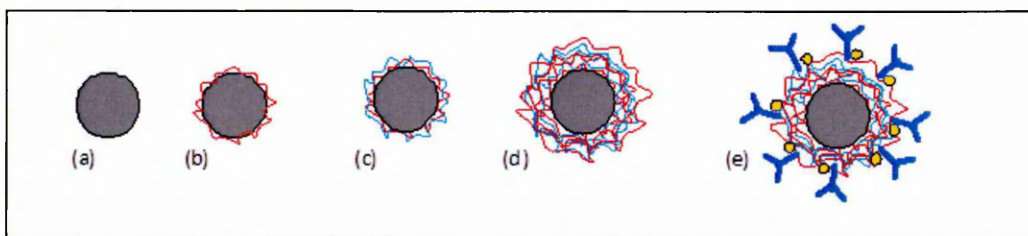


Figure 8.1. Formation of polyelectrolyte capsules: (a) Original CaCO_3 core particle containing negative charge on the surface; (b) after coating with PAH layer; (c) after coating with PSS layer; (d) after deposition of several bilayers of PAH/PSS; (e) After further functionalisation of a capsule with Protein A and IgG molecules.

Core particles (CaCO_3 or MnCO_3) which are commercially available in different sizes, e.g. 2, 4, 6 μm , typically contain a negative charge on the surface and thus can be coated with a PAH layer by a simple mixing CaCO_3 suspension with PAH 2mg/ml aqueous solution. The mixture should be stirred for 10-15 minutes and then let to sediment. Following the same procedure, the layers of PSS and PAH can be deposited consecutively (using intermediate rinsing with water) resulting in the formation of a PAH/PSS shell on the surface of the core particle (Fig. 8.1 d). This core particle can then

be dissolved in HCl solution ($\text{pH} \approx 2$) and the capsule can be filled with some other liquid (e.g. drug) following the original idea using such capsules for targeted drug delivery [207]. The capsules can be further modified with antibodies (Fig. 8.1 d) for particular bio-sensing or bio-medical applications [208-210]. Shell thickness is determined by the number of layers but is typically of few nanometres. The variable size of the capsules can be fully controlled from 50 nm to tens of micrometres, depending on the size of the core particle and the number of layers deposited and the solution conditions (e.g., pH, ionic strength, etc.) used during fabrication. This polyelectrolyte multilayer coating can be easily and reproducibly formed on any charged surface, and the core of the particles can be dissolved, making hollow capsules that can be refilled with substances of interest and the permeability can be tuned to a wide class of substances through designed layer thickness. Temperature has an effect on the manufacturing of the capsules (causing shrinkage of capsules with compensated charges which results in an increase in the wall thickness and a drastic reduction in permeability). A typical SEM picture of microcapsule Fig. 8.2 shows clearly its porous and thus chemically permeable structure [68].

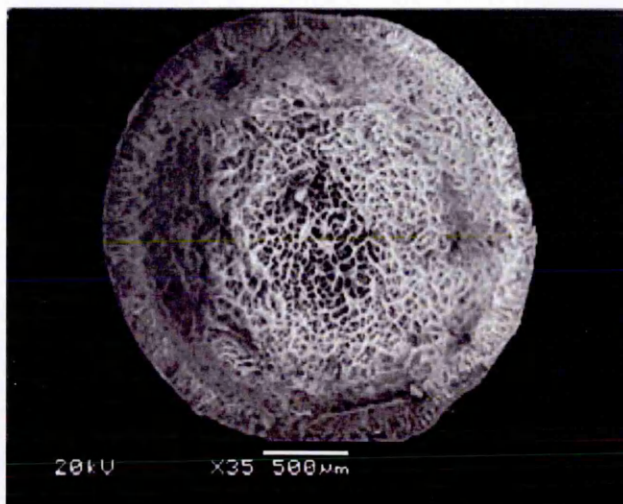
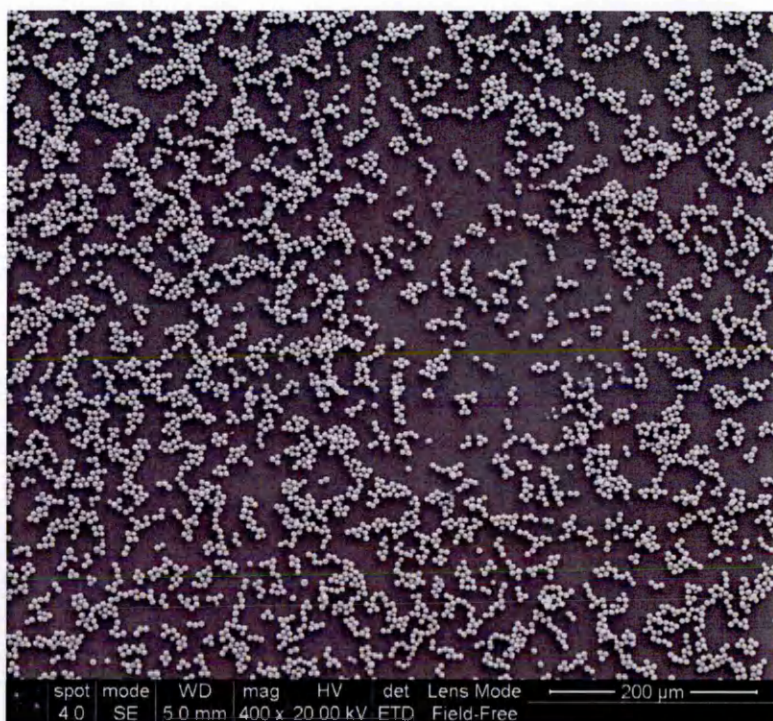


Figure 8.2. Typical SEM image of the cross-section view of prepared hollow microcapsule [68]

In this project, the capsules functionalized with antibodies has been utilized for purification of substances contaminated with toxins, e.g. aflatoxin B1 and microcystin-LR. For this purpose, we have prefer to keep the inorganic core intact in order to have the particles heavy and thus enable them to sediment quickly.

8.3 Preparation of micro-particles

To prepare micro-capsules for modification with antibody MC10E7, it is mixed with MnCO_3 , which has a diameter of $4\mu\text{m}$ in a suspension of PAH 2mg/ml aqueous solution. The mixture should be stirred for 10-15 minutes and then let to sediment. Following the same procedure, the layers of PSS and PAH can be deposited consecutively (using intermediate rinsing with water) resulting in the formation of a PAH/PSS shell on the surface of the core particle. Such a procedure can be repeated many times until the desired number of layers is reached (typically 3-4 bilayers of PAH/PSS. Adding NaCl into a solution of PAH or PSS increases the ion strength and thus the thickness of the shell. A series of SEM images in Figure 8.3, taken at different magnifications, show the result micro-particles.



(a)

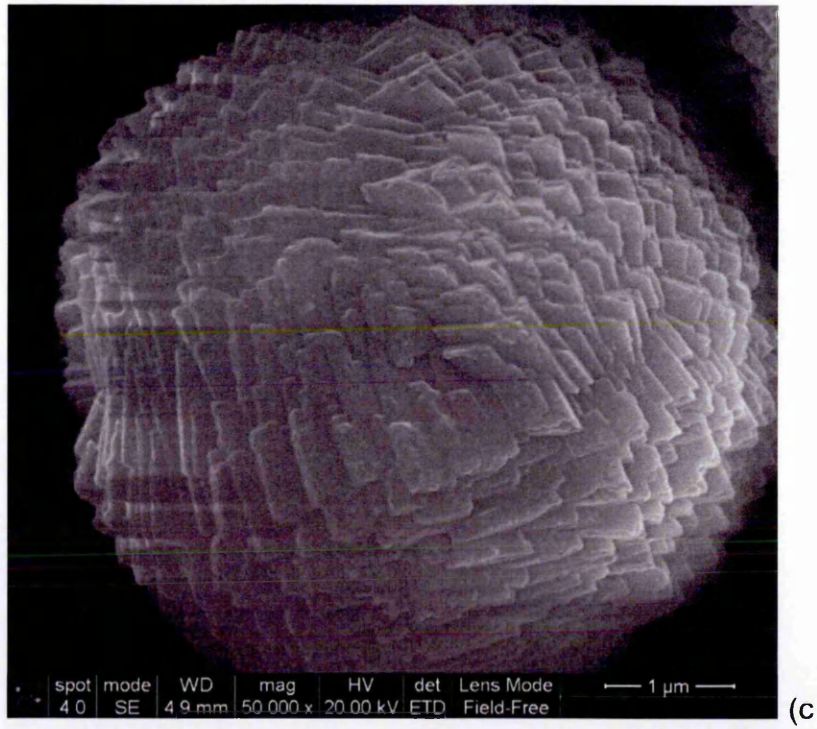


Figure 8.3 Microcapsules which have a 4 μm diameter core.(a) captured in resolution 200 μm ,(b) captured in resolution 5 μm , and (c) captured in resolution 1 μm .

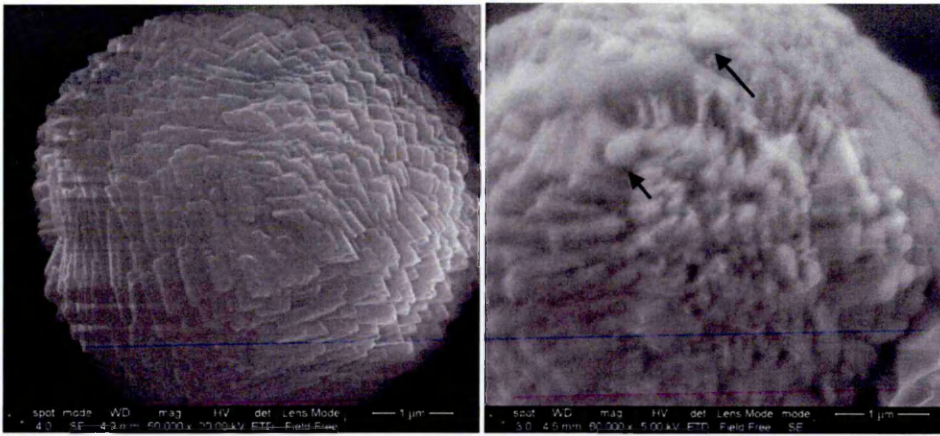


Figure 8.4 Microcapsules with 6 μ m diameter core after depositing many layers of (PAH/PSS) and coated with an enzyme.

8.3.1 UV-visible measurement

The procedure described in 8.3 involves the original MnCO_3 core particle of 4-6 μ m in diameter containing a positive charge on the surface being coated first with poly-anionic PSS layer and then with a poly-cationic PAH layer. Such procedure was repeated several times to form particles coated with 3 to 4 PSS/PAH bi-layers. These particles were functionalised further with Protein G and then with MC10E7 antibodies and later were used as an absorbent for MC-LR. The purification protocol is rather simple: functionalized microparticles, when mixed with aqueous solution containing MC-LR, bind MC-LR, molecules, then heavy microparticles sediment on the bottom of a sample tube leaving the purified solution above as shown in Fig. 7.7 in Chapter 7. The concentration of MC-LR in solution at different stages of purification was monitored using UV-visible spectroscopy and TIRE methods [213, 214].

A typical series of UV-visible spectra of aqueous solution containing naturally produced MC-LR is shown in Figure 8.5 As one can see, the magnitude of the absorption peak of MC-LR is decrease with the time of treatment with functionalized microparticles. Many concentration of MC-LR were prepared beginning with 0.1 μ g to 1000 μ g, Mixed with a 1:1 capsule with the dilution of the MC-LR after enabled the TIRE measurement.

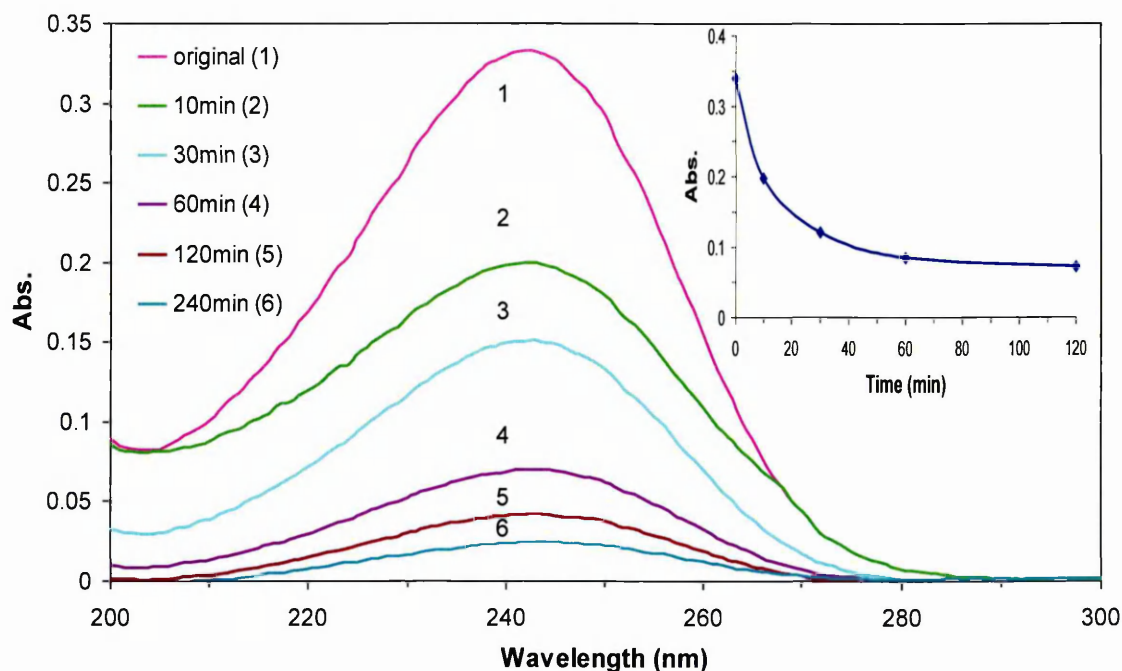


Figure 8.5 UV-visible absorption spectra of MC-LR (25.9 µg/ml) concentration recorded during treatment with functionalized microparticles. Inset: The reduction of the amplitude of absorption peak with time of treatment.

8.3.2 TIRE measurements

The TIRE spectra measurements were carried out on samples of the MC-LR toxin produced by *M. aeruginosa* culture. The graph in Figure 8.7 shows a 1.4 nm increase in the adsorbed layer thickness due to binding of MC-LR toxin to MC10E7 antibodies. After treatment MC-LR solutions with functionalized microparticles, the response was reduced to 0.8 nm which is believed to be caused by partial absorption of MC-LR on functionalized microparticles as shown in Fig. 8.6. The thickness increment appeared to be about half the original. Different concentrations of naturally produced MC-LR were obtained by dilution of the original MC-LR extract of 25.9 µg/ml concentration.

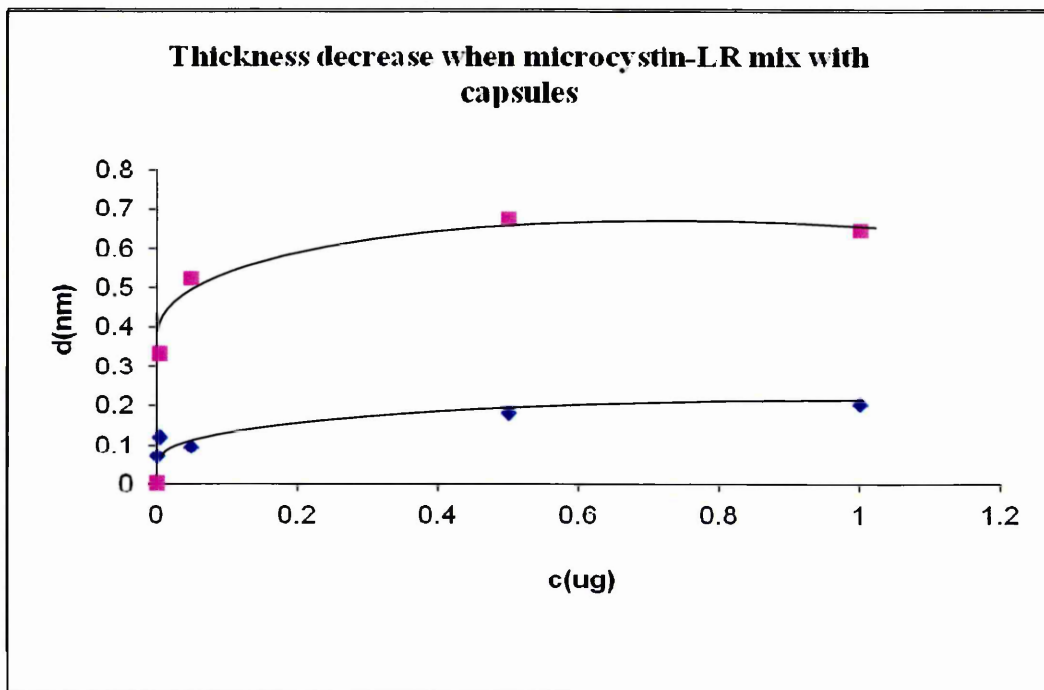


Figure 8.6 TIRE measurements taken on commercial MC-LR samples before and after treatment with functionalized capsules demonstrate the effect of purification.

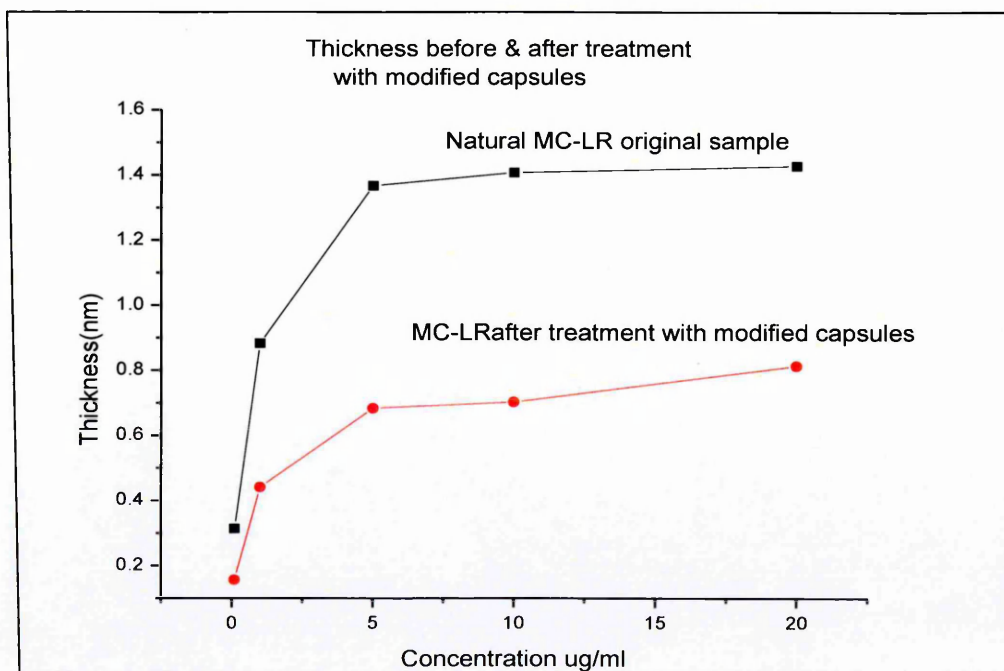


Figure 8.7 TIRE data: thickness increment concentration of natural MC-LR: (a) in original MC-LR solution; and (b) after treatment with functionalized micro-particles for 60min.

8.4 Comparison between purification of natural and commercial toxin by microcapsules

In this study, these particles were used as a tool for the recovery and/or purification of molecules in their associated environments. To observe the efficiency of these capsules the measurement were taken with both commercial and natural MC-LR. The TIRE measurements, UV-visible, were used.

TIRE measurements showed similar effect, after treatment natural solutions of MC-LR with functionalized microparticles, the thickness appeared to be about two times smaller.

In Fig 8.8 the concentration exponentially decay with the time, and the abs. decreased in length after treatment with functionalized microcapsules. And in Fig 8.9 the standard curve for natural toxin decreased in length after treatment with microcapsules.

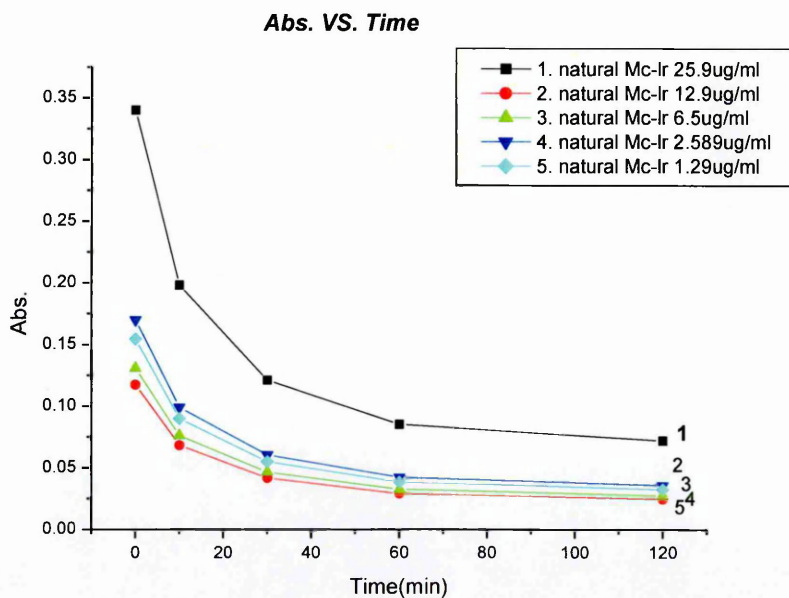


Fig. 8.8 Effect of microparticle treatment on concentration of MC-LR: Abs. at 238 nm.

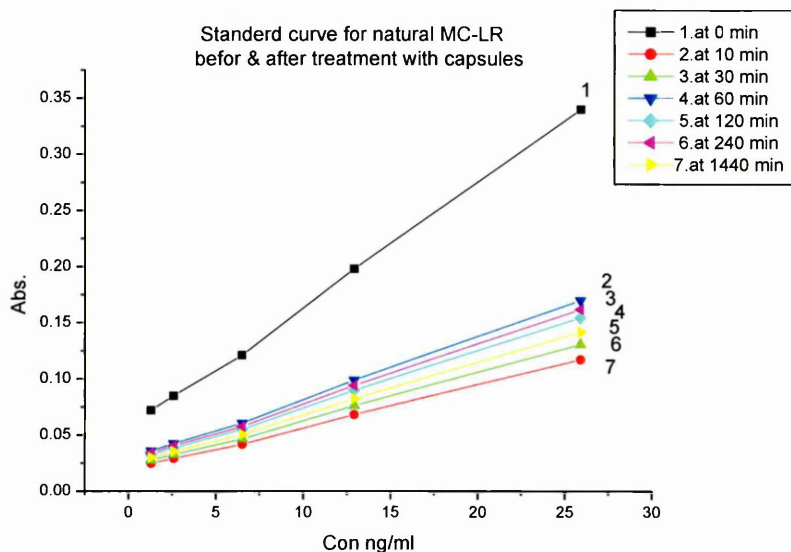
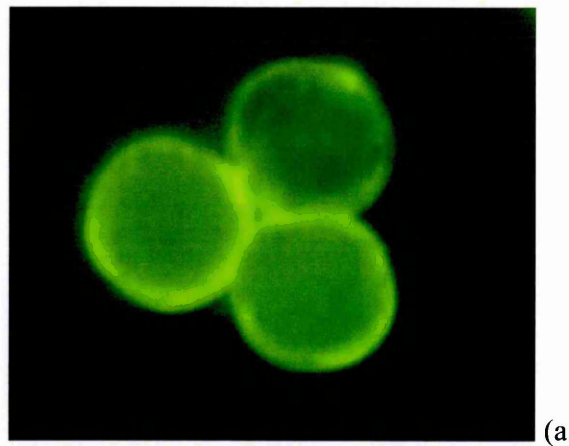


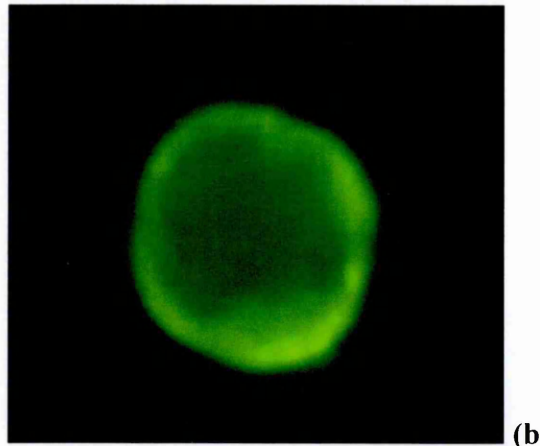
Figure 8.9 standard curves for MC-LR after treatment with capsules.

8.5 Removing the core of the microcapsules

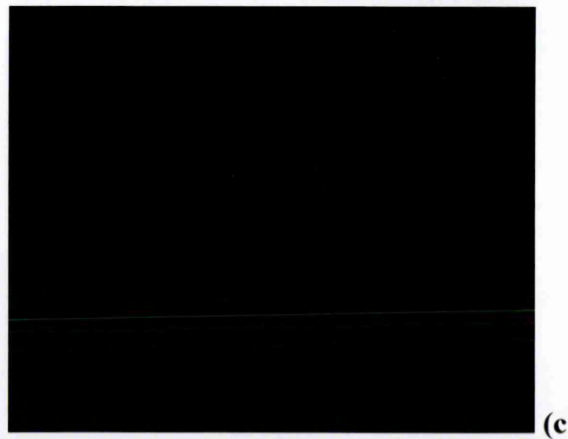
Multilayered polyelectrolyte microcapsules [211,212] have been fabricated to encapsulate various classes of (drug, enzymes, antibodies molecules), by using polymers that can respond and release their payload. In our work the core MnCO_3 $6\mu\text{m}$ was used, along with polymers (PAH, PSS), to form polyelectrolyte micro-capsules of eight layers (PAH/ PSS), as shown in Fig. 8.10a, and 8.10b. After preparing these capsules and removing the core by using (HCl 0.01 M) to change the pH to 2, after rinsing the sediment with water to remove the dissolved core and capture its image with fluorescence microscopy, the capsules without a core appear shrunken, as shown in Fig. 8.10c. After this, the capsules were filled with dye immersed in water (pH 4), and this dye will go inside the capsules because of the change in pH.



(a)



(b)



(c)

Figure 8.10 (a) Microcapsules with core MnCO_3 $6\mu\text{m}$ and eight layers (PAH/ PSS).
(a and (b) Microcapsule before removing the core. and (c) Microcapsule after removing
the core. Images were taken by fluorescence microscopy.

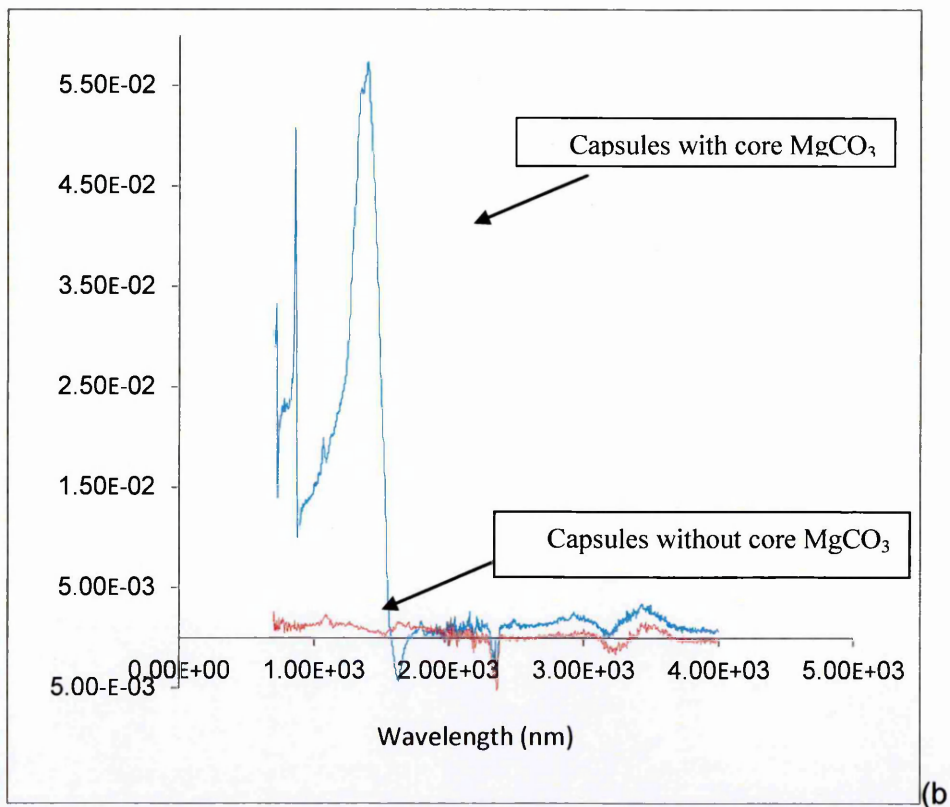
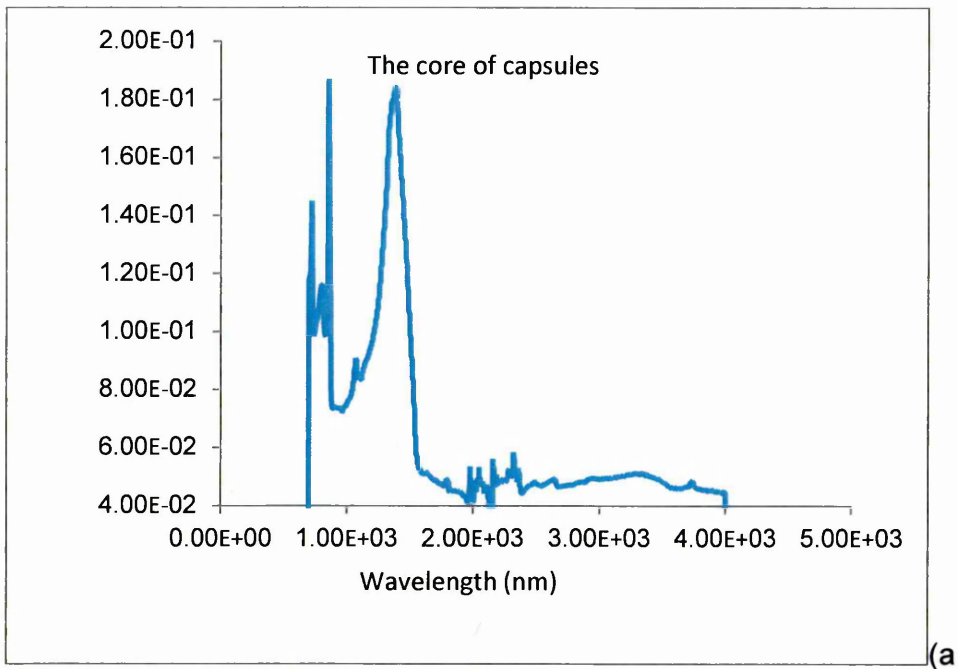


Figure 8.11 (a) Microcapsules with core MgCO_3 tested in FT-IR appear in wavelength 1000 nm, and (b) microcapsules without core in wavelength 1000 nm the core not found.

In Fig 8.11 after removing the core of microcapsules, these capsules were examined by FT-IR spectroscopy, to prove that these microcapsules have lost their core. Two samples were prepared using about 100 μ l from original capsules and the other from those which their core were removed. To the measure the material of the core $MnCO_3$ its appeared at 1000nm, and then the original microcapsules which have core and finally these microcapsules without core, there is no peak appear in 1000nm this mean these microcapsules have not core.

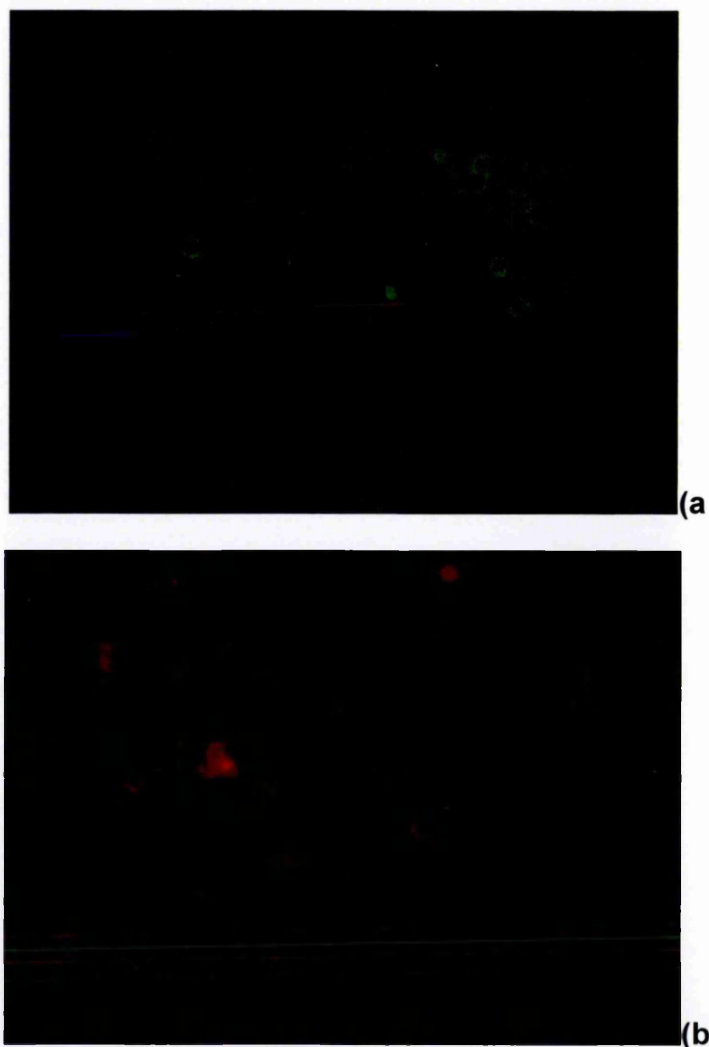
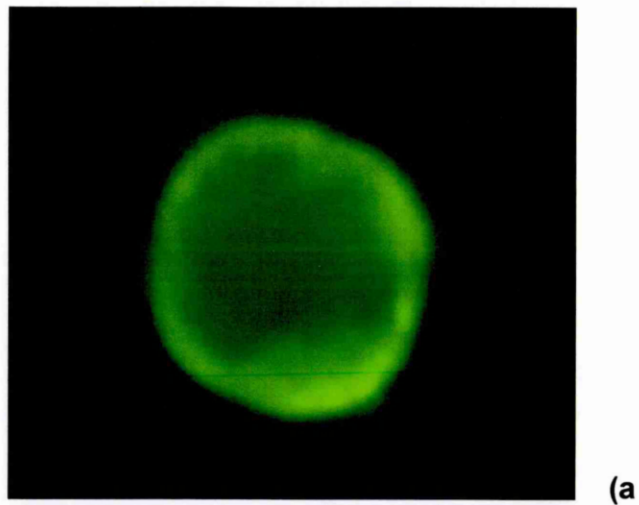


Figure 8.12 (a) microcapsules stained with SYTO-9 Green Fluorescence stain, and (b) Propidium iodide red Fluorescence stain.

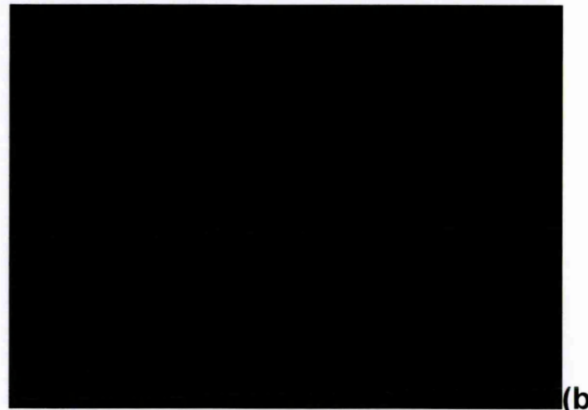
The process involves adding 0.3 μl of SYTO-9 Green Fluorescence stain to 50 μl of microcapsules 6 μm core diameter. This is mixed by centrifuges at the speed of 3000 rpt; then 10 ml of the capsule solution is dropped on the glass slide, covered by a cover slide and viewed under 100x blue light. The same method was used to stain microcapsules with Propidium iodide red Fluorescence stain, viewed under 100x purple light.

Hollow microcapsule filled with dye

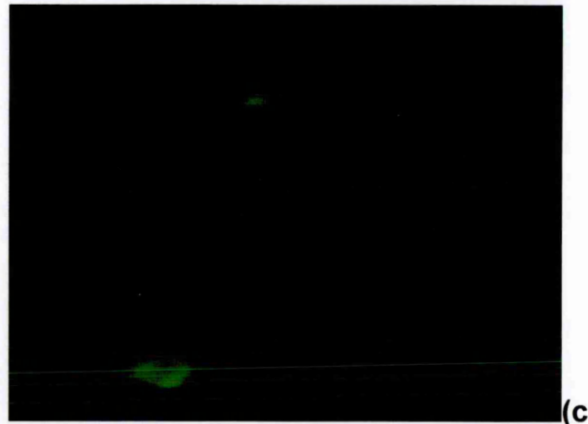
Hollow micro-capsules were prepared by layer-by-layer (LBL) on the 6 μm diameter using oppositely charged polymers polysodium 4-styrene sulfonic acid and polyethelendi-hydro-chlorid then the core removed with (0.1 M) HCL, the capsules appear shrinkage under the fluorescence microscopy. After that the capsules are filled with organic dye (SYTO-9 Green Fluorescence) by changing the PH to 4. The dye goes inside the capsules. A fluorescence microscope was used to visualize the polymer shell, as shown in Figure 8.13.



(a)



(b)



(c)

Figure 8.13 Processes of fill microcapsules with organic dye: a) Capsules of 6 μm stained with fluorescence dye under 100x; (b) Microcapsules after removing the core appears shrinkage; (c) microcapsules after are filled with organic dye and stained with fluorescence dye (SYTO-9 Green Fluorescence stain) under 100x.

8.6 Microcystin-LR removal by electrolysis

Since it was shown recently that microcystin-LR can be degraded photo-catalytically, The degradation process is based on the generation of highly reactive oxygen species (e.g., $\text{HO}\cdot$, $\text{O}\cdot^{2-}$) using Ag_3PO_4 under low pH. Maximum MC-LR degradation rates of 99.98% were obtained within 5 h. But the disadvantage the reaction must be under low pH [232]. This section describes the attempts of using electrolysis of solutions containing MC-LR to reduce its concentration.

A simple experiment was carried out in a sample tube filled with a MC-LR natural extract with two stainless steel electrodes between which the DC voltage of 3V was applied. The initial concentration of microcystin-LR was 25.9 $\mu\text{g/ml}$.

UV-visible spectra measurements were carried out on liquid samples taken at different stages of such treatment in order to monitor the amount of MC-LR in the sample. The results of such measurements presented in Figure 8.14 are showing the reduction of the absorption peak amplitude which indicates the reduction in MC-LR concentration. Also it appeared that the absorption peak was shifted to the shorter wavelengths during electrolysis. The latter fact can be explained by changes in the π -conjugated electron system of MC-LR molecules.

It is known that the position of the absorption band of aromatic molecules depends on the number of π -conjugated electrons in the molecule; the reduction of numbers of π -conjugated electrons causes a “blue” spectral shift. Also a white insoluble layer was formed on the anode after several hours of electrolysis which is most likely the result of flocculation of organic chemicals present, such as microcystin LR. According to [216, 217], a possible mechanism for MC-LR modification involves electrochemical reactions on iron (stainless steel) electrodes, as a result of which Fe^{2+} and Fe^{3+} are formed and react subsequently with MC-LR to form iron-colloid precipitates. Most-likely the Adda group and heptapeptide ring of microcystin (see chemical structure in Fig.2.1) are affected. This model links well with the observed “blue” spectral shift due to disruption of π conjugated electrons.

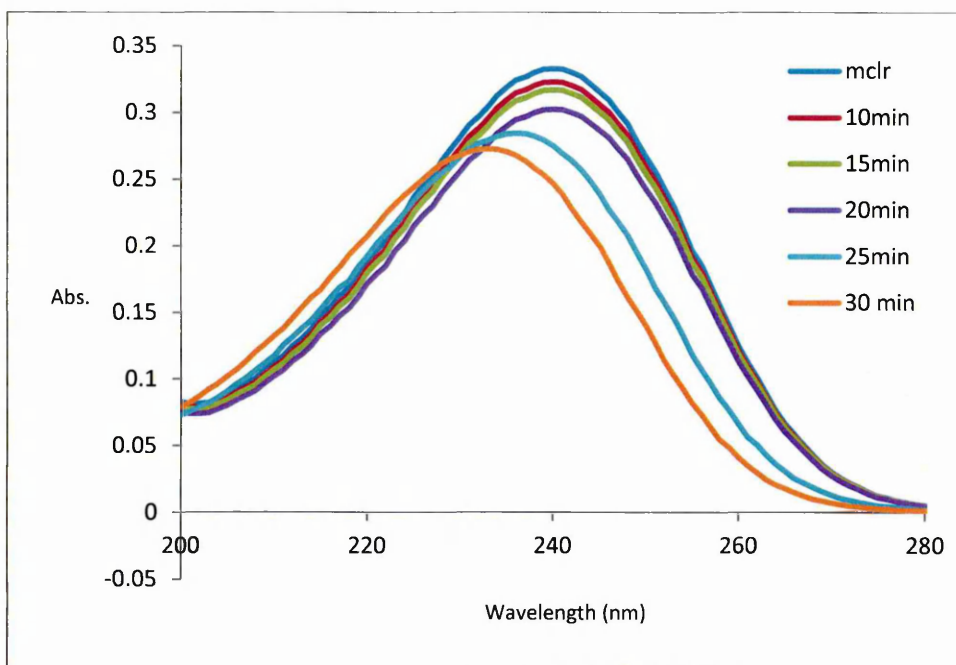


Figure 8.14 Absorption spectra of Microcystin-LR samples during electrolysis.

After 24 hours of continuous electrolysis, the MC-LR peak disappeared completely. The formation of white deposit on the anode was observed after prolonged electrolysis.

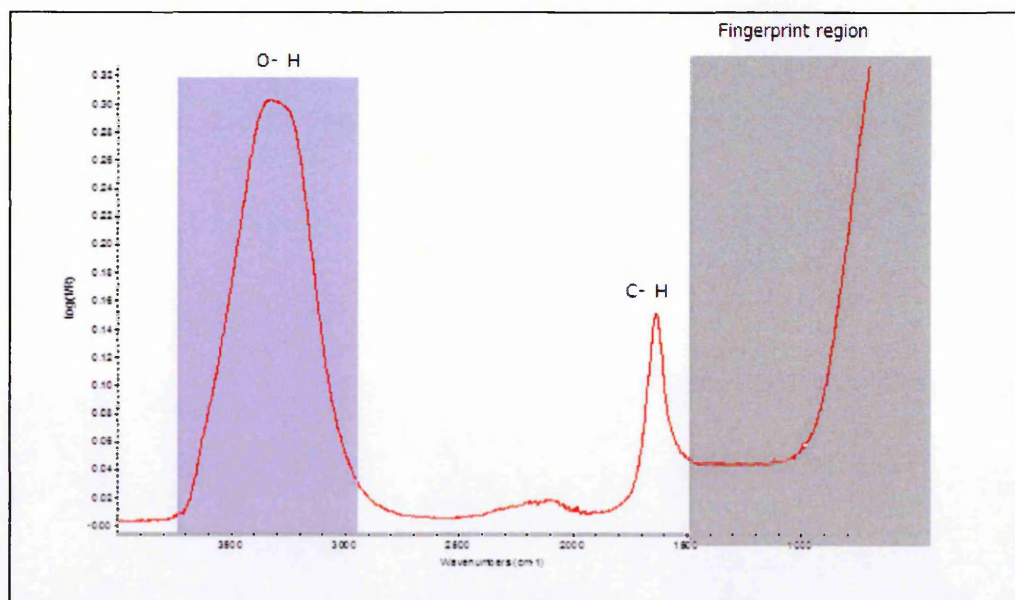


Figure 8.15 FT-IR spectrum of MC-LR solution after 24h electrolysis.

Interestingly, the electrolysis of the same solution in the same cell but with gold-coated electrodes did not show the formation of white deposit. Also, the peak of microcystin-LR at 238 nm was reduced in the intensity but there was no shift to the shorter

wavelengths. The experiment was repeated with the commercial MC-LR with the same outcome.

FT-IR measurements in Figure 8.15 showed no traces of signature vibration bands associated with MC-LR after 24 h electrolysis. The observed fact was showed that degradation of MC-LR is related to the electrochemical reaction on steel (Fe) electrodes as was suggested in [216, 217].

Conclusions

Functionalized microparticules with antibodies successfully reduced MC-LR concentration in aqueous solution, and these particules worked better when keep their core, it deposited more quickly than those without core.

The reduction of ferrate in water is caused by oxygen radicals and peroxide radicals (O_2^{-2} and HO_2^-) radicals these radicals make ferrate a stronger oxidizer and the ferric ion makes it a good coagulants, so that toxin removal after a 30 min contact time was 93%. MCLR reacted with ferrate [228].

CHAPTER 9

CONCLUSION AND FUTURE WORK

9.1 Conclusions

The method of total internal reflection ellipsometry (TIRE) was exploited in the study of protein-protein interaction using the example of interaction of protein chaperon and its receptor in plants. In this work, the interaction of chaperones Hsp 70 and Hsp90 with their receptors OEP61 naturally present in chloroplast membranes were studied using TIRE. For this purpose, chloroplast membranes were successfully deposited on gold coated glass slides using Langmuir-Schaefer technique, which was reported for the first time. Apart from confirming binding between chaperons and respective receptors, this work showed a clear separation of specific and no-specific binding in terms of both the sensor response (i.e. thickness increment) and the affinity of binding. The methodology developed in this work opens exciting possibilities of studying fundamental cellular processes and rapid screening of drugs that target membrane proteins.

Optical methods of total internal reflection ellipsometry (TIRE), UV-visible and FT-IR spectroscopies were successfully adapted for detection of microcystin-LR either in purified form available commercially or naturally produced by algae. The method of TIRE was particularly promising because it was proved to be capable of detection of Microcystin LR in low concentrations down to 0.1ng/ml in direct immunoassay with specific monoclonal antibodies MC10E7. The above immune reaction is highly specific according to the results of the binding kinetics which yielded the values of the association constant in the range of $10^7 - 10^8$ (l/mol). In addition to comprehensive TIRE methodology, a much simpler method of UV-visible spectroscopy was utilized for detection of concentration of microcystin in solutions.

The process of production of microcystin LB by *M. aeruginosa* was studied in more detail. The roles of environmental factors (such as temperature, pH, salinity, nutrients) on both *M. aeruginosa* growth and MC-LR production were evaluated. The generation rate of MC-LR was found to be the optimal conditions for bacteria growth (20-25 C°, light-dark natural cycles, and balanced nutrients). Extra nutrients increase rate of generation of MC-LR, while the presence of NaCl substantially reduced bacteria growth and therefore the production of MC-LR.

The second part of this work was focused on purification of substances contaminated with microcystin. The methodology of using polyelectrolyte coated microparticles functionalized with specific antibodies was first tested on another type of toxin, i.e. Aflatoxin B1 from mycotoxin family. The developed method was adapted for purification of substances containing microcystin LR. This time, polyelectrolyte coated microparticles of 4 and 6 μm in diameter were further functionalized with antibodies specific to MC-LR and successfully used as a sorbent for MC-LR either in purified form or produced naturally by *M. aeruginosa*.

Another simple technique of direct electrolysis can be used for MC-LR cleansing. This process may involve the coagulation of MC-LR with Fe^{3+} ions appearing as a result of the electrochemical reaction on iron electrodes.

9.2 Future work

TIRE method appeared to be a very promising analytical tool in biosensing and showed great potential for many applications including environmental control and and biomedicine. At the same time, TIRE technique based on spectroscopic ellipsometry is a bench-top instrument suitable for in-lab testing. It will be useful to develop a portable sensor which can be used for medical and environmental testing. Planar waveguide devices seem to be the most promising way of doing so.

This research may lead to a number of possible applications in the areas of environmental pollution control, water industry, and biomedicine. Microparticles functionalized with MC10E7 antibodies act as an absorbent for MC-LR in water solutions, and could be used in future for purification of substances contaminated microcystin-LR. This method, however, might be too expensive for decontamination of large quantities of water (contaminated ponds, swimming pools, and water reservoirs), therefore microparticles will more suitable for purification of small samples, maybe to treat food poisoning, and similar application.

Finally, a simple technique of electrolysis was attempted to treat water samples contaminated with microcystin. It appeared to be promising for future application in water purification in a large scale but require more detailed study.

References:

- [1] Lloyd L. Medsker, David Jenkins, and Jerome F. Thomas. (1968). Odorous compounds in natural waters. an earthy-smelling compound associated with blue-green algae and Actinomycetes University of California, Berkeley, *Calif. Sci. Technol.*, **6** (2), 461-464.
- [2] Aceroa Juan L., Rodrigueza Eva, Meriluoto Jussi. (2005). Kinetics of reactions between chlorine and the cyanobacterial toxins microcystins. *Water Research*. **39** , 1628-1638.
- [3] Kull Tomas P. J., Backlund Peter H., Karlsson Krister M., and Meriluoto Jussi A. O. (2004). Oxidation of the cyanobacterial hepatotoxin microcystin-LR by Chlorine Dioxide: Reaction kinetics, characterization, and toxicity of reaction products. *Environ. Sci. Technol.*, **38** (22), 6025-6031.
- [4] WHO. (1998.). Cyanobacterial toxins: Microcystin-LR. guidelines for drinking water quality. world health organization, Geneva.
- [5] Sangolkar Lalita N., Maske Sarikar S., Chakrabarti Tapan. (2006). Methods for determining microcystins (peptide hepatoxins) and microcystin-producing cyanobacteria. *Water Research*. **40** , 3485-3496.
- [6] Hyenstrand P., Metcalf J.S., Beattie K. A. And Codd G. A. (2001). Effects of adsorption to plastics and solvent conditions in the analysis of the cyanobacterial toxin microcystin-LR by high performance liquid chromatography, *Water Source*. **35** , 3508-3511.
- [7] Campas M., Marty Jean-Louis, (2007). Highly sensitive amperometric immunosensors for microcystin detection in algae. *Biosensors and Bioelectronics*. **22** , 1034-1040.
- [8] Jayaraj R., akshmana Rao P.V. L. (2006). Protein phosphorylation profile and adduct formation in liver and kidney of microcystin-LR treated mice, *Toxicon*. **48** , 272-277.
- [9] Lawton Linda A., Heather Chambers, Edwards Christine, Nwaopara Assumpta A., Healy Mike. (2010). Rapid detection of microcystin in cells and water, *Toxicon*. **55** , 973-978.
- [10] Herranz Sonia. Bockova Marketa. Marazuela Maria Dolores. Homola Jiri. Cruz Moreno-Bondi Maria. (2010). An SPR biosensor for the detection of microcystins in drinking water, *Anal. Bioanal. Chem*. **398** , 2625-2634.
- [11] Nabok A., Tsagorodskaya A., Holloway A., Starodub N.F., Gojster O. (2007). Registration of T-2mycotoxin with total internal reflection ellipsometry and QCM impedance methods, *Biosensors and Bioelectronics*. **22** , 885-890.

- [12] Yan-Lei Su, Jin-ru Li, Long Jiang. (2004). Chromatic immunoassay based on polydiacetylene vesicles. *Colloids and Surfaces B: Biointerfaces*. **38** , 29-33.
- [13] Baier W., Loleit M., Fischer B., Jung G., Neumann U., Web M., Weckesser J., Hoffmann P., Bessler W.G., Mittenbuhler K. (2000). Generation of antibodies directed against the low-immunogenic peptide-toxins microcystin-LR/RR and nodularin, *International Journal of Immunopharmacology*. **22** , 339-353.
- [14] Nabok A. V., Hassan A.K., Ray A.K.. (1999). Optical and electrical characterisation of polyelectrolyte self-assembled thin films. *Material science and Engineering*. **9** , 505-508.
- [15] Sadovoy AV, Lomova MV, Antipina MN, Braun NA, Sukhorukov GB and Kiryukhin MV. (2013). Layer-by-layer assembled multilayer shells for encapsulation and release of fragrance. *Acs Applied materials and Interfaces*. **5** (18), 8948-8954.
- [16] Nabok A., Tsargorodskaya A., Mustafa M.K., Szekacs I., Starodub N.F., Szekacs A. (2011). Detection of low molecular weight toxins using optical phase detection techniques, *Sensors and Actuators B, Chemical*. **154** , 232-237.
- [17] Nabok A., Parkinson D., Mustafa M. K., Tsargorodskaya A. (2010). Detection of amyloid precursor protein using ellipsometry immunosensor with a view of alzheimer's disease diagnostics. *Sensors & Transducers*, **120** , 53-61.
- [18] Sung-Hye Cho, Chang-Hee Lee, Jang Mi-Ran, Young-Wook Son, Sang-Mok L., Choi In-Sun, Kim So-Hee, Kim Dai-Byung. (2008). Aflatoxins contamination in spices and processed spice products commercialized in korea, *Food Chem*. **107** , 1283-1288.
- [19] Saleemullah A. I., Amjad Iqbal, Khalil I. A., Hamidullah Shah .(2006). Aflatoxin contents of stored and artificially inoculated cereals and nuts. *Food Chem*. **98** , 699-703.
- [20] Kershaw S.J. (1982). Occurrence of aflatoxins in oilseeds providing cocoa-butter substitutes. *Appl. Environ. Microbiol.*, **43** , 1210-1212.
- [21] Moss M. O. (2002). Risk assessment for aflatoxins in foodstuffs, *Int. Biodetector. Biodegrad*. **50** , 137-142.
- [22] Yu Jorn C.C. and Lai EPC. (2004). Polypyrrole film on miniaturized surface plasmon resonance sensor for ochratoxin A detection. *Synthetic Metals, Elsevier* **143** , 253-258.
- [23] Wild C.P. and Gong Y.Y. (2010). Mycotoxins and human disease: A largely ignored global health issue, *Carcinogenesis*. **31** , 71-82.
- [24] Webster M.T., Groome N., Francis P.T., Pearce B.R., Sherriff F.E., Thinakaran G., Felsenstein K.M., Wasco W., Tanzi R.E. and Bowen D.M. (1995). A novel protein, amyloid precursor-like protein-2, is present in human brain, cerebrospinal-fluid and conditioned media, *Biochem. J*. **310** , 95-99.
- [25] Hudler G. W. (1998). *Magical mushrooms, mischievous mold. new jersey: Princeton university press.*

- [26] Peraica M., Radic B., Lucic A. , and Pavlovic M. (1999). Toxic effects of mycotoxins in humans Bull . *Wold Health Organ.* **77** , 754-766.
- [27] Williams J. H., Phillips T. D., Pauline E. J., Stiles J. K., Curtis M. J., And Aggarwal D.(2004). Human aflatoxicosis in developing countries: A review of toxicology, exposure, potential health consequences, and interventions, The American journal ..., *Am Soc Nutrition* **80** , 1106-1122.
- [28] Sulyok M., Krska R. and Schuhmacher R. (2007). A liquid chromatography/tandem mass spectrometric multi-mycotoxin method for the quantification of 87 analytes and its application to semi-quantitative screening of moldy food samples, *Anal. Bioanal.Chem.* **389** , .1505-1523.
- [29] Sarensen L. K. , and Elbaek T. H. (2005). Determination of mycotoxins in bovine milk by liquid chromatography tanden mass spectrometry, *Jurnal of Chromatography B*, **820** , 183-196.
- [30] Thusu R. (2010). Strong growth predicted for biosensors market. weekly.
- [31] Global industry Analyte Inc... (2008). Biosensors in medical diagnostics-global business report .
- [32] Turko I. V., Lepesheva G. I. and Chashchin V. L. (1992). Direct antigen-detection in langmiur-blodgett-flims of immunoglobulin-G modified with coproporphyrin-I , *Anal. Chim. Acta.* **265** , 21-26.
- [33] Defillipo K. A., and Grayeski M. L. (1991). Flow-injection chemiluminescent method for an enzyme-labeled DNA probe , *Anal. Chim. Acta.* **249** , 155-162.
- [34] Jayaraj R., Lakshmana Rao P.V. (2006). Protien phosphorylation profile and adduct formation in liver and kidney of microcystin-LR treated mice. *Toxicon.* **48** , . 272-277.
- [35] Lawton A., Heather Chambers, Edwards C., Assumpta A. Nwaopara, Healy M. (2010). Rapid detection of microcystin in cells and water. *Toxicon.* **55** , 973-978.
- [36] Herranz S. Bockova M., Dolores Marazuela M., Homola Jiri., Maria Cruz Moreno-Bondi; (2010). An SPR biosensor for the detection of microcystins in drinking water, *Anal. Bioanal. Chem.* **398**, 2625-2634.
- [37] Nabok A., Kamarulzaki M. M., Tsagorodskaya A. and Nikolaj F. S. (2011). Detection of aflatoxin B1 with a label-free ellipsometry immunosensor. *BioNanoScience*, **1** , 38-45.
- [38]- Bohuslav Uher. (2010). Cyanobacteria and algae as significant. Book.Lap lambert academic publishing AG & co KG.
- [39] Stoyneva, Maya P. (2000). Planktic green algae of bulgarian coastal wetlands.*Hydrobiologia.* **438** , 25-41.
- [40] Olson, Theodore A. (1960). Algae in water supplies. *American Journal of Public Health and the Nation's Health*, **50** , 1621-1622.

- [41] Hyenstrand P., Metcalf J.S., Beattie K. A. , and Codd G. A. (2001). Effects of adsorption to plastics and solvent conditions in the analysis of the cyanobacterial toxin microcystin-LR by high performance liquid chromatography. *Water Source*. **35** , 3508-3511.
- [42] David R. (2012). Environmental microbiology: Tampering with cyanobacterial mats. *Nature Reviews Microbiology*. **10** , 239.
- [43] Lehman P.W., Boyer G., Satchwell M., Waller S.(2008). The influence of environmental conditions on the seasonal variation of microcystis cell density and microcystins concentration in san francisco estuary. *Hydrobiologia*. **600** , 187-204.
- [44] Liu J., Yue C., Yonghui D., Zhenkun S., Dong G., Bo To, Dongyuan Zhao. (2010) Magnetic 3-D ordered macroporous silica templated from binary colloidal crystals and its application for effective removal of microcystin. *Microporous and Mesoporous Materials*, **130** (26-31).
- [45] Pouria Shideh, Andrade A de, Barbosa J., Cavalcanti R. L., Barreto V. T. S., Ward C. J., Preiser W., Grace K Poon, Neild G. H., Codd G. A.(1998) ,Fatal microcystin intoxication in haemodialysis unit in Caruaru, Brazil. *Lancet*. **352**, 21–26.
- [46] Huang Winn-Jung , Cheng Bai-Ling , Cheng Yung-Ling. (2007). Adsorption of microcystin-LR by three types of activated carbon. *Journal of Hazardous Materials* ,**141**, 115–122.
- [47] Tao Lin, Wei Chen, Leilei Wang. (2010). Particle properties in granular activated carbon filter during drinking water treatment. *Journal of Environmental Sciences*. **22** , 681-688.
- [48] Miguel Pelaeza, Polycarpos Falarasb, Vlassis Likodimosb, Athanassios G. Kontosb, Armah A. de la Cruzc, Kevin O’shead, Dionysios D. Dionysioua. (2010). Synthesis, structural characterization and evaluation of sol–gel-based NF-TiO2 films with visible light-photoactivation for the removal of microcystin-LR. *Applied catalysis B: Environmental*. **99** , 378-387.
- [49] Robert W. MacKintosh, Kevin N. Dalby, David G. Campbell, Patricia T.W. Cohen, Philip Cohen, Carol MacKintosh.(1995), The cyanobacterial toxin microcystin binds covalently to cysteine-273 on protein phosphatase. *FEBS Letters*. *FEBS Letters* **371** ,236—240.
- [50] Sangolkar Lalita N., Maske Sarikar S., Chakrabarti T. (2006). Methods for determining microcystins(peptide hepatoxins) and microcystin-producing cyanobacteria. *Water Research*. **40** , 3485-3496.
- [51] Lopez C.B., Jewett E.B., Dortch, Q., Walton B.T., Hudnell H.K. (2008). Scientific Assessment of Freshwater Harmful Algal Blooms. Interagency Working Group on Harmful Algal Blooms, Hypoxia, and Human Health of the Joint Subcommittee on Ocean Science and Technology. Washington, DC.

- [52] Campas M., Marty Jean-Louis. (2007). Highly sensitive amperometric immunosensors for microcystin detection in algae., *Biosensors and Bioelectronics*. **22** , 1034-1040.
- [53] Kull Tomas P. J., Backlund Peter H., Karlsson Krister M., and Meriluoto Jussi A. O. (2004). Oxidation of the cyanobacterial hepatotoxin microcystin-LR by ChlorineDioxide: Reaction kinetics, characterization, and toxicity of reaction products. *Environ. Sci. Technol.* **38** (22), 6025-6031.
- [54] Nabok A., Tsargorodskaya A., Gauthier D., Davis F., Higson S.P.J., Berzina T., L. Cristofolini, Fontana M.. (2009). Hybridization of genomic DNA adsorbed electrostatically onto cationic surfaces, *Journal of Physical Chemistry B*. **113** , 7897-7902.
- [55] Jayaraj R., akshmana P.V. L, Rao, (2006). Protein phosphorylation profile and adduct formation in liver and kidney of microcystin-LR treated mice, *Toxicol.***48**, 272-277.
- [56] Stoyneva, Maya P., (2000), Planktic green algae of Bulgarian coastal wetlands, *Hydrobiologia*. **438**,(1), 25-41.
- [57] Olson Theodore A.(1960), Algae in water supplies, *Am. J. Public Health Nations Health*. **50**, (10),1621-1622.
- [58] Cyanobacteria Environmental Microbiology Reports,(2010), **2**, 2, 340 – 341.
- [59] Mohamed Z. A. (2001), Alum and Lime-Alum Removal of Toxic and Nontoxic Phytoplankton from the Nile River Water: Laboratory Study, *Water Resources Management* **15**, 213–221.
- [60] Pelaez M., Falaras P., Likodimos V., Kontos A. G., Armah A. de la Cruz, Kevin O'shea, Dionysios D. Dionysiou, (2010), Synthesis, structural characterization and evaluation of sol-gel-based NF-TiO₂ films with visible light-photoactivation for the removal of microcystin-LR. *Applied Catalysis B: Environmental* **99**, 378–387.
- [61] Ochimsen M.J., Carmichael W., Denisem Card J., Cookson S., Holmes C. M., Antunes M. B., Demelofilh D. A., Lyra T., Barreot V., Azevedo S. F. O., Arvis A. J.(1998). Liver failure and death after exposure to microcystins at a hemodialysis center in Brazil. *The New England Journal of Medicine* **338**,873- 878.
- [62] Garcia L.Villada, Rico M., Altamirano Maria, Sanchez-Martin L., Lopez-Rodas V., Eduardo Costas(2004). Occurrence of copper resistant mutants in the toxic cyanobacteria, *Microcystis aeruginosa*, characterization and future implications in the use of copper sulphate as algacide. *Water research*, **38**, 2207-2213.
- [63] NOAA. (2006) Harmful algal blooms in the Great Lakes. NOAA Great Lakes Environmental Research Laboratory, National Oceanic and Atmospheric Administration.
<http://www.glerl.noaa.gov/res/Centers/HumanHealth/hab/EventResponse/>

- [64] Vesterkvist P.S.M., Meriluoto J.A.O. (2003). Occurrence of microcystins MC-LW and MC-LF in Dutch surface waters and their contribution to total microcystins toxicity. *Toxicon*. **41**. 349-355.
- [65] Tsuji K., Watanuki T., Kondo F., Watanabe M. F., Suzuki S., Nakazawa H., Suzuki M. H., Uchida, Ken-Ichi Harada, (1995). Stability of microcystins from cyanobacteria—II. Effect of UV light on decomposition and isomerization. *Toxicon*. **33**,(12),1619-1631.
- [66] Gan N, Sun X, Song L., (2010), Activation of Nrf₂ by microcystin-LR provides advantages for liver cancer cell growth, *Chem. Res, Toxicol* **23**, 1477- 1484.
- [67] Kondo F, Ikai Y, Oka H, Okumura M, Ishikawa N, et al. (1992) Formation, characterization, toxicity of the glutathione and cysteine conjugates of toxic heptapeptide microcystins. *Chem Res Toxicol*. **5**, 591-596.
- [68] Miller MJ, Hutson J, Fallowfield HJ. (2005), The adsorption of cyanobacterial hepatoxins as a function of soil properties. *J. Water Health.*, **3**(4), 47-339.
- [69] Mohamed Zakaria A., El-Sharouny Hassan M., Ali Wafaa S. (2007), Microcystin concentrations in the Nile river sediments and removal of microcystin-LR by sediments during batch experiments. *Arch. Environ, Toxicon*, **52**, 489-495.
- [70] Andreasen K., B. T. (1999). Validation of urine drug-of-abuse testing methods for ketobemidone using thin-layer chromatography and liquid chromatography-electrospray mass spectrometry. *J Chromatogr B. Biomed Sci Appl.* **736** (1-2), 13-103.
- [71] Sajewicz M, Staszek D, Natic M, Waksmundzka- Hajnos M, Kowalska T, (2011). TLC-MS versus TLC-LC-MS fingerprints of herbal extracts. part III. application of reversed-C18 stationary phase. *J. Chromatogr Sci.* **44** (7), 7-560.
- [72] Engvall Eva, Perlmann Peter. (1971). Enzyme-linked immunosorbent assay (ELISA) quantitative assay of immunoglobulin G. *Immunochemistry*. **8** (9), 871-874.
- [73] Wayne W. Carmichael and Jisi An. (1999). Using an enzyme linked immunosorbent assay (ELISA) and a protein phosphatase inhibition assay (PPIA) for the detection of microcystins and nodularins. *Natural Toxins*. **7** (6), 377-385.
- [74] Lawton Linda A., Chambers Heather, Edwards Christine, Nwaopara Assumpta A., Healy Mike. (2010). Rapid detection of microcystins in cells and water. *Toxicon*. **55** (5), 973-978.
- [75] Herranz Sonia. Bockova Marketa. Marazuela Maria Dolores. Homola Jiri. Moreno-Bondi Maria Cruz. (2010). An SPR biosensor for the detection of microcystins in drinking water, *Anal. Bioanal. Chem.* **398** , 2625-2634.
- [76] Winn-Jung Huang, Bai-Ling Cheng, Yung-Ling Cheng. (2007). Adsorption of microcystin-LR by three types of activated carbon. *Hazardous Materials*. **141** , 115-122.
- [77] Tao Lin, Wei Chen, Leilei Wang. (2010). Particle properties in granular activated carbon filter during drinking water treatment. *Environmental Sciences*. **22** (5), 681-688.

- [78] Nabok A.V. , Tsargorodskaya A., Hassan A.K., Starodub N.F. (2005). Total internal reflection ellipsometry and SPR detection of low molecular weight environmental toxins. *Applied Surface Science*. **246** (4), 381-386.
- [79] Brooks Steven L., Ashby Robert E., Turner Anthony P.F., Calder Michael R., Clarke David J. (1987). Development of an on-line glucose sensor for fermentation monitoring. *Biosensors*. **3** (1), 45-56.
- [80] Sai a V.V.R., Tapanendu Kundub, Deshmukhc Chitra, Titusc Susan, Pradeep Kumarc, Soumyo Mukherjia. (2010). Label-free fiber optic biosensor based on evanescent wave absorbance at 280nm. *Sensors and Actuators B*. **143** , 724-730.
- [81] Rekha K., Thakur M. S. and Karanth N. G. (2000). Biosensors for the detection of organophosphorous pesticides. *Informa Health Care*. **20** , 213-235.
- [82] Gutiérrez M., Alegret S., del Valle M.. (2007). Potentiometric bioelectronic tongue for the analysis of urea and alkaline ions in clinical samples. *Biosensors and Bioelectronics*. **22** (9-10), 2171-2178.
- [83] Hicks G. P. , Updike S. J. (1967). The enzyme electrode, *Nature*, **214**,986-988.
- [84] Guilbault, G. G. , and Montalvo, J.(1969). A urea specific enzyme electrode, *J. Am.Chem. Soc.***91**,2164.
- [85] Blackburn G. F., Shah H. P., Kenten J. H., Leland J., Kamin R. A., Link J., Peterman J., Powell M. J., A. Shah, D. B. Talley, S. K. Tyagi, E. Willkins, T. G. Wu and R. J. Massae,(1991), Electrochemiluminescence Detection for Development of Immunoassays and Dna Probe Assays for Clinical Diagnostics, *Clin. Chem.*, **37**,1534-1539.
- [86] Rocks B.F., Patel N. and Bailey M.P., (1991) Use of a silver-enhanced gold-labeled immunoassay for detection of antibodies to the human-immunodeficiency-virus in whole-blood samples *Ann. Clin. Biochem.*, **28**,155-129.
- [87] Jansen E. H. M., Vandenberg R.H.and Zomer G.,(1989), characteristics and detection principles of a new enzyme label producing a longe-term chemi-luminescent signal, *J. Biolumin. Chemilumin.*, **4**,129-135.
- [88] Betazzo. U, Ehrlich S. D. and Bernardi g., (1973),radioactive labelling and analysis of 3 – Terminal nucleotides of DNA fragments. *Biochim. Biophys. Acta*, **312**,192-201.
- [89] Hypia T., (1985), detection of adenovirus in nasopharyngeal specimens by radioactiveand nonradioactive dna probe , *J. Clin. Microbial*. **21**, 730-733.
- [90] Ricci F., Volpe G., micheli L., and palleschi G.,(2007), a review on novel developments and applications of immunoscensors in food analysis, *Anal. Chim. Acta*, **605**, 111-129.
- [91] Janis K. (1997), Immunology. W.h.freeman & co.
- [92] Wild D., Ed.(2005). The immunoassay handbook. London: *Elsvier*.

- [93] Dan Dua, Feng Yanb, Shengli Liuc, Huangxian Jua, (2003) Immunological assay for carbohydrate antigen 19-9 using an electrochemical immunosensor and antigen immobilization in titania sol-gel matrix . *Journal of Immunological Methods*, **283** , 67-75
- [94] Elgersma A. V. , Zsom R. L. J., Norde W. and Lyklema J. (1991), The adsorption of different types of monoclonal immunoglobulin on positively and negatively charged polystyrene lattices, *Colloids and Surfaces*, **54**, 89-101.
- [95] Bagchi P. and Birnbaum S. M., (1981), Effect of ph on the adsorption of immunoglobulin-g on anionic poly(vinyltoluene) model latex- particales, *J. Colloid Interface Sci.***83**, 460-478.
- [96] Schramm W., Paek S. and Voss G. (1993) Strategies for the immobilization of antibodies, *Immunomethode*, **3**, 93-103.
- [97] Hicks G. P. and Updike S. J. (1967) The enzyme electrode, *nature*. **214** , 986.
- [98] Edeleman G. M. (1972). Antibody structure and molecular immunology,*Science* . , 830-840.
- [99] Gerdes J., Lemke H., Baisch H., Wacker H.H., Schwab U.and Stein H. (1984). Cell cycle analysis of a cell proliferation-associated human nuclear antigen defined by the monoclonal antibody ki-67.*Immunology*. **133** , 1710-1715.
- [100] Donasik Yoo, Aiping Wu, Jinkyu Lee, Michael F. Rubner.(1997).New electro-active self-assembled multilayer thin films based on alternately adsorbed layers of polyelectrolytes and functional dye molecules, *Synthetic Metals*.**85** (1-3), 1425- 1426.
- [101] Yuri Lvov , Heinrich Haas , Gero Decher , Helmuth Moehwald , Albert Mikhailov , Boris Mtchedlishvily , Ekaterina Morgunova , Boris Vainshtein(1994). Successive Deposition of Alternate Layers of Polyelectrolytes and a Charged Virus, *Langmuir*, **10** (11), 4232-4236.
- [102] Janeway CA Jr, Travers P, Walport M, et al. (2001). Immunobiology: The immune system in health and disease .5th edition. Garland science. .
- [103] RE Bird, KD Hardman, JW Jacobson, S Johnson, BM Kaufman, SM Lee, T Lee, SH Pope, GS Riordan, M Whitlow. (1988). Single-chain antigen-binding proteins. *Science*. **242** , 423-426.
- [104] Mayer G., Immunoglobulins-structure and function. Microbiology. 5th edition, H edition, 110-113.
- [105] Hornbeck P., Winston S. E., Fuller S. A. (2001). Enzyme-Linked immunosorbent assays (ELISA). Current protocols in molecular biology.
- [106] Indyk H. E., Evans E. A., Bostrom Caselunghe M.C. (2000). Determination of biotin and folate in infant formula and milk by optical biosensor-based immunoassay. *AOAC International*. **83** , 1141-1148.

- [107] Nagata K. and Handa H. Springer-Verlag. (2000). Real-time analysis of biomolecular interactions: Applications of biacore. Tokyo.
- [108] Azzam R.M.A. and Bashara N.M.,(1978). Ellipsometry and Polarized. *Surface Technology*, 7, (3) 269.
- [109] Woollam J.A.Co.Inc, (2001), Guide to using WVASE32, Software for Spectroscopic Ellipsometry Data Acquisition and Analysis. New York: Wex Tech Systems Inc.
- [110] Arwin H. (1998), Spectroscopic ellipsometry and biology: recent developments and challenges, *Thin Solid film* 764-774.
- [111] Sai V.V.R., Tapanendu Kundu, Chitra Deshmukh, Susan Titus, Pradeep Kumar, Soumyo Mukherji,(2010), Label-free fiber optic biosensor based on evanescent wave absorbance at 280nm. *Sensors and Actuators B* **143**, 724–730.
- [112] Nabok A., Tsargorodskaya A., Frank Davis, Seamus Higson P.J. (2007) The study of genomic DNA adsorption and subsequent interactions using total internal reflection ellipsometry. *Biosensors and Bioelectronics* **23**, 377-383.
- [113] Malmqvist M.(1993). Surface plasmon resonance for detection and measurement of antibody-antigen affinity and kinetics. *Curr Opin Immunol.* **5**,282-286.
- [114] Alexander Szabo, Lesley Stolz and Russ Granzow(1995). Surface plasmon resonance and its use in biomolecular interaction analysis (BIA). *Current Opinion in Structural Biology*, **5**(5), 699-705.
- [115] Herranz S., Bockova M. Marazuela M.D. Homola J. Moreno-Bondi M. C. (2010). An SPR biosensor for the detection of microcystins in drinking water, *Anal. Bioanal. Chem.***398**, 2625-2634.
- [116] Kabashin A. V., and Nikitin P.I.,(1998), “Surface plasmon resonance interferometer for bio- and chemical-sensors, *Opt. Commun.* **150** (1-6), 5–8.
- [117] Nabok A.V., Hassan A.K., Ray A.K.; (1999) Optical and electrical characterisation of polyelectrolyte self-assembled thin films. *Material Science and Engineering C* (8-9), 505-508.
- [118] Nabok A., Parkinson D., Mustafa M. K., Tsargorodskaya A.,(2010) Detection of amyloid precursor protein using ellipsometry immunosensor with a view of Alzheimer's disease diagnostics, *Sensors & Transducers*,**120** (9), 53-61.
- [119] Westphal P. and Bornmann A.,(2002) bioelcular detection by surface Plasmon enhanced ellipsometry, *Sensors and Actuators, B: Chemical*, **84**,.278-282.
- [120] Arwin A., Poksinski M. and Johansen K. (2004) total internal reflection ellipsometry: principles and applications,*Appl. Opt.***43**,3028-3036.

- [121] Nabok A.V., Tsargorodskava A., Hassan A.K. and Starodub N.F. ,(2005), total internal reflection ellipsometry and SPR detection of low molecular weight environmental toxins. *Applied Surface Science*,**246**,381-386.
- [122] Kim H. , Jung S., Kim S. , Suh I., Kim W.J., Jung J.,Yuk, J.S. Kim Y. and k. Ha,(2006), high-throughput analysis of mumps virus and the virus-specific monoclonal antibody on the arrays of a cationic polyelectrolyte with a spectral SPR Biosensor, *Proteomics*, **6**, 6426-6432.
- [123] Anne Zeck, Anja Eikenberg, Michael G. Weller, Reinhard Niessner,(2001). Highly sensitive immunoassay based on a monoclonal antibody specific for [4-arginine]microcystins *Analytica Chimica Acta*. **441**,1–13.
- [124] Woollam J.A Co. Inc,(2001).Guide to using WVASE32, Software for Spectroscopic Ellipsometry Data Acquisition and analysis. New York,Wex Tech systems Inc.,
- [125] Hiroyuki Fujiwara,(2007). Spectroscopic Ellipsometry: Principles and Applications. England: John Wiley& Son Ltd.
- [126] Nabok A. (2005). Organic and inorganic nanostructure, artech house, boston.
- [127] Indyk H. E., Evans E. A., Bostrom Caselunghe M.C . (2000), Determination of biotin and folate in infant formula and milk by optical biosensor-based immunoassay.*AOAC international*. **83** , 1141-1148.
- [128] Anne Zeck, Anja Eikenberg, Michael G. Weller. (2001). Reinhard niessner highly sensitive immunoassay based on a monoclonal antibody specific for [4-arginine]microcystins. *Analytica Chimica Acta*. **441** , 1-13.
- [129] Shane Beck. (1998). Across the spectrum: Instrumentation for UV/Vis spectrophotometry,the scientist magazine technology profile,chart 1.
- [130] Andruch V., Kocúrová L., Balogh I. S., Škrliková J. (2012). Recent advances in couplingsingle-drop and dispersive liquid–liquid microextraction with UV-vis spectrophotometry and related detection techniques. *Microchemical Journal Elsevier* **102** , 1-10.
- [131] Bosch Ojeda C., Sanchez Rojas F. (2013) Recent applications in derivative ultraviolet/visible absorption spectrophotometry.*microchemical journal*, **106** , 1-16.
- [132] Filipický T., Říha M., Hrdina R., Vávrová K., Mladěnka P. (2013). Mathematical calculations of iron complex stoichiometry by direct UV–Vis spectrophotometry. *Bioorganic Chemistry*. **49** , 1-8.
- [133] Josep M. Vergès, Juan I. Morales. (2014). The gigapixel image concept for graphic SEM documentation.applications in archeological use-wear studies.*Micron*. **65** , 15-19.
- [134] Jiruše J., Havelka M., Lopour F. (2014). Novel field emission SEM column with beam deceleration technology. *Ultramicroscopy. Elsevier* **146** , 27-32.

- [135] Chunli Zheng, Yafei Ding, Xiaoqing Liu, Yunkai Wu, Liang Ge. (2014). Highly magneto-responsive multilayer microcapsules for controlled release of insulin. *International Journal of Pharmaceutics*. **475** (1-2), 17-24.
- [136] Woodward J.D., Wepf R.A. (2014), Macromolecular 3D SEM reconstruction strategies: Signal to noise ratio and resolution. *Ultramicroscopy*. **144** , 43-49.
- [137] Orkun Ersoy. (2010). Surface area and volume measurements of volcanic ash particles by SEM stereoscopic imaging. *Journal of Volcanology and Geothermal research*. **190** (3-4), 290-296.
- [138] İlker R. Çapoğlu, Jeremy D. Rogers, Allen Taflove, Vadim Backman. (2012). Chapter 1 - the microscope in a computer: Image synthesis from three-dimensional full-vector solutions of Maxwell's equations at the nanometer scale. *progress in optics*. **57** , 1-91.
- [139] Perkins W.D. (1986). Fourier transform-infrared spectroscopy. part 1. instrumentation. topics in chemical instrumentation. ed. frank A. settle, Jr. *Journal of Chemical Education*. **63** , 5-10.
- [140] Smith B. C. (1996). Fundamentals of fourier transform infrared spectroscopy, CRC press.
- [141] Saptari V. (2003). Fourier-transform spectroscopy instrumentation engineering, SPIE publication, bellingham. .
- [142] Cheng X., Irimia D., Dixon M., Sekine K., Demirci U., Lee Z., Tompkins R. G., William R. and Toner M. (2007). A microfluidic device for practical label-free CD4+ T cell counting of HIV-infected subjects. *Lab. Chip* **7** , 170-178.
- [143] Kubitscheck U. (2013). Fluorescence microscopy: From principles to biological applications. (Book), 1-539.
- [144] Hausmann, Michael. (1997). High-precision distance microscopy of 3D nanostructures by a spatially modulated excitation fluorescence microscope. *Optical Biospies and Microscopic Techniques*. **3197** , 217.
- [145] Bailey B., Farkas D.L., Taylor D.L., and Lanni F. (1993). Enhancement of axial resolution in fluorescence microscopy by standing-wave excitation, *Nature*. **366** , 44-48.
- [146] Konstatinides K., and Rasure J. (1994). The khoros software development environment for image and signal processing IEEE trans. *Image proc.* **3** (3), 243-252.
- [147] Gunkel, M. (2009). Dual color localization microscopy of cellular nanostructures. *Biotechnology Journal*. **4** (6), 38-927.
- [148] Nabok A. V. and Richardson T., Frank Davis and Stirling Charles J. M., (1997). Cadmium sulfide nanoparticles in Langmuir–Blodgett films of calixarenes. *Langmuir*. **13** (12), 3198-3201.

[149] Nabok A.V. Author Vitae, Hassan A.K. , Ray A.K , Omar O., Kalchenko V.I. (1997). Study of adsorption of some organic molecules in calix[4]resorcinolarene LB films by surface plasmon resonance. *Sensors and Actuators B: Chemical.* **45** (2), 115-121.

[150] RAY, Hassan A. K., and Nabok, A. V. (2003). Nanocomposite organic films on silicon. *Nanotechnology, IEEE transact.* **2** (3), 149-153.

[151] Ebrahim S. (2012) Harvard college, properties of silk III fibroin at the air-water interface.

[152] Nabok A. V. (2000). Registration of immunoglobuline AB/AG reaction with planar polarization interferometer. *Biochemical and Biomolecular Sensing.* 4200 .

[153] Hassan, A. K., Nabok, A. V., Ray, A. K., Lucke, A., Smith, K., Strilling, C. J. M. and DAVIS, F. (1999). Thin films of calix-4-resorcinarene deposited by spin coating and Langmuir-Blodgett techniques: determination of film parameters by surface plasmon resonance. *Materials Science and Engineering C*, **8-9**, 251-255.

[154] Ebrahim S. (2012). Harvard college, properties of silk III fibroin at the air-water interface.

[155] Hayward D., Pethrick R. A. , Tiwaporn Siri Wittayakorn. (1992). Dielectric studies of heterogeneous phase polymer systems: Poly(ethylene oxide) inclusions in polycarbonate - a model system. *Macromolecules.* **25** (2), 1480-1486.

[156] Sze-Shun Wong , Hajime Takano , and Marc D. Porter. (1998). Mapping orientation differences of terminal functional groups by friction force microscopy. *Anal. Chem.* **70** (24), 5209-5212.

[157] Haberska K., Ruzgas T. (2009) Polymer multilayer film formation studied by in situ ellipsometry and electrochemistry. *Bioelectrochemistry.* **76** , 153-161.

[158] González-Maeso J. (2010) Anxious interactions. *Nature Neuroscience.* **13** , 524-526.

[159] Maynard JA, Lindquist NC, Sutherland JN, Lesuffleur A, Warrington AE, et al. (2009). Surface plasmon resonance for high-throughput ligand screening of membrane-bound proteins. *Biotechnol J.* **4** , 1542-1558.

[160] Nabok A, Tsargorodskaya A. (2008). The method of total internal reflection ellipsometry for thin film characterisation and sensing. *Thin Solid films.* **516** , 8993-9001.

[161] Arwin H, Poksinski M, Johansen K. (2004). Total internal reflection ellipsometry: Principles and applications. *Appl Optics.* **43** , 3028-3036.

[162] Kriechbaumer V, Tsargorodskaya A, Mustafa MK, Vinogradova T, Lacey J, et al. (2011). Study of receptor-chaperone interactions using the optical technique of spectroscopic ellipsometry. *Biophys J.* **101** , 504-511.

- [163] Von Loeffelholz O, Kriechbaumer V, Ewan RA, Jonczyk R, Lehmann S, et al. (2011). OEP61 is a chaperone receptor at the plastid outer envelope. *Biochem J.* **438** , 143-153.
- [164] Wickner W, Schekman R. (2005). Protein translocation across biological membranes. *Science.* **310** , 1452-1456.
- [165] Abell BM, Rabu C, Leznicki P, Young JC, High S. (2007). Post-translational integration of tail-anchored proteins is facilitated by defined molecular chaperones. *J Cell Sci.* **120** , 1743-1751.
- [166] Nabok A., Tsargorodskaya, A., Mustafa, M. K., Szekacs, I., Starodub, (2011). Detection of low molecular weight toxins using optical phase detection techniques. *Sensors Actuators B Chemical*, **154** , 232-237.
- [167] Nabok A., Tsargorodskaya, A., Holloway, A., Starodub, N. F. (2007). Specific binding of large aggregates of amphiphilic molecules to respective antibodies. *Langmuir.* **23** , 8485-8490.
- [168] Kershaw S. J. (1982). Occurrence of aflatoxin in oilseeds providing cocoa-butter substitutes. *Appl. Environ. Microbiol.* **43** , 1210-1212.
- [169] Yu J. C. C. and Lai E. P. C. (2004). Polypyrrole film on miniaturized surface plasmon resonance sensor for ochratoxin A detection, *Synth. Met.* **143** , 253-258.
- [170] Nabok, A. V., Daves, F., Hassan, A. K., RAY, A. K., Majeed, R. and Ghassemlooy, Z. (1999). Polyelectrolyte self-assembled thin films containing cyclo-tetrachromotropyrene for chemical and bio-sensing. *Materials Science and Engineering C*, **8-9**, 123-126.
- [171] Nabok A., Tsargorodskaya A., Davis F., Higson S. P.J, (2007). The study of DNA hybridisation using total internal reflection ellipsometry, *Biosensors & Bioelectronics*, **23** (3), 377-383.
- [172] Nabok A., Tsargorodskaya A. (2008). The method of total internal reflection ellipsometry for thin film characterisation and sensing, *Thin Solid Films*, **516** (24), 8993-9001.
- [173] Nabok A., Tsargorodskaya A., Gauthier D., Davis F., Higson S.P.J., T. Berzina, L. Cristofolini, Fontana M., (2009). Hybridization of genomic DNA adsorbed electrostatically onto cationic surfaces, *Journal of Physical Chemistry B*, **113** , 7897-7902.
- [174] Nabok A.V. , Tsargorodskaya A., Holloway A., Starodub N.F., Demchenko A. (2007). Specific binding of large aggregates of amphiphilic molecules to respective antibodies, *Langmuir*, **23** (16), 8485-8490.
- [175] Nabok A., Heriot S.Y., Richardson T. H. (2005). Optical study of langmuir-schaeffer films of gold colloid nanoparticles, *Phys. Status Solid*, **242** (4), 797-802.

- [176] Mustafa M.K., Nabok A., Parkinson D., Tothill I.E., Salam F., Tsargorodskaya A., (2010). Detection of beta- amyloid peptide (1-16) and amyloid precursor protein (APP770) using spectroscopic ellipsometry and QCM techniques: A step forward towards alzheimers disease diagnostics, *Biosensors & Bioelectronics*, **26** , 1332-1336.
- [177] Nabok A., Tsargorodakaya A., Suryajaya. (2008). Ellipsometry study of ultra thin layers of evaporated gold, *Phys. Stat. Solid C*, **23** (5), 1150-1155.
- [178] Nabok, A. V., Ray, A. K., Hassan, A. K., Omar, O., Taylor, R., Richardson, T. and Pavier, M. (1998). Inclusion phenomenon in mixed floating layers containing phthalocyanines. *Thin Solid Films*, **327**, 104-108.
- [179] Mackintosh C., Beattie K. A., Klump S., Cohen P.H., Codd G. A. (1990). Cyanobacterial microcystin-LR is a potent and specific inhibitor of protein phosphatases 1 and 2A from both mammals and higher plants. *FEBS Lett*, **264**(2) 187-192.
- [180] Carmichael, Carmichael W.W. (1992). Cyanobacteria secondary metabolites-the cyanotoxins. *Journal of Applied Bacteriology*, **72** , 445-459.
- [181] Lindner P., Molz R., Yacoub-George E., Durkop A., Wolf H. (2004) Development of a highly sensitive inhibition immunoassay for microcystin-LR. *Analytica Chimica Acta* . **521** (1), 37-44.
- [182] Anne Zeck , Michael G. Weller , Don Bursill and Reinhard Niessner, (2001). Generic microcystin immunoassay based on monoclonal antibodies against adda. *Analyst*. **126** , 2002-2007.
- [183] Zeck A., Weller M. G., Niessner R. (2001). Highly sensitive immunoassay based on a monoclonal antibody specific for [4-arginine]microcystins. *Analytica Chimica Acta* . **441** (1), 1-13.
- [184] Claire S. Peyratout Dr. and Lars Dähne Dr. Tailor-made polyelectrolyte microcapsules: From multilayers to smart containers. *Angewandte Chemie International edition*. **43** (29), 3762-3783.
- [185] Kenne G., Deon van der Merwe. (2013). Classification of toxic cyanobacterial blooms by fourier-transform infrared technology (FTIR). *Advances in microbiology*, **3** , 1-8.
- [186] Frank Higgins. (2013). Onsite quantitative FTIR analysis of water in turbine oil.
- [187] Sabine Ja hnichen, Benedict M. Long, Thomas Petzoldt. (2011). Microcystin production by microcystis aeruginosa: Direct regulation by multiple environmental factors. *Harmful Algae*. **12** , 95-104.
- [188] Zhou Yang , Linlin Geng , Wei Wang , Jing Zhang. (2012). Combined effects of temperature, light intensity, and nitrogen concentration on the growth and polysaccharide content of microcystis aeruginosa in batch culture. *Biochemical Systematics and Ecology*. **41** , 130-135.

- [189] Dittmann E., Börner T.(2005). Genetic contributions to the risk assessment of microcystin in the environment. *Toxicology and Applied Pharmacology*. **203** , 192-200.
- [190] Sielaff H., Dittmann E., Tandeau de Marsac N., Bouchi C., von Döhren H., Börner T., Schwecke T. (2003). The mcyF gene of the microcystin biosynthetic gene cluster from *Microcystis aeruginosa* encodes an aspartate racemase, *Biochemical journal, immediate publication* .
- [191] KRÜGER G.H.J., Eloff J. N. (1983). Effect of CO₂ and HCO₃⁻ on photosynthetic oxygen evolution by *Microcystis aeruginosa*. *Zeitschrift für Pflanzenphysiologie* **112** (3), 231-236.
- [192] Taghavi D., Farhadian O., Mahboobi Soofiani N., Keivany Y. (2013). Effects of different light/dark regimes and algal food on growth, fecundity, ephippial induction and molting of freshwater cladoceran, *Ceriodaphnia Quadrangula*, *Aquaculture*. **410-411** , 190-196.
- [193] Karina Hesse, , Elke Dittmann, Thomas Börner. (2001). Consequences of impaired microcystin production for light-dependent growth and pigmentation of *Microcystis aeruginosa* PCC 7806, *FEMS Microbiology Ecology* . **37** (1), 39-43.
- [194] Zhou Yang , Linlin Geng, Wei Wang, Jing Zhang. (2012). Combined effects of temperature, light intensity, and nitrogen concentration on the growth and polysaccharide content of *Microcystis aeruginosa* in batch culture. *Biochemical Systematics and Ecology*. **41**, 130-135.
- [195] Carlos J. Pestana, Petra J. Reeve, , Gayle Newcombe. (2014). Extraction method for total microcystins in cyanobacteria-laden sludge, *Journal of Chromatography B* . **965** , 61-64.
- [196] Carmen Rojo, , Matilde Segura , Francisco Cortés , María A. Rodrigo . (2013). Allelopathic effects of microcystin-LR on the germination, growth and metabolism of five charophyte species and a submerged angiosperm. *Aquatic Toxicology*. **144-145**, 1-10.
- [197] Xi Hu, Yunguo Liu, Guangming Zeng, Xinjiang Hu, Yaqin Wang, Xiaoxia Zeng. (2014). Effects of limonene stress on the growth of and microcystin release by the freshwater cyanobacterium *Microcystis aeruginosa* FACHB-905, *Ecotoxicology and Environmental Safety* **105** , 121-127.
- [198] Timothy W. Davis, Dianna L. Berry, Gregory L. Boyer, Christopher J. Gobler. (2009). The effects of temperature and nutrients on the growth and dynamics of toxic and non-toxic strains of *Microcystis* during cyanobacteria blooms, *Harmful Algae*. **8** (5), 715-725.
- [199] Yanfang Chen, Fengbo He, Yong Ren, Hong Peng, , Kaixun Huang. (2014). Fabrication of chitosan/PAA multilayer onto magnetic microspheres by LbL method for removal of dyes. *Chemical Engineering Journal*. **249**, 79-92.
- [200] Shideh Pouria, A de Andrade, J Barbosa, R L Cavalcanti, V T S Barreto, C J Ward, W Preiser, Grace K Poon, G H Neild, G A Codd (1998). Fatal microcystin intoxication in haemodialysis unit in caruaru, Brazil. *Lancet* . **352** , 21-26.

- [201] Winn-Jung Huang, Bai-Ling Cheng, Yung-Ling Cheng. (2007). Adsorption of microcystin-LR by three types of activated carbon. *Journal of Hazardous Materials*. **141**, 115-122.
- [202] Tao Lin, Wei Chen, Leilei Wang. (2010). Particle properties in granular activated carbon filter during drinking water treatment. *Journal of Environmental Sciences*, **22** (5), 681-688.
- [203] Lalita N. Sangolkar, Sarika S. Maske, Pradeep L. Muthal, Sanjay M. Kashyap, Tapan Chakrabarti. (2009). Isolation and characterization of microcystin producing *microcystis* from a central Indian water bloom. *Harmful Algae*. **8** (5), 674-684.
- [204] Emad Y. A. Al-Sultan. (2011). The isolation, the purification and the identification of hepatotoxin microcystin-LR from two cyanobacterial species and studying biological activity on some aquatic organisms. *Journal of Basrah Researches Sciences*. **37**, 39-57.
- [205] Straub C., Quillardet P., Vergalli J., Tandeau de Marsac N., Humbert J. F. (2011), A Day in the Life of *Microcystis aeruginosa* Strain PCC 7806 as Revealed by a Transcriptomic Analysis. *Plos One. Journal Pone*.
- [206] Sabine Jaehnichen a, Benedict M. Long, Thomas Petzoldt. (2011). Microcystin production by *microcystis aeruginosa*: Direct regulation by multiple environmental factors. *Harmful Algae* 12 (2011) 95–104. **12**, 95-104.
- [207] Qin Wei, Yanfang Zhao, Bin Du, Dan Wu, Yanyan Cai, Kexia Mao, He Li, and Caixia Xu. (2011). Nanoporous PtRu alloy enhanced nonenzymatic immunosensor for ultrasensitive detection of microcystin-LR. *Advanced Functional Material*. **21** (21), 4193-4198.
- [208] Sharma V. K., Triantis M. T. M., Antoniou G. X., Pelaez He M., Han C., Song W., Shea K. E. O, Cruz A. A. de la, Kaloudis T., Hiskia A., Dionysios D. Dionysiou,. (2012). Destruction of microcystins by conventional and advanced oxidation processes: A review. *Separation and Purification Technology*. **91**, 3-17.
- [209] Liu J., Huang Y., Kumar A., Tan A., Jin S., Mozhi A., Xing-Jie Liang. (2013). pH-sensitive nano-systems for drug delivery in cancer therapy. *Biotechnology Advances*, **32**, (4), 693-710.
- [210] Xiaoxue Song, Huanbin Li, Weijun Tong, Changyou Gao. (2014). Fabrication of triple-labeled polyelectrolyte microcapsules for localized ratiometric pH sensing. *Journal of Colloid and Interface Science* **416**, 252-257.
- [211] Alireza Abbaspourrad, Sujit S. Datta, and David A. Weitz. (2013). Controlling release from pH-responsive microcapsules. *Langmuir*, **29** (41), 12697-12702.
- [212] Feng Z., Wang Z., Gao C., Shen J. (2007). Hollow microcapsules with a complex polyelectrolyte shell structure fabricated by polymerization of 4-vinylpyridine in the presence of poly(sodium 4-styrenesulfonate) and silica particles. *Materials Letters*. **61**, 2560-2564.

- [213] Bao-ling yuan, Jiu-Hui Qu, Ming-Lai Fu. (2002). Removal of cyanobacterial microcystin-LR by ferrate oxidation- coagulation. *Toxicon*. **40** , 1129-1134.
- [214] Alice Hudder, Weihua Song, Kevin E. O'Shea, Patrick J. Walsh. (2007). Toxicogenomic evaluation of microcystin-LR treated with ultrasonic irradiation, *Toxicology and Applied Pharmacology*. **220** , 357-364.
- [215] He X., Pelaez M., Judy A. Westrick , Kevin E. O'Shea , A., H.,T., Triantis, T., Kaloudis, Mihaela I. Stefan f, Armah A. de la Cruz , Dionysios D. Dionysiou . (2012). Efficient removal of microcystin-LR by UV-C/H₂O₂ in synthetic and natural water samples. *Water Research*. **4** (6), 1501-1510.
- [216] Dai G., Quan C., Zhang X. , Jin Liu, L., Song. (2012). Nanqin gan. fast removal of cyanobacterial toxin microcystin-LR by a low-cytotoxic microgel-fe(III) complex. *Water Research*. **46** , 1482-1489.
- [217] Liana L., Caoa X., Wu Y., Sunb D., Loub D., (2014). A green synthesis of magnetic bentonite material and its application for removal of microcystin-LR in water. *Applied Surface Science*. **289**, 245-251.
- [218] Geshan Z., Yong Cai Zhang, M., Nadagoudac, C., Hana, Kevin O'Shead, Said M. El-Sheikhe, Adel A. Ismaile, D., D. Dionysioua. (2014). Visible light-sensitized S, N and C co-doped polymorphic TiO₂ for photocatalytic destruction of microcystin-LR. *Applied catalysis B: Environmental*. **144** , 614-621.
- [219] Liu X., Chen Z., Zhou N., Shen J., M., Ye. (2010). Degradation and detoxification of microcystin-LR in drinking water by sequential use of UV and ozone. *Journal of Environmental Sciences*. **22** (12), 1897-1902.
- [220] Pelaez M., Armah A. de la Cruz, Elias Stathatos, Polycarpos Falaras, Dionysios D. Dionysiou, (2009). Visible light-activated N-F-codoped TiO₂ nanoparticles for the photocatalytic degradation of microcystin-LR in water. *Catal Today*. **144** , 19-25.
- [221] Hong Zhang, Qing Huang, Zhigang Ke, Linfang Yang, Xiangqin Wang, Zengliang Yu. (2012). Degradation of microcystin-LR in water by glow discharge plasma oxidation at the gas-liquid interface and its safety evaluation. *Water Research*. **46** , 6554-6562.
- [222] Jacobs L. C.V., Peralta-Zamora P. , Campos F. R., Pontarolo R.. (2013). Photocatalytic degradation of microcystin-LR in aqueous solutions. *Chemosphere*. **90** , 1552-1557.
- [223] Wenjuan Liao , Yanrong Zhang, Mi Zhang , Muthu Murugananthan , Sachio Yoshihara. (2013). Photoelectrocatalytic degradation of microcystin-LR using Ag/AgCl/TiO₂ nanotube arrays electrode under visible light irradiation. *Chemical Engineering Journal*. **231** , 455-463.
- [224] Jungju Lee, Harold W. Walker. (2011). Adsorption of microcystin-Lr onto iron oxide nanoparticles. *colloids and surfaces A: Physicochem. Eng. Aspects*. **373**, 94-100.
- [225] Warhurst A.M., IRaggett S.L., McConnachie G.L., Pollard S.J.T., Chipofyad V., Codd G.A. (1997). Adsorption of the cyanobacterial hepatotoxin microcystin-LR by a

low-cost activated carbon from the seed husks of the pan-tropical tree, moringa oleifera. *The science of the total Environment*. **207**, 207-211.

[226] Nyboma S.M.K., DzigaHeikkilä D., J.E., Kull T.P.J., Salminen S.J., Meriluoto. J.A.O. (2012). Characterization of microcystin-LR removal process in the presence of probiotic bacteria. *Toxicon*. **59** , 171-181.

[227] Hangjun Zhang, Guoying Zhu, Xiuying Jia, Ying Ding, Mi Zhang, (2011). Removal of microcystin-LR from drinking water using a bamboo-based charcoal adsorbent modified with chitosan. *Journal of Environmental Sciences* . **23** (12), 1983-1988.

[228] Baoling Yuan, Yanbo Li, Xiaodan Huang, Huijuan Liu, Jiuhui Qu. (2006). Fe(VI)-assisted photocatalytic degradating of microcystin-LR using titanium dioxide. *Journal of Photochemistry and Photobiology A: Chemistry* . **178** , 106-111.

[229] Jin Z., Guo, K., Tian-Fang X., Rui S., Xue. (2013). An immunosensor for microcystins based on Fe₃O₄, au magnetic nanoparticle modified screen-printed electrode. *Chin J Anal Chem*. **41** (9), 1353-1358.

[230] Dai G. , Quan C. , Zhang X. , J., Liu , L., Song. (2012). Fast removal of cyanobacterial toxin microcystin-LR by a low-cytotoxic microgel-fe(III) complex. *Water Research*. **46** , 1482-1489.

[231] Baoling Yuan , Yanbo Li , Xiaodan Huang, Huijuan Liu , Jiuhui Qu. (2006) Fe(VI)-assisted photocatalytic degradating of microcystin-LR using titanium dioxide. *Photochemistry and Photobiology A: Chemistry* **178**, 106–111.

[232]Xin Sui, Xiangrong Wang, Honghui Huang, Guotao Peng, Shoubing Wang,Zhengqiu Fan(2014). A Novel Photocatalytic Material for Removing Microcystin-LR under Visible Light Irradiation: Degradation Characteristics and Mechanisms, DOI: 10.1371, *Journal.Pone*.0095798.